Supplementary information

Photocleavable luminescent conjugates of 2-(2-aryl-5-(piperidin-1-yl)-2*H*-1,2,3-triazol-4-yl)thiazoles and aminoacids, diagnostic and drugs

Timur O. Fomin,[a] Vitalii A. Krasilnikov, [a] Vadim A. Shevyrin,[a] Artem S. Minin,[a,b] Enrico Benassi*[c] and Nataliya P. Belskaya*[a]

[a] Department of Technology for Organic Synthesis, Ural Federal University, 19 Mira Str., Yekaterinburg, 620002, Russia. E-mail: n.p.belskaya@urfu.ru
[b] M. N. Mikheev Institute of Metal Physics, Ural Branch of Russian Academy of Sciences, 18 S. Kovalevskaya Str., Yekaterinburg, 620108, Russia
[c] TIES Srl, Piazza Renato Simoni 1, Verona 37122, Italy. E-mail: ebenassi3@gmail.com

Table of contents

1. Experimental section

^{1}H NMR and ^{13}C NMR spectra were recorded using a Bruker Avance II spectrometer (Karlsruhe, Germany; 400 MHz for ^{1}H and 100 MHz for ^{13}C) and a Bruker Avance NEO spectrometer (Karlsruhe, Germany; 600 MHz for ^{1}H and 150 MHz for ^{13}C). Chemical shifts are reported in parts per million (ppm) relative to tetramethylsilane for ^{1}H NMR and relative to the residual solvent signals for ^{13}C NMR as an external reference. Coupling constants (J) are given in hertz (Hz). Signal splitting patterns are described as singlet (s), doublet (d), triplet (t), quartet (q), quintet (quin), sextet (sext), multiplet (m), broad (br), doublet of doublets (dd), doublet of triplets (dt), or AA′XX′ (spin system of para-substituted benzene with two different substituents). High resolution mass spectra were obtained using a Agilent 1290 Infinity II high-performance liquid chromatography system equipped with a UV diode array detector and tandem quadrupole time-of-flight (Q-TOF) accurate mass detector Agilent 6545 Q-TOF LC– MS (Agilent Technologies Inc., Santa Clara, CA, USA). The Q-TOF instrument were operated with an electrospray ion source in positive ion mode. Fourier transform infrared (FTIR) spectra were obtained using an attenuated total reflection (ZnSe) FTIR spectrometer in the range of 4000–500 cm^{-1}. Melting points were determined using a microscopic melting point meter without correction. UV-Vis absorption spectra were recorded on a Shimadzu UV-1800 spectrometer. The fluorescence of the sample solution was measured using a Hitachi F-7000 spectrophotometer (Tokyo, Japan). The absorption and emission spectra were recorded in Toluene, 1,4-dioxane, $CHCl_3$, EtOH, MeOH, EtOAc, Acetone, DMF, MeCN, DMSO and DMSO-H_2O (1:1; 1:9, v/v), MeCN-H_2O (1:9, v/v), Acetone-H_2O (1:9, v/v) using 10.00-mm quartz cells. The excitation wavelengths were the absorption maxima. Atmospheric oxygen contained in the solutions was not removed. The concentration of the compound in the test solution was 5.0×10^{-5} M for absorption and 5.0×10^{-6} M for fluorescence measurements. Microscopic examination was performed using the equipment of the Shared Research Center of Scientific Equipment SRC IIP UrB RAS. After staining and washing, living cells were examined using a confocal laser scanning microscope (LSM-710, Carl Zeiss) with a multichannel QUASAR detector (34 channels). The images were obtained using an immersion lens (40x/1.3 Oil). To obtain informative fluorescent images, ZEN software was used in special lambda mode (λ mode), allowing for the determination of the emission range with maximum contrast.

The reactions were monitored by analytical thin-layer chromatography (TLC) on aluminum-backed silica-gel plates (Sorbfil UV–254). Visualization of the components was accomplished using UV light (254 and 365 nm). The products were purified by column chromatography using a silica-gel (0.035–0.070, 60 Å) and recrystallized from ethanol. 2-Aryl-2*H*-1,2,3-triazole-4-carbonitriles **8a-d** were prepared according to the published procedure[1,2].

General Procedure for the synthesis of compounds 4a-d.

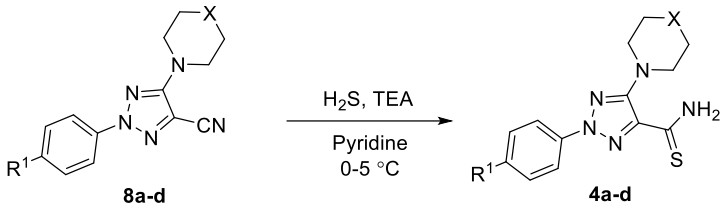

8a-d **4a-d**

8a: R^1 = MeO, X = CH_2 **4a:** R^1 = MeO, X = CH_2, 19h, 91%
8b: R^1 = Br, X = CH_2 **4b:** R^1 = Br, X = CH_2, 20h, 90%
8c: R^1 = MeCO, X = CH_2 **4c:** R^1 = MeCO, X = CH_2, 21h, 89%
8d: R^1 = MeCO, X = O **4d:** R^1 = MeCO, X = O, 22h, 85%

Scheme S1.

Dry hydrogen sulfide was bubbled through a cooled (0–5 °C) solution of 7.0 mmol of 2-aryl-1,2,3-triazolecarbonitriles **8a–d** in 20 ml in pyridine and 1.0 ml (7.0 mmol) of TEA for 1.5 h with continuous stirring. The mixture was left at 0–5 °C overnight, then ethanol (50 ml) is added and the reaction mixture poured into 200 g of crushed ice. The resulting precipitate was filtered off, washed with water and crystallised from ethanol.

2-(4-Methoxyphenyl)-5-(piperidin-1-yl)-2*H*-1,2,3-triazole-4-carbothioamide (4a). Yellow

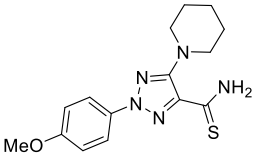

powder, yield 91%; mp = 146-148 °C. ^{1}H NMR ($CDCl_3$, 400 MHz): δ 1.61-1.65 (m, 2H, CH_2); 1.71–1.76 (m, 4H, CH_2); 3.23 (t, J = 5.3 Hz, 4H, CH_2), 3.84 (s, 3H, OCH_3); 6.95 7.96 (AA′XX′, J = 9.0 Hz, 4H, CH_{Ar}); 7.55 (br. s, 1H, $CONH_2$); 8.85 (br. s, 1H, $CONH_2$). ^{13}C NMR ($CDCl_3$, 100 MHz): 23.9, 25.8 (2C), 52.9 (2C), 55.7, 114.4 (2C), 120.6 (2C), 133.1, 135.5, 156.1, 159.5, 189.9. FT-IR (neat) ν_{max} (cm^{-1}): 3421, 3252; 3143; 2933, 2837-2810. HRMS (ESI-TOF) *m/z*: $[M+H]^+$ Calcd. for $C_{15}H_{19}N_5OS$+H 318.1389; Found 318.1392

2-(4-Bromophenyl)-5-(piperidin-1-yl)-2*H*-1,2,3-triazole-4-carbothioamide (4b). Light-yellow

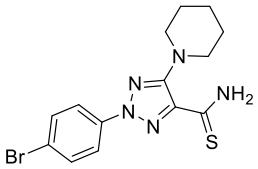

powder, yield 90%; mp = 176-178 °C. ^{1}H NMR ($CDCl_3$, 400 MHz): δ 1.61–1.68 (m, 2H, CH_2); 1.70–1.78 (m, 4H, $2CH_2$); 3.24 (t, J = 5.3 Hz, 4H, $2CH_2$); 7.54 (br, 1H, NH); 7.58 and 7.93 (AA′XX′, J = 8.2 Hz, 4H, CH_{Ar}); 8.74 (br, 1H, NH). ^{13}C NMR ($CDCl_3$, 100 MHz): 23.9, 25.8 (2C), 52.7 (2C), 120.5 (2C), 121.6, 132.5 (2C), 136.2, 138.3, 156.4, 189.8. FT-IR (neat) ν_{max} (cm^{-1}): 3388, 3247, 3147, 2992, 2969, 2932, 2851, 2810, 2750. HRMS (ESI-TOF) *m/z*: $[M+H]^+$ Calcd. for $C_{14}H_{16}BrN_5S$+H 366.0383; Found 366.0383.

2-(4-Acetylphenyl)-5-(piperidin-1-yl)-2*H*-1,2,3-triazole-4-carbothioamide (4c). Yellow powder,

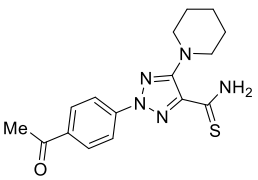

yield 89%; mp = 188-190 °C. ^{1}H NMR ($CDCl_3$, 400 MHz): δ 1.61–1.68 (m, 2H, CH_2); 1.72–1.78 (m, 4H, $2CH_2$); 2.63 (s, 3H, CH_3); 3.28 (t, J = 5.3 Hz, 4H, $2CH_2$,); 7.62 (br, 1H, NH); 8.05 and 8.13 (AA′XX′, J = 8.5 Hz, 4H, CH_{Ar}); 8.68 (br, 1H, NH). ^{13}C NMR ($CDCl_3$, 100 Hz.): 23.9, 25.7 (2C), 26.8, 52.6 (2C),

118.7 (2C), 129.8 (2C), 136.1, 136.7, 142.3, 156.7, 189.7, 196.9. FT-IR (KBr) ν_{max} (cm^{-1}): 3285, 3179, 3004, 2967, 2899, 2854, 2827, 2739, 2693, 1682. HRMS (ESI-TOF) *m/z*: [M+H]+ Calcd. for $C_{16}H_{19}N_5OS$+H 330.1383; Found 330.1389.

2-(4-Acetylphenyl)-5-morpholino-2*H*-1,2,3-triazole-4-carbothioamide (4d). Yellow powder, yield 85%; mp = 190-192 °C. ^{1}H NMR ($CDCl_3$, 400 MHz): δ 2.63 (s, 3H, CH_3); 3.45 (t, J = 4.5 Hz, 4H, $2CH_2$); 3.89 (t, J = 4.5 Hz, 4H, $2CH_2$); 7.56 (br, 1H, NH); 8.05 and 8.10 (AA′XX′, J = 8.8 Hz, 4H, CH_{Ar}); 8.26 (br, 1H, NH).^{13}C NMR ($CDCl_3$, 100 MHz): 26.8 (2C), 51.2 (2C), 66.6, 118.6 (2C), 129.9 (2C), 135.8, 136.2, 142.1, 157.0, 189.0, 196.8. FT-IR (KBr) ν_{max} (cm^{-1}): 3285, 3179, 3004, 2967, 2899, 2854, 2827, 1682. HRMS (ESI-TOF) *m/z*: $[M+H]^+$ Calcd. for $C_{15}H_{17}N_5O_2S$+H 332.1176; Found 332.1178

General Procedure for the synthesis of compounds 3a-d:

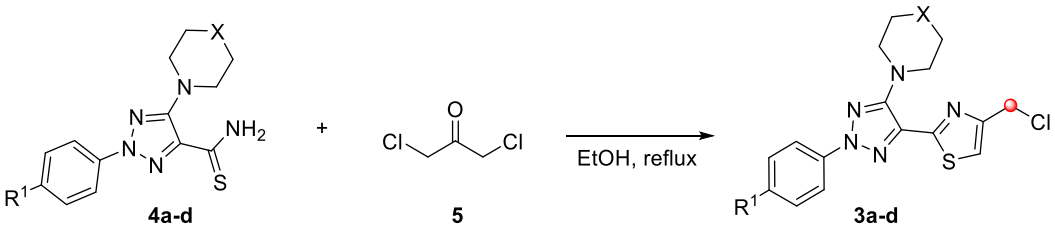

3a, 4a: R^1 = MeO X = CH_2 **3c, 4c:** R^1 = MeCO X = CH_2
3b, 4a: R^1 = Br X = CH_2 **3d, 4d:** R^1 = MeCO X = O

Scheme S2.

1.143 g (9.0 mmol) of 1,3-dichloroacetone was added to a solution of 4.5 mmol 2-aryl-1,2,3-triazole-4-carbothioamide **4** in 30 ml of ethanol. The reaction was steered while the starting compound was consumed (TLC) and the mixture was cooled in an ice bath. The resulting precipitate was filtered off, washed with petroleum ether, and then crystallised from ethanol.

4-(Chloromethyl)-2-(2-(4-methoxyphenyl)-5-(piperidin-1-yl)-2*H*-1,2,3-triazol-4-ylthiazole (3a). Yellow powder, yield 78%; mp = 98-100 °C. ^{1}H NMR ($CDCl_3$, 400 MHz): δ 1.62–1.67 (m, 2H, CH_2); 1.79 (quin, J = 5.1 Hz, 4H, $2CH_2$); 3.37 (t, J = 5.1 Hz, 4H, $2CH_2$); 3.85 (s, 3H, CH_3); 4.76 (s, 2H, CH_2); 6.97 and 7.96 (AA′XX′, J = 9.1 Hz, 4H, CH_{Ar}); 7.30 (s, 1H, CH). ^{13}C NMR ($CDCl_3$, 100 MHz): 24.3, 25.6 (2C), 41.2, 51.4 (2C), 55.7, 114.4 (2C), 117.1, 119.9 (2C), 132.1, 133.5, 152.9, 155.1, 158.9, 159.6. FT-IR (KBr) ν_{max} (cm^{-1}): 3109, 3057, 2997, 2938, 2859, 2812, 2760. HRMS (ESI-TOF) *m/z*: $[M+H]^+$ Calcd. for $C_{18}H_{20}ClN_5OS$+H 390.1150; Found 390.1156.

2-(2-(4-Bromophenyl)-5-(piperidin-1-yl)-2*H*-1,2,3-triazol-4-yl)-4-(chloromethyl)thiazole (3b). Light-yellow powder, yield 91%; mp = 104-106 °C. ^{1}H NMR ($CDCl_3$, 400 MHz): δ 1.62–1.68 (m, 2H, CH_2); 1.75–1.82 (m, 4H, $2CH_2$); 3.38 (t, J = 4.9 Hz, 4H, $2CH_2$); 4.76 (s, 2H, CH_2); 7.33 (s, 1H, CH); 7.57 and 7.92 (AA′XX′, J = 8.6 Hz, 4H, CH_{Ar}). ^{13}C NMR ($CDCl_3$, 100 MHz): 24.3, 25.5 (2C), 41.1, 51.2 (2C), 117.5, 119.9 (2C), 120.5, 132.4 (2C), 133.0, 138.6, 153.1, 155.4, 159.3. FT-IR (KBr) ν_{max} (cm^{-1}): 3118, 3089, 3023, 2974, 2936, 2818, 2714. HRMS (ESI-TOF) *m/z*: $[M+H]^+$ Calcd. for $C_{17}H_{17}BrClN_5S$+H 438.0149; Found 438.0139.

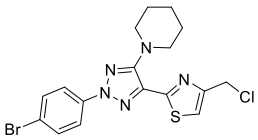

1-(4-(4-(4-(Chloromethyl)thiazol-2-yl)-5-(piperidin-1-yl)-2*H*-1,2,3-triazol-2-yl)phenyl)ethan-1-one (3c). Yellow powder, yield 75%; mp = 148-150 °C. ^{1}H NMR ($CDCl_3$, 400 MHz): δ 1.62–1.69 (m, 2H, CH_2); 1.74–1.84 (m, 4H, $2CH_2$); 2.63 (s, 3H, CH_3); 3.41 (t, J = 5.2 Hz, 4H, $2CH_2$); 4.77 (s, 2H, CH_2); 7.35 (s, 1H, CH); 8.06 and 8.12 (AA′XX′, J = 8.4 Hz, 4H, CH_{Ar}). ^{13}C NMR ($CDCl_3$, 100 MHz): 24.2, 25.5 (2C), 26.8, 31.1, 41.1, 51.1 (2C), 117.8, 118.0 (2C), 129.9 (2C), 133.8, 135.3, 142.5, 153.2, 155.7, 159.1, 197.0. FT-IR (KBr) ν_{max} (cm^{-1}): 3110, 3060, 2934, 2849, 2825, 1679. HRMS (ESI-TOF) *m/z*: $[M+H]^+$ Calcd. for $C_{19}H_{20}ClN_5OS$+H 402.1150; Found 402.1156.

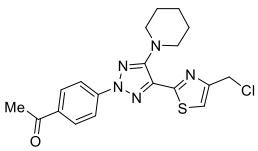

1-(4-(4-(4-(Chloromethyl)thiazol-2-yl)-5-morpholino-2*H*-1,2,3-triazol-2-yl)phenyl)ethan-1-one (3d). Yellow powder, yield 71%; mp = 128-130 °C. ^{1}H NMR ($CDCl_3$, 400 MHz): δ 2.64 (s, 3H, CH_3); 3.53 (t, J = 4.8 Hz, 4H, $2CH_2$); 3.94 (t, J = 4.8 Hz, 4H, $2CH_2$); 4.74 (s, 2H, CH_2); 7.34 (s, 1H, CH); 8.06 and 8.12 (AA′XX′, J = 8.5 Hz, 4H, CH_{Ar}). ^{13}C NMR ($CDCl_3$, 100 MHz): 26.8, 41.0, 50.0 (2C), 66.6 (2C), 117.9, 118.0 (2C), 129.9 (2C), 133.5, 135.5, 142.3, 153.1, 154.6, 159.1, 196.9. FT-IR (KBr) ν_{max} (cm^{-1}): 3104, 2994, 2977, 2950, 2916, 2892, 2856, 2831, 1682. HRMS (ESI-TOF) *m/z*: $[M+H]^+$ Calcd. for $C_{18}H_{18}ClN_5O_2S$+H 404.0942; Found 404.0950.

General Procedure for the synthesis of compounds 6a-d

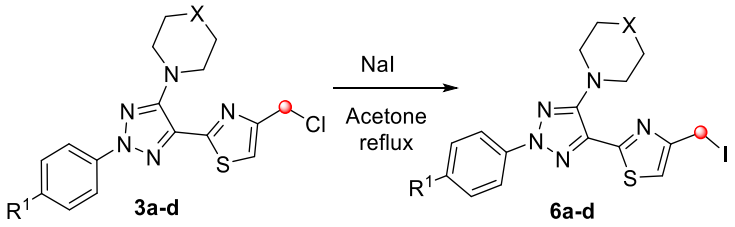

Scheme S3.

The solution of 2.5 mmol 4-(chloromethyl)thiazole **3a-d,** 1.87 g (12.5 mmol) NaI in 30 ml of acetone, was refluxed until the reaction was complete (TLC). Then ethyl acetate (70 ml) was added and the mixture was washed with 80 ml × 2 of a 0.15 M NaCl solution and organic layer was dried over

anhydrous Na_2SO_4. Afterward, the solvent was evaporated under reduced pressure and the product was purified using liquid column chromatography (eluent – chloroform).

4-(Iodomethyl)-2-(2-(4-methoxyphenyl)-5-(piperidin-1-yl)-2*H*-1,2,3-triazol-4-yl)thiazole (6a). Yellow powder, yield 65%; mp = 96-98 °C. ^{1}H NMR ($CDCl_3$, 400 MHz): δ 1.62–1.67 (m, 2H, CH_2); 1.79–1.85 (m, 4H, $2CH_2$); 3.40 (t, J = 5.3 Hz, 4H, $2CH_2$); 3.85 (s, 3H, CH_3); 4.58 (s, 2H, CH_2); 6.97 and 7.95 (AA′XX′, J = 9.1 Hz, 4H, CH_{Ar}); 7.22 (s, 1H, CH).^{13}C NMR ($CDCl_3$, 100 MHz): -1.0, 24.3, 25.8 (2C), 51.2 (2C), 55.7, 114.4 (2C), 115.6, 119.9 (2C), 132.0, 133.5, 153.6, 155.1, 158.9, 159.4. FT-IR (KBr) ν_{max} (cm^{-1}): 3086, 2994, 2936, 2918, 2842, 2817. HRMS (ESI-TOF) *m/z*: $[M+H]^+$ Calcd. for $C_{18}H_{20}IN_5OS$+H 482.0506; Found 482.0522.

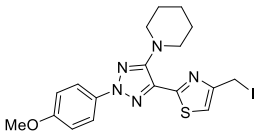

2-(2-(4-Bromophenyl)-5-(piperidin-1-yl)-2*H*-1,2,3-triazol-4-yl)-4-(iodomethyl)thiazole (6b). Brown powder, yield 79%; mp = 94-96 °C. ^{1}H NMR ($CDCl_3$, 400 MHz): δ 1,63–1,68 (m, 2H, CH_2); 1.78–1.84 (m, 4H, $2CH_2$); 3.40 (t, J = 5.3 Hz, 4H, $2CH_2$); 4.58 (s, 2H, CH_2); 7.24 (s, 1H, CH); 7.56 and 7.93 (AA′XX′, J = 9.0 Hz, 4H, CH_{Ar}).^{13}C NMR ($CDCl_3$, 100 MHz): -1.2, 24.3, 25.7 (2C), 51.0 (2C), 115.9, 119.8 (2C), 120.4, 132.3 (2C), 132.9, 138.6, 153.8, 155.3, 159.0. FT-IR (KBr) ν_{max} (cm^{-1}): 3109, 2936, 2851. HRMS (ESI-TOF) *m/z*: $[M+H]^+$ Calcd. for $C_{17}H_{17}BrIN_5S$+H 531.9486; Found 531.9497.

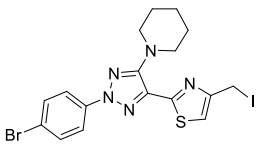

1-(4-(4-(4-(Iodomethyl)thiazol-2-yl)-5-(piperidin-1-yl)-2*H*-1,2,3-triazol-2-yl)phenyl)ethan-1-one (6c). Yellow powder, yield 90%; mp = 140-142 °C. ^{1}H NMR ($CDCl_3$, 400 MHz): δ 1.63–1.69 (m, 2H, CH_2); 1.79–1.86 (m, 4H, $2CH_2$); 2.63 (s, 3H, CH_3); 3.43 (t, J = 5.4 Hz, 4H, $2CH_2$); 4.58 (s, 2H, CH_2); 7.26 (s, 1H, CH); 8.05–8.11 (AA′XX′, J = 8.7 Hz, 4H, CH_{Ar}).^{13}C NMR ($CDCl_3$, 100 MHz.): 1.3, 24.3, 25.7 (2C), 26.8, 51.0 (2C), 116.2, 117.9, 129.8 (2C), 133.6, 135.2, 142.5, 153.9, 155.6, 158.8, 197.0. FT-IR (KBr) ν_{max} (cm^{-1}): 3099, 2928, 2854, 2811, 1680. HRMS (ESI-TOF*) m/z*: $[M+H]^+$ Calcd. for $C_{19}H_{20}IN_5OS$+H 494.0506; Found 494.0516.

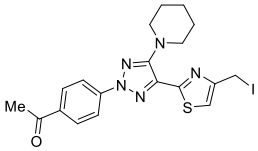

1-(4-(4-(4-(Iodomethyl)thiazol-2-yl)-5-morpholino-2*H*-1,2,3-triazol-2-yl)phenyl)ethan-1-one (6d). Yellow powder, yield 80%; mp = 158-160 °C. ^{1}H NMR ($CDCl_3$, 400 MHz): δ 2.64 (s, 3H, CH_3); 3.55 (t, 4H, $2CH_2$, J = 4.7 Hz); 3.97 (t, J = 4.7 Hz); 4.56 (s, 2H, CH_2); 7.26 (s, 1H, CH); 8.06 and 8.12 (AA′XX′, J = 8.9 Hz, 4H, CH_{Ar}).^{13}C NMR ($CDCl_3$, 100 MHz): -1.3, 26.8, 49.8 (2C), 66.8 (2C), 116.1, 118.0 (2C), 129.9 (2C), 133.4, 135.5, 142.3, 153.8, 154.6, 158.7, 196.9. FT-IR (KBr) ν_{max} (cm^{-1}): 3100, 3074, 3006, 2967, 2904, 2886, 2848, 2758, 2684, 1683. HRMS (ESI-TOF) *m/z*: $[M+H]^+$ Calcd. for $C_{18}H_{18}IN_5O_2S$+H 496.0299; Found 496.0323.

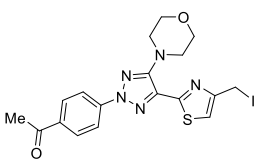

Synthesis of compounds 1a-o

Table S1. Optimization of reaction conditions for ATT-CH_2Cl **3c** alkylation of carboxylic acid **2e**

Entry	*N*-Boc-Gly (eq.)	NaI (eq.)	Base	Base (eq.)	Solvent	T (°C)	Time (h)	Yield (%)
1	1.2	0	$NaHCO_3$	1.3	DMF	50	60	12
2	1.2	0	Na_2CO_3	1.3	DMF	50	60	18
3	1.2	0	Na_2CO_3	1.3	Acetone	56	42	15
4	1.2	0.1	Na_2CO_3	1.3	Acetone	56	42	21
5	1.2	0	K_2CO_3	1.3	DMF	50	60	51
6	1.2	0	K_2CO_3	1.3	Acetone	56	37	27
7	1.2	0.1	K_2CO_3	1.3	Acetone	56	37	32
8	1.2	0	Cs_2CO_3	1.3	DMF	50	12	86

General Procedures for the synthesis of compounds 1a-q

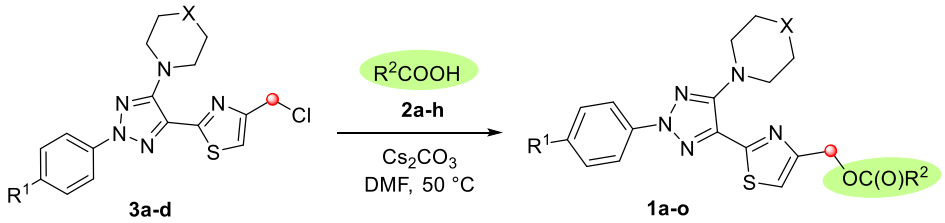

Scheme S4.

Procedure 1: Carboxylic acid **2** (0.36 mmol) was added to a solution of 0.3 mmol 4-(chloromethyl)thiazole **3** in 5 ml of DMF, followed by 0.127 g (0.39 mmol) of Cs_2CO_3. The mixture was then heated at 50 °C with stirring. Ethyl acetate (70 ml) was added after the reaction was completed (TLC) and the mixture was washed with 80 ml × 3 of a 0.15 M NaCl solution. The organic extract was dried (anhydrous Na_2SO_4), and the solvent was evaporated under vacuum. Finally, the product was separated and purified using liquid column chromatography with a mixture of EtOAc and *n*-Hexane (1:4, v/v).

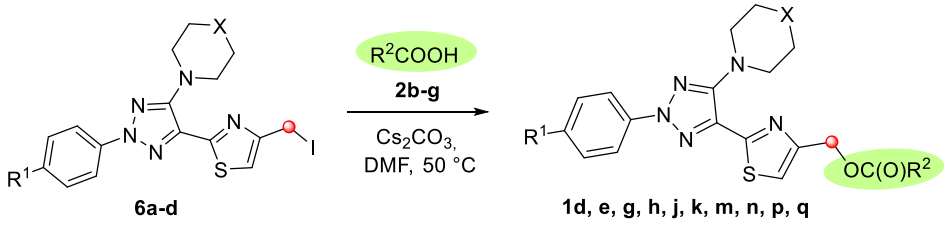

Scheme S5.

Procedure 2: Carboxylic acid **2** (0.36 mmol) was added to a solution of 0.3 mmol 4-(iodomethyl)thiazole **6** in 5 ml of DMF, followed by 0.127 g (0.39 mmol) of Cs_2CO_3. The mixture was then heated at 50 °C with stirring. Ethyl acetate (70 ml) was added after the reaction was completed (TLC) and the mixture was washed with 80 ml × 3 of a 0.15 M NaCl solution. The organic extract was dried (anhydrous Na_2SO_4), and the solvent was evaporated under vacuum. Finally, the

product was separated and purified using liquid column chromatography with a mixture of EtOAc and *n*-Hexane (1:4).

2-(2-(4-Methoxyphenyl)-5-(piperidin-1-yl)-2*H*-1,2,3-triazol-4-yl)thiazol-4-yl)methyl (*tert*-butoxycarbonyl)glycinate (1a). White powder, yield 69% (Procedure 1); mp = 94-96 °C. ^{1}H NMR ($CDCl_3$, 400 MHz): δ 1.45 (s, 9H, $3CH_3$); 1.62–1.68 (m, 2H, CH_2); 1.74–1.80 (m, 4H, $2CH_2$); 3.35 (t, J = 5.1 Hz, 4H, $2CH_2$); 3.85 (s, 3H, CH_3); 3.99 (d, J = 4.7 Hz, 2H, CH_2); 5.03 (br, 1H, NH); 5.36 (s, 2H, CH_2); 6.96 and 7.96 (AA′XX′, J = 9.1 Hz, 4H, CH_{Ar}); 7.30 (s, 1H, CH). ^{13}C NMR ($CDCl_3$, 100 MHz): 24.3, 25.6 (2C), 28.4 (3C), 42.6, 51.4 (2C), 55.7, 62.8, 80.2, 114.4 (2C), 117.7, 119.9 (2C), 132.2, 133.2, 155.1, 155.8, 158.9, 159.5, 170.2. FT-IR (KBr) ν_{max} (cm^{-1}): 3112, 3095, 2935, 2833, 1758, 1675. HRMS (ESI-TOF) *m/z*: $[M+H]^+$ Calcd. for $C_{25}H_{32}N_6O_5S$+H 529.2228; Found 529.2241.

(2-(2-(4-Methoxyphenyl)-5-(piperidin-1-yl)-2*H*-1,2,3-triazol-4-yl)thiazol-4-yl)methyl (*tert*-butoxycarbonyl)-*L*-leucinate (1b). Beige powder, yield 66% (Procedure 1); mp = 86-88 °C. ^{1}H NMR ($CDCl_3$, 400 MHz): δ 0.90–0.97 (m, 6H, $2CH_3$); 1.44 (s, 9H, $3CH_3$); 1.49–1.56 (m, 1H, CH); 1.62–1.65 (m, 2H, CH_2); 1.66–1.74 (m, 2H, CH_2); 1.74–1.80 (m, 4H, $2CH_2$); 3.36 (t, 4H, $2CH_2$); 3.85 (s, 3H, CH_3); 4.33–4.44 (m, 1H, CH); 4.81- 4.91 (m, 1H, NH); 5.36 (s, 2H, CH_2); 6.96 and 7.96 (AA′XX′, J = 8.8 Hz, 4H, $4CH_{Ar}$); 7.29 (s, 1H, CH). ^{13}C NMR ($CDCl_3$, 100 MHz): 22.0, 23.0, 24.3, 24.9, 25.6 (2C), 28.5 (3C), 41.8, 51.4 (2C), 52.4, 55.7, 62.8, 80.0, 114.4 (2C), 117.2, 119.9 (2C), 132.3, 133.5, 151.5, 155.0, 155.6, 159.4, 173.3. FT-IR (KBr) ν_{max} (cm^{-1}): 3136, 3090, 3064, 2994, 2957, 2933, 2872, 2854, 2816, 2757, 1734, 1685. HRMS (ESI-TOF) *m/z*: $[M+H]^+$ Calcd. for $C_{29}H_{40}N_6O_5S$+H 585.2859; Found 585.2871.

(2-(2-(4-Methoxyphenyl)-5-(piperidin-1-yl)-2*H*-1,2,3-triazol-4-yl)thiazol-4-yl)methyl (*tert*-butoxycarbonyl)-*L*-methioninate (1c). Beige powder, yield 62% (Procedure 1); mp = 108-110 °C. ^{1}H NMR ($CDCl_3$, 400 MHz): δ 1.44 (s, 9H, $3CH_3$); 1.62–1.66 (m, 2H, CH_2); 1.74–1.79 (m, 4H, $2CH_2$); 1.93–2.02 (m, 1H, CH); 2.06 (s, 3H, CH_3); 2.12–2.21 (m, 1H, CH); 2.51–2.55 (m, 2H, CH_2); 3.35 (t, J = 5.3 Hz, 4H, $2CH_2$); 3.85 (s, 3H, CH_3); 4.49 (br, 1H, CH); 5.15 (br, 1H, NH); 5.37 (s, 2H, CH_2); 6.97 and 7.96 (AA′XX′, J = 8.9 Hz, 4H, $4CH_{Ar}$); 7.31 (s, 1H, CH). ^{13}C NMR ($CDCl_3$, 100 MHz): 15.6, 24.3, 25.6 (2C), 28.4 (3C), 30.1, 32.3, 51.4 (2C), 53.1, 55.7, 62.9, 80.2, 114.4 (2C), 117.5, 119.9 (2C), 132.2, 133.5, 151.3, 155.1, 158.9, 159.5, 172.2. FT-IR (neat) ν_{max} (cm^{-1}): 2997, 2968, 2934, 2851, 2821, 1739, 1685. HRMS (ESI-TOF) *m/z*: $[M+H]^+$ Calcd. for $C_{28}H_{38}N_6O_5S_2$+H 603.2418; Found 603.2435.

(2-(2-(4-Bromophenyl)-5-(piperidin-1-yl)-2*H*-1,2,3-triazol-4-yl)thiazol-4-yl)methyl (*tert*-butoxycarbonyl)glycinate (1d). Light beige, yield 73% (Procedure 2); mp = 106-108 °C. ^{1}H NMR ($CDCl_3$, 400 MHz): δ 1.45 (s, 9H, $3CH_3$); 1.62–1.67 (m, 2H, CH_2); 1.74–1.80 (m, 4H, $2CH_2$); 3.36 (t, J = 5.5 Hz, 2H, CH_2); 3.96–4.04 (m, 2H, CH_2); 4.98–5.08 (m, 1H, NH); 5.37 (s, 2H, CH_2); 7.33 (s, 1H, CH); 7.57 and 7.93 (AA′XX′, J = 9.0 Hz, 4H, $4CH_{Ar}$). ^{13}C NMR ($CDCl_3$, 100 MHz): 24.2, 25.5 (2C), 28.5 (2C), 42.6, 51.3 (3C), 62.7, 80.3, 118.1, 119.9 (2C), 120.5, 132.4 (2C), 133.1, 138.6, 151.4, 155.4, 159.2, 170.3. FT-IR (KBr) ν_{max} (cm^{-1}): FT-IR (KBr) ν_{max} (cm^{-1}): 3372, 3111, 2978, 2961, 2935, 2849, 2831, 1758. HRMS (ESI-TOF) *m/z*: $[M+H]^+$ Calcd. for $C_{24}H_{29}BrN_6O_4S$+H 577.1233; Found 577.1242.

(2-(2-(4-Bromophenyl)-5-(piperidin-1-yl)-2*H*-1,2,3-triazol-4-yl)thiazol-4-yl)methyl (*tert*-butoxycarbonyl)-*L*-leucinate (1e). White powder, yield 16 % (Procedure 1); yield 67% (Procedure 2); mp = 110-112 °C. ^{1}H NMR ($CDCl_3$, 400 MHz): δ 0.92–0.97 (m, 6H, $2CH_3$); 1.44 (s, 9H, $3CH_3$); 1.49–1.55 (m, 1H, CH); 1.61–1.67 (m, 2H, CH_2); 1.68–1.73 (m, 2H, CH_2); 1.74–1.80 (m, 4H, $2CH_2$); 3.37 (t, J = 5.3 Hz, 4H, $2CH_2$); 4.32–4.45 (m, 1H, CH); 4.83-4.97 (m, 1H, NH); 5.36 (s, 2H, CH_2); 7.33 (s, 1H, CH); 7.57 and 7.93 (AA′XX′, J = 8.5 Hz, 4H, $4CH_{Ar}$). ^{13}C NMR ($CDCl_3$, 100 MHz): 22.0. 23.0, 24.2, 24.9, 25.5 (2C), 28.5 (3C), 41.8, 51.3 (2C), 52.4, 62.8, 80.1, 117.6, 119.9 (2C), 120.5, 132.4 (2C), 133.2, 138.6, 151.7, 155.3, 155.6, 159.0, 173.4. FT-IR (KBr) ν_{max} (cm^{-1}): 3107, 2963, 2935, 2872, 2850, 2811, 2759, 1759, 1690. HRMS (ESI-TOF) *m/z*: $[M+H]^+$ Calcd. for $C_{28}H_{37}BrN_6O_4S$+H 635.1836; Found 635.1846.

(2-(2-(4-Acetylphenyl)-5-(piperidin-1-yl)-2*H*-1,2,3-triazol-4-yl)thiazol-4-yl)methyl (*tert*-butoxycarbonyl)glycinate (1f). Yellow powder, yield 86% (Procedure 1); mp = 138-140 °C. ^{1}H NMR ($CDCl_3$, 400 MHz): δ 1.45 (s, 9H, $3CH_3$); 1.63–1.68 (m, 2H, CH_2); 1.74–1.82 (m, 4H, $2CH_2$); 2.63 (s, 3H, CH_3); 3.39 (t, J = 4.9 Hz, 4H, $2CH_2$); 3.99 (d, J = 5.6 Hz, 2H, CH_2); 5.03 (br, 1H, NH); 5.37 (s, 2H, CH_2); 7.36 (s, 1H, CH); 8.06 and 8.13 (AA′XX′, J = 8.8 Hz, 4H, $4CH_{Ar}$). ^{13}C NMR ($CDCl_3$, 150 MHz): 24.2, 25.4 (2C), 26.8, 28.4 (3C), 42.6, 51.2 (2C), 62.7, 80.3, 118.0 (2C), 118.4, 129.9 (2C), 133.9, 135.3, 142.5, 155.7, 155.8, 159.0, 170.3, 197.0. FT-IR (KBr) ν_{max} (cm^{-1}): 3092, 2983, 2939, 2921, 2853, 1753, 1689. HRMS (ESI-TOF) *m/z*: $[M+H]^+$ Calcd. for $C_{26}H_{32}N_6O_5S$+H 541.2228; Found 541.2239.

(2-(2-(4-Acetylphenyl)-5-(piperidin-1-yl)-2*H*-1,2,3-triazol-4-yl)thiazol-4-yl)methyl (*tert*-butoxycarbonyl)-*L*-leucinate (1g). Light-yellow powder, yield 20% (Procedure 1); yield 81% (Procedure 2); mp = 108-110 °C. ^{1}H NMR ($CDCl_3$, 600 MHz): δ 0.89–1.00 (m, 6H, $2CH_3$); 1.44 (s, 9H, $3CH_3$); 1.50–1.55 (m, 1H, CH); 1.62–1.75 (m, 2H, CH_2) and (m, 2H, CH_2); 1.75–1.85 (m, 4H, $2CH_2$); 2.64 (s, 3H, CH_3); 3.42 (t, J = 5.2 Hz, 4H, $2CH_2$); 4.34–4.45 (m, 1H, CH); 4.86-4.96 (m, J = 5.2 Hz, 1H, NH); 5.33–5.41 (m, 2H, CH_2); 7.36 (s, 1H, CH); 8.06 and 8.13 (AA′XX′, J = 8.8 Hz, 4H, CH_{Ar}). ^{13}C NMR ($CDCl_3$, 150 MHz): 22.0, 23.0, 24.1, 24.9, 25.3 (2C), 26.8, 28.5 (3C), 41.8, 51.4 (2C), 52.3, 62.7, 80.1, 117.9, 118.0 (2C), 129.9 (2C), 134.0, 135.4, 142.5, 151.9, 155.6, 158.7, 173.4, 197.0. FT-IR (neat) ν_{max} (cm^{-1}): 3355, 2996, 2958, 2934, 2875, 2850, 2825, 1734, 1679. HRMS (ESI-TOF) *m/z*: $[M+H]^+$ Calcd. for $C_{30}H_{40}N_6O_5S$+H 597.2854; Found 597.2859.

(2-(4-Acetylphenyl)-5-(piperidin-1-yl)-2*H*-1,2,3-triazol-4-yl)thiazol-4-yl)methyl (*tert*-butoxycarbonyl)-*L*-methioninate (1h). Yellow powder, yield 25% (Procedure 1); yield 61% (Procedure 2); mp = 84-86 °C. ^{1}H NMR ($CDCl_3$, 400 MHz): δ 1.44 (s, 9H, $3CH_3$); 1.64–1.69 (m, 2H, CH_2); 1.74–1.81 (m, 4H, $2CH_2$); 1.92–2.01 (m, 1H, CH); 2.06–2.12 (m, 1H, CH); 2.51 –2.56 (m, 2H, CH_2); 2.63 (s, 3H, CH_3); 3.40 (t, J = 5.3 Hz, 4H, $2CH_2$); 4.43–4.56 (m, 1H, CH); 5.05-5.27 (m, 1H, NH); 5.38 (s, 2H, CH_2); 7.36 (s, 1H, CH); 8.05 and 8.12 (AA′XX′, J = 9.0 Hz, 4H, CH_{Ar}). ^{13}C NMR ($CDCl_3$, 150 MHz): 15.7, 24.2, 25.5 (2C), 26.8, 28.4 (3C), 30.1, 32.2, 51.2 (2C), 53.0, 62.9, 80.3, 118.0 (2C), 118.3, 129.9 (2C), 133.9, 135.3, 142.5, 151.6, 155.7, 159.0, 172.2, 197.1. FT-IR (KBr) ν_{max} (cm^{-1}): 3108, 3055, 2976, 2938, 2853, 2826, 2768, 1742, 1717, 1667. HRMS (ESI-TOF) *m/z*: $[M+H]^+$ Calcd. for $C_{29}H_{38}N_6O_5S_2$+H 615.2418; Found 615.2426.

(2-(2-(4-Acetylphenyl)-5-(piperidin-1-yl)-2*H*-1,2,3-triazol-4-yl)thiazol-4-yl)methyl 4-((*tert*-butoxycarbonyl)amino)butanoate (1i). Yellow powder, yield 41% (Procedure 1); mp = 80-82 °C. ^{1}H NMR ($CDCl_3$, 400 MHz): δ 1.43 (s, 9H, $3CH_3$); 1.63–1.67 (m, 2H, CH_2); 1.75–1.80 (m, 4H, $2CH_2$); 1.82-1.89 (m, 2H, CH_2); 2.44 (t, J = 7.2 Hz, 2H, CH_2); 2.63 (s, 3H, CH_3); 3.13–3.22 (m, 2H, CH_2); 3.37–3.41 (m, 4H, $2CH_2$); 4.64 (br, 1H, NH); 5.31 (s, 2H, CH_2); 7.33 (s, 1H, CH); 8.05 and 8.12 (AA′XX′, J = 8.5 Hz, 4H, CH_{Ar}). ^{13}C NMR ($CDCl_3$, 100 MHz): 24.2, 25.5 (2C), 26.7, 28.5 (3C), 31.6, 40.0, 51.2 (2C), 62.1, 79.4, 117.9, 118.0 (2C), 129.9 (2C), 133.9, 135.3, 142.5, 152.2, 155.7, 156.1, 158.9, 173.0, 197.0. FT-IR (neat) ν_{max} (cm^{-1}): 3359, 3322, 3280, 2979, 2931, 2896, 2852, 2821, 1740, 1699, 1676. HRMS (ESI-TOF) *m/z*: $[M+H]^+$ Calcd. for $C_{28}H_{36}N_6O_5S$+H 569.2541; Found 569.2555.

(2-(2-(4-Acetylphenyl)-5-(piperidin-1-yl)-2*H*-1,2,3-triazol-4-yl)thiazol-4-yl)methyl 5-((3a*R*,4*R*,6a*S*)-2-oxohexahydro-1*H*-thieno[3,4-*d*]imidazol-4-yl)pentanoate (1j). Yellow

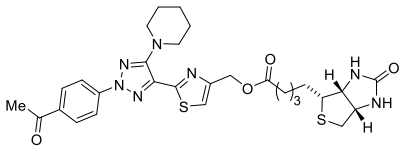

powder, yield 18% (Procedure 1); yield 74% (Procedure 2); mp = 96-98 °C. ^{1}H NMR ($CDCl_3$, 600 MHz): δ 1.42–1.49 (m, 2H, CH_2); 1.63–1.80 (m, 2H, CH_2) and (m, 6H, $3CH_2$) and (m, 4H, $2CH_2$); 2.42 (t, J = 7.4 Hz, 2H, CH_2); 2.63 (s, 3H, CH_3); 2.70 (d, J = 12.9 Hz, 1H, CH); 2.87 (dd, J = 12.9, 5.0 Hz, 1H, CH); 3.13 (q, J = 6.1 Hz, 1H, CH); 3.39 (t, J = 5.4 Hz, 4H, $2CH_2$); 4.29 (t, J = 6.1 Hz, 1H, CH); 4.47 (t, J = 6.1 Hz, 1H, CH); 5.15 (s, 1H, NH); 5.29 (s, 2H, CH_2); 5.70 (s, 1H, NH); 7.34 (s, 1H, CH); 8.05 and 8.12 (AA′XX′, J = 8.2 Hz, 4H, $4CH_{Ar}$). ^{13}C NMR ($CDCl_3$, 150 MHz): 24.21, 24.89, 25.45 (2C), 26.77, 28.37, 28.44, 33.91, 40.65, 51.18 (2C), 55.51, 60.19, 61.99, 62.03, 117.95 (2C), 118.03, 129.87 (2C), 133.90, 135.26, 142.48, 152.21, 155.67, 158.84, 163.47, 173.43, 197.04. FT-IR (KBr) ν_{max} (cm^{-1}): 3106, 2933, 2853, 1704, 1683. HRMS (ESI-TOF) *m/z*: $[M+H]^+$ Calcd. for $C_{29}H_{35}N_7O_4S_2$+H 610.2265; Found 610.2281.

(2-(2-(4-Acetylphenyl)-5-(piperidin-1-yl)-2*H*-1,2,3-triazol-4-yl)thiazol-4-yl)methyl (*S*)-3-(4-(bis(2-chloroethyl)amino)phenyl)-2-((*tert*-butoxycarbonyl)amino)propanoate (1k). Light yellow powder, yield 63% (Procedure 2); mp = 140-142 °C. ^{1}H NMR ($CDCl_3$, 400 MHz): δ 1.43 (s, 9H,

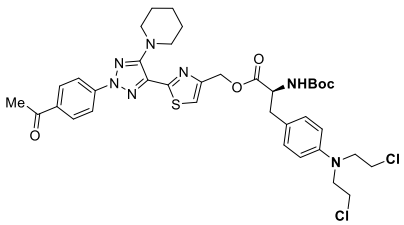

$3CH_3$); 1.62–1.68 (m, 2H, CH_2); 1.74–1.81 (m, 4H, $2CH_2$); 2.64 (s, 3H, CH_3); 2.99–3.07 (m, 2H, CH_2); 3.40 (t, J = 5.1 Hz, 4H, $2CH_2$); 3.56–3.61 (m, 4H, $2CH_2$); 3.63–3.69 (m, 4H, $2CH_2$); 4.55–4.66 (m, 1H, CH); 4.93–5.07 (m, 1H, CH); 5.35 (s, 2H, CH_2); 6.55 and 6.97 (AA′XX′, J = 8.5 Hz, 4H, CH_{Ar}); 7.25 (s, 1H, CH); 8.06 and 8.13 (AA′XX′, J = 8.8 Hz, 4H, CH_{Ar}). ^{13}C NMR ($CDCl_3$, 100 MHz): 24.2, 25.5 (2C), 26.8 (2C), 28.5 (3C), 37.3, 40.5, 51.2 (2C), 53.6 (2C), 54.7, 62.7, 80.1, 112.2 (2C), 118.0 (2C), 118.3, 124.8, 129.9 (2C), 130.8 (2C), 133.8, 135.3, 142.5, 145.3, 151.6, 155.3, 155.6, 158.9, 171.9, 197.0. FT-IR ν_{max} (cm^{-1}): 3100, 3009, 2975, 2939, 2927, 2876, 2850, 2825 2800, 1742, 1678. HRMS (ESI-TOF) *m/z*: $[M+H]^+$ Calcd. for $C_{37}H_{45}Cl_2N_7O_5S$+H 770.2658; Found 770.2663.

(2-(2-(4-Acetylphenyl)-5-morpholino-2*H*-1,2,3-triazol-4-yl)thiazol-4-yl)methyl (*tert*-butoxycarbonyl)glycinate (1l). White powder, yield 46% (Procedure 1); mp = 132-134 °C. ^{1}H

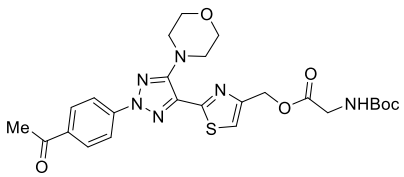

NMR ($CDCl_3$, 400 MHz): δ 1.45 (s, 9H, $3CH_3$); 2.64 (s, 3H, CH_3); 3.50–3.55 (m, 4H, $2CH_2$); 3.89–3.94 (m, 4H, $2CH_2$); 3.98 (d, J = 5.0 Hz, 2H, CH_2); 5.03 (br, 1H, NH); 5.35 (s, 2H, CH_2); 7.36 (s, 1H, CH); 8.06 and 8.12 (AA′XX′, J = 8.9 Hz, 4H, CH_{Ar}). ^{13}C NMR ($CDCl_3$, 100 MHz): 26.8, 28.4 (3C), 42.6, 50.1 (2C), 62.5, 66.6 (2C), 80.3, 118.1 (2C), 118.5 129.9 (2C), 133.6, 135.5, 142.3, 151.6, 154.6, 155.8, 159.0, 170.2, 196.9. FT-IR (neat) ν_{max} (cm^{-1}): 3106,

2998, 2967, 2921, 2897, 2863, 2827, 1765, 1718, 1675. HRMS (ESI-TOF) *m/z*: $[M+H]^+$ Calcd. for $C_{25}H_{30}N_6O_6S$+H 543.2020; Found 543.2034.

(2-(2-(4-Acetylphenyl)-5-morpholino-2*H*-1,2,3-triazol-4-yl)thiazol-4-yl)methyl 4-((*tert*-butoxycarbonyl)amino)butanoate (1m). Yellow powder, yield 31% (Procedure 1); yield 82% (Procedure 2); mp = 100-102 °C. ^{1}H NMR ($CDCl_3$, 400 MHz): δ 1.43 (s, 9H, $3CH_3$); 1.86 (quin, J = 7.2 Hz, 2H, CH_2); 2.44 (t, J = 7.2 Hz, 2H, CH_2); 2.64 (s, 3H, CH_3); 3.13–3.22 (m, 2H, CH_2); 3.53 (t, J = 4.3 Hz, 4H, $2CH_2$); 3.92 (t, J = 4.3 Hz, 4H, $2CH_2$); 4.63 (br, 1H, NH); 5.29 (s, 2H, CH_2); 7.34 (s, 1H, CH); 8.07 and 8.13 (AA′XX′, J = 8.6 Hz, 4H, CH_{Ar}). ^{13}C NMR ($CDCl_3$, 150 MHz): 25.5, 26.8, 28.5 (3C), 31.5, 40.0, 50.1 (2C), 62.0, 66.6 (2C), 79.4, 118.0 (2C), 129.9 (2C), 133.7, 135.5, 142.3, 152.2, 154.6, 156.1, 158.8, 173.0, 197.0. FT-IR (KBr) ν_{max} (cm^{-1}): 3145, 3054, 3010, 2979, 2861, 2770, 1735, 1710, 1680. HRMS (ESI-TOF) *m/z*: $[M+H]^+$ Calcd. for $C_{27}H_{34}N_6O_6S$+H 571.2333; Found 571.2347.

(2-(2-(4-Methoxyphenyl)-5-(piperidin-1-yl)-2*H*-1,2,3-triazol-4-yl)thiazol-4-yl)methyl 4-methoxybenzoate (1n). Light yellow powder, yield 90% (Procedure 2); mp = 46-48 °C. ^{1}H NMR ($CDCl_3$, 400 MHz): δ 1.60–1.67 (m, 2H, CH_2); 1.76–1.83 (m, 4H, $2CH_2$); 3.40 (t, 4H, $2CH_2$, J = 4.9 Hz); 3.85 (s, 3H, CH_3); 3.86 (s, 3H, CH_3); 5.53 (s, 2H, CH_2); 6.92 and 8.06 (AA′XX′, J = 8.8 Hz, 4H, CH_{Ar}); 6.97 and 7.97 (AA′XX′, J = 9.0 Hz, 4H, CH_{Ar}); 7.35 (s, 1H, CH). ^{13}C NMR ($CDCl_3$, 100 MHz): 24.1, 25.3 (2C), 51.7 (2C), 55.6, 55.7, 62.3, 113.8 (2C), 114.4 (2C), 117.2, 120.0 (2C), 122.5, 132.0 (2C), 132.6, 133.4, 152.4, 152.2, 159.1, 163.7, 166.1. FT-IR (KBr) ν_{max} (cm^{-1}): 3085, 3074, 3010, 2939, 2925, 2836, 2818, 2764, 1721. HRMS (ESI-TOF) *m/z*: $[M+H]^+$ Calcd. for $C_{26}H_{27}N_5O_4S$+H 506.1862; Found 506.1873.

(2-(2-(4-Methoxyphenyl)-5-(piperidin-1-yl)-2*H*-1,2,3-triazol-4-yl)thiazol-4-yl)methyl 4-nitrobenzoate (1o). Orange powder, yield 88% (Procedure 1); mp = 116-118 °C. ^{1}H NMR ($CDCl_3$, 400 MHz): δ 1.60 – 1.66 (m. 2H, CH_2); 1.72 – 1.78 (m, 4H, $2CH_2$); 3.36 (t, J = 5.4 Hz, 4H, $2CH_2$); 3.85 (s, 3H, CH_3); 5.58 (s, 2H, CH_2); 6.97 and 7.96 (AA′XX′, J = 9.1 Hz, 4H, $4CH_{Ar}$); 8.26 and 8.29 (AA′XX′, J = 9.2 Hz, 4H, $4CH_{Ar}$). ^{13}C NMR ($CDCl_3$, 100 MHz): 24.3, 25.6 (2C), 51.4 (2C), 55.7, 63.2, 114.4 (2C), 118.2, 120.0 (2C), 123.7 (2C), 131.1 (2C), 132.2, 133.5, 135.5, 150.8, 151.1, 155.1, 158.9, 159.8, 164.5. FT-IR (KBr) ν_{max} (cm^{-1}): 3146, 3108, 3077, 3055, 3004, 2927, 2839, 2758, 1730. HRMS (ESI-TOF) *m/z*: $[M+H]^+$ Calcd. for $C_{25}H_{24}N_6O_5S$+H 521.1607; Found 521.1610.

(2-(2-(4-Bromophenyl)-5-(piperidin-1-yl)-2*H*-1,2,3-triazol-4-yl)thiazol-4-yl)methyl 4-methoxybenzoate (1p). White powder, yield 78% (Procedure 2); mp = 112-114 °C. ^{1}H NMR

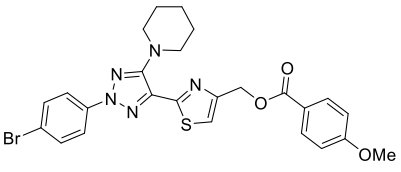

($CDCl_3$, 400 MHz): δ 1.61–1.66 (m. 2H, CH_2); 1.72–1.79 (m, 4H, $2CH_2$); 3.37 (t, J = 5.4 Hz, 4H, $2CH_2$); 3.87 (s, 3H, CH_3); 5.53 (s, 2H, CH_2); 6.93 and 7.93 (AA′XX′, J = 8.9 Hz, 4H, CH_{Ar}); 7.37 (s, 1H, CH); 7.57 and 8.06 (AA′XX′, J = 8.9 Hz, 4H, CH_{Ar}). ^{13}C NMR ($CDCl_3$, 100 MHz): 24.2, 25.5 (2C), 51.2 (2C), 55.6, 62.3, 113.8 (2C), 117.5, 119.8 (2C), 120.4, 122.4, 132.0 (2C), 132.3 (2C), 133.2, 138.5, 152.5, 155.4, 158.9, 163.7, 166.1. FT-IR (KBr) ν_{max} (cm^{-1}): 3124, 3010, 2918, 2854, 2818, 2768, 1710. HRMS (ESI-TOF) *m/z*: $[M+H]^+$ Calcd. for $C_{25}H_{24}N_5O_3S$+H 554.0861; Found 554.0868.

(2-(2-(4-Acetylphenyl)-5-(piperidin-1-yl)-2*H*-1,2,3-triazol-4-yl)thiazol-4-yl)methyl 4-methoxybenzoate (1q). Light yellow powder, yield 83% (Procedure 2); mp = 140-142 °C. ^{1}H NMR

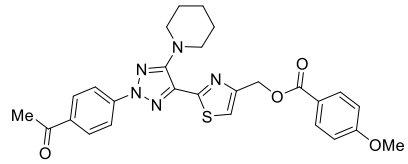

($CDCl_3$, 400 MHz): δ 1.59-1.67 (m, 2H, CH_2); 1.76 (quin, J = 5.4 Hz, 4H, $2CH_2$); 2.63 (s, 3H, CH_3); 3.40 (t, J = 5.4 Hz, 4H, $2CH_2$); 3.86 (s, 3H, CH_3); 5.53 (s, 2H, CH_2); 6.93 (d, J = 8.7 Hz, 2H, CH_{Ar}); 7.40 (s, 1H, CH); 8.02 – 8.08 (m, 4H, CH_{Ar}); 8.10 – 8.15 (m, 2H, CH_{Ar}). ^{13}C NMR ($CDCl_3$, 100 MHz): 24.2, 25.5 (2C), 26.7, 51.2 (2C), 55.6, 62.3, 113.8 (2C), 117.7, 118.0 (2C), 122.4, 129.9 (2C), 132.0 (2C), 134.0, 135.2, 142.5, 152.6, 155.7, 158.8, 163.7, 166.1, 197.0. FT-IR (KBr) ν_{max} (cm^{-1}): 3102, 3057, 3023, 3014, 2989, 2937, 2855, 2828, 2767, 1709, 1678. HRMS (ESI-TOF) *m/z*: $[M+H]^+$ Calcd. for $C_{27}H_{27}N_5O_4S$+H 518.1857; Found 518.1864.

Procedure for the synthesis of compound 7c:

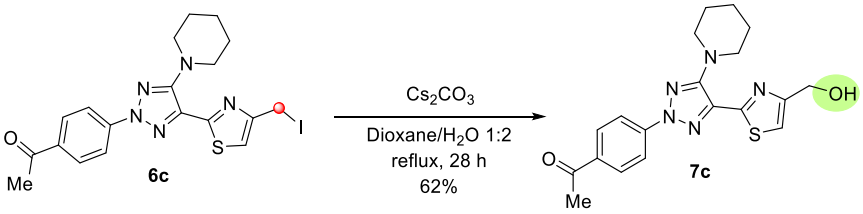

Scheme S6.

Procedure 1: A mixture of 4-(iodomethyl)thiazole **6c** (0.3 mmol), 10 ml of 1,4-dioxane, 20 ml of H_2O, and 0.147 g (0.45 mmol) of Cs_2CO_3 was refluxed until the reaction was complete. The resulting mixture was poured onto crushed ice (100 g). The aqueous mixture was then acidified with 0.1 M HCl to pH 7. The product was extracted with ethyl acetate (3 × 30 ml). The combined organic extracts were dried over anhydrous Na_2SO_4, and the solvent was evaporated under reduced pressure. The crude product was purified by column chromatography using a mixture of chloroform and ethanol (4:1, v/v) as the eluent.

Procedure for the synthesis of compounds 7a,b:

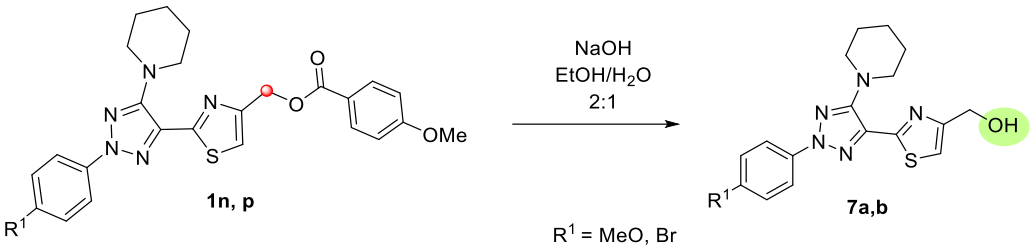

Scheme S7.

Procedure 2: A mixture of hybrids **1n, p** (0.3 mmol), 15 ml of ethanol, 7.5 ml of water, and 120 mg (2.0 mmol) of NaOH was refluxed until the reaction was complete. The resulting mixture was poured onto crushed ice (100 g). The aqueous mixture was then acidified with 0.1 M HCl to pH 7. The product was extracted with ethyl acetate (3 × 30 ml). The combined organic extracts were dried over anhydrous Na_2SO_4, and the solvent was evaporated under reduced pressure. The crude product was purified by column chromatography using a mixture of chloroform and ethanol (4:1 v/v) as the eluent.

(2-(2-(4-Methoxyphenyl)-5-(piperidin-1-yl)-2*H*-1,2,3-triazol-4-yl)thiazol-4-yl)methanol (7a).

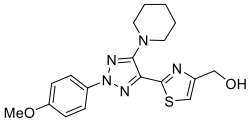

Procedure 2. Light yellow powder, yield 75%; mp = 100-102 °C. ^{1}H NMR ($CDCl_3$, 400 MHz): δ 1.61-1.67 (m, 2H, CH_2); 1.77 (quin, J = 5.4 Hz, 4H, $2CH_2$); 2.44 (br, 1H, OH); 3.34 (t, J = 5.4 Hz, 4H, $2CH_2$); 3.85 (s, 3H, CH_3); 4.84 (s, 2H, CH_2); 6.96 and 7.96 (AA′XX′, J = 9.2 Hz, 4H, CH_{Ar}); 7.19 (s, 1H, CH). ^{13}C NMR ($CDCl_3$, 100 MHz): 24.3, 25.6 (2C), 51.5 (2C), 55.7, 61.5, 114.4 (2C), 119.9 (2C), 132.4, 133.5, 155.1, 157.0, 158.9, 159.3. FT-IR (KBr) ν_{max} (cm^{-1}): 3108, 3077, 3001, 2961, 2932, 2857, 2833, 2763, 2360, 2342, 2036, 1884. HRMS (ESI-TOF) *m/z*: $[M+H]^+$ Calcd. for $C_{18}H_{21}N_5O_2S$+H 372.1489; Found 372.1493.

(2-(2-(4-Bromophenyl)-5-(piperidin-1-yl)-2*H*-1,2,3-triazol-4-yl)thiazol-4-yl)methanol (7b).

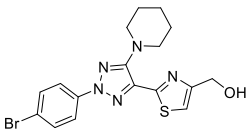

Procedure 2. Yellow-brown oil, yield 88%. ^{1}H NMR ($CDCl_3$, 400 MHz): δ 1.62–1.68 (m, 2H, CH_2); 1.74–1.80 (4H, $2CH_2$); 2.36 (br, 1H, NH); 3.35 (t, 4H, $2CH_2$, J = 5.4 Hz); 4.85 (s, 2H, CH_2); 7.22 (s, 1H, CH); 7.57 and 7.92 (AA′XX′, J = 9.0 Hz, 4H, CH_{Ar}). ^{13}C NMR ($CDCl_3$, 100 MHz): 24.2, 25.5 (2C), 51.3 (2C), 61.4, 114.8, 119.9 (2C), 120.5, 132.4 (2C), 133.3, 138.6, 155.4, 157.1, 159.0. FT-IR (KBr) ν_{max} (cm^{-1}): 3099, 2995, 2968, 2935, 2917, 2850. HRMS (ESI-TOF) *m/z*: $[M+H]^+$ Calcd. for $C_{17}H_{18}BrN_5OS$+H 420.0494; Found 420.0488.

1-(4-(4-(4-(Hydroxymethyl)thiazol-2-yl)-5-(piperidin-1-yl)-2*H*-1,2,3-triazol-2-yl)phenyl)ethan-1-one (7c). Procedure 1. Yellow powder, yield 62%; mp = 168-170 °C. ^{1}H NMR ($CDCl_3$, 400 MHz):

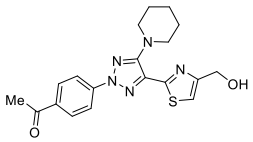

δ 1.62–1.67 (m, 2H, CH_2); 1.74–1.81 (m, 4H, $2CH_2$); 2.44 (t, J = 6.1 Hz, 1H, OH); 2.63 (s, 3H, CH_3); 3.38 (t, J = 4.8 Hz, 4H, $2CH_2$); 4.86 (d, J = 6.1 Hz, 2H, CH_2); 7.25 (s, 1H, CH); 8.05 and 8.12 (AA′XX′, J = 8.6 Hz, 4H, CH_{Ar}). ^{13}C NMR ($CDCl_3$, 100 MHz): 24.2, 25.5 (2C), 26.7, 51.2 (2C), 61.4, 115.1, 118.0 (2C), 129.8 (2C), 134.0, 135.2, 142.5, 155.7, 158.8, 197.0. FT-IR (KBr) ν_{max} (cm^{-1}): 3099, 2995, 2968, 2935, 2917, 2850. HRMS (ESI-TOF) *m/z*: $[M+H]^+$ Calcd. for $C_{19}H_{21}N_5O_2S$+H 384.1489; Found 384.1502.

2. NMR ^{1}H and ^{13}C spectra of compounds

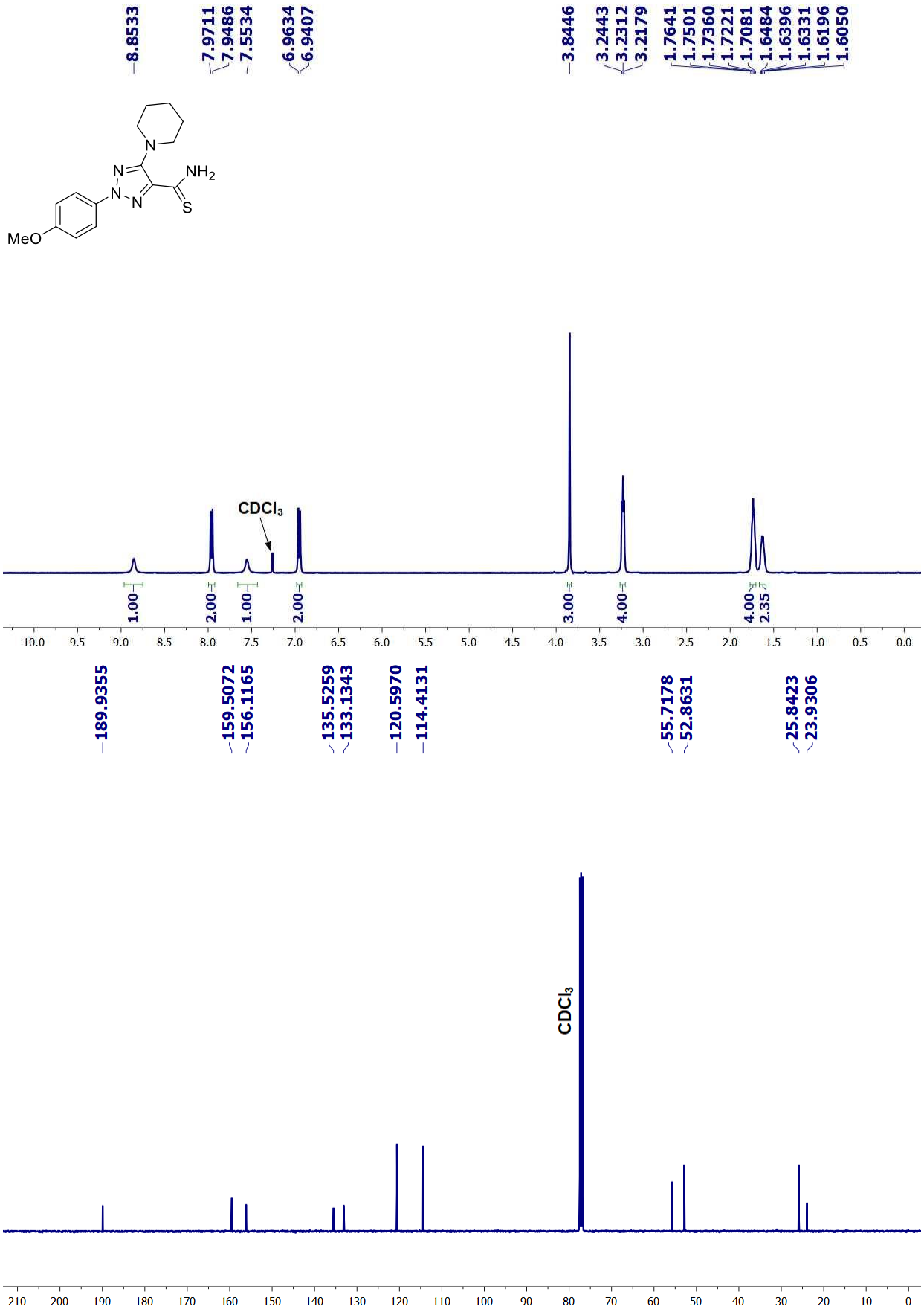

Fig. S1. ^{1}H NMR (400 MHz, $CDCl_3$, TMS) and ^{13}C NMR (100 MHz, $CDCl_3$) spectra of 2-(4-methoxyphenyl)-5-(piperidin-1-yl)-2*H*-1,2,3-triazole-4-carbothioamide (**8a**).

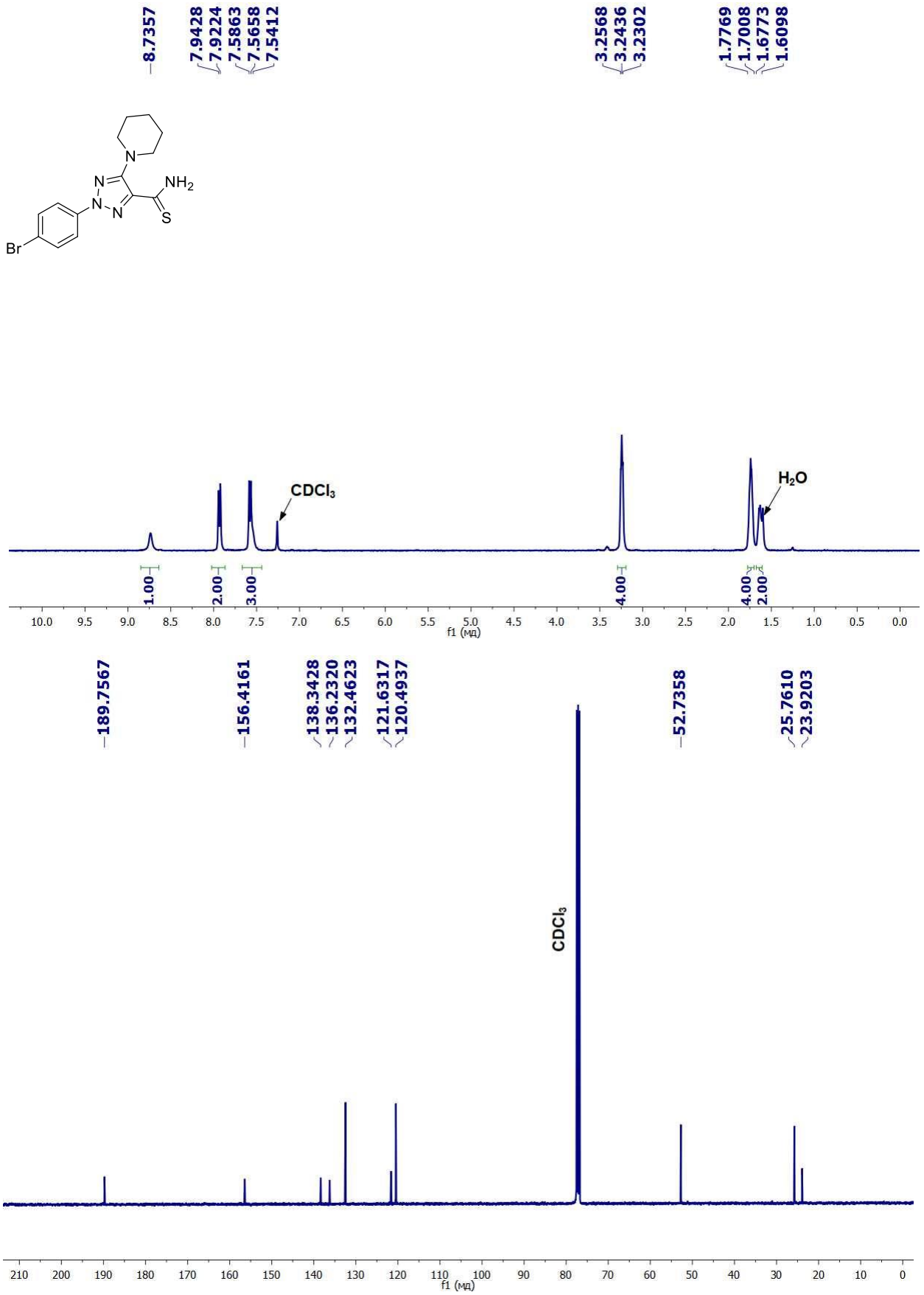

Fig. S2. ^{1}H NMR (400 MHz, $CDCl_3$, TMS) and ^{13}C NMR (100 MHz, $CDCl_3$) spectra of 2-(4-acetylphenyl)-5-morpholino-2*H*-1,2,3-triazole-4-carbothioamide (**8b**).

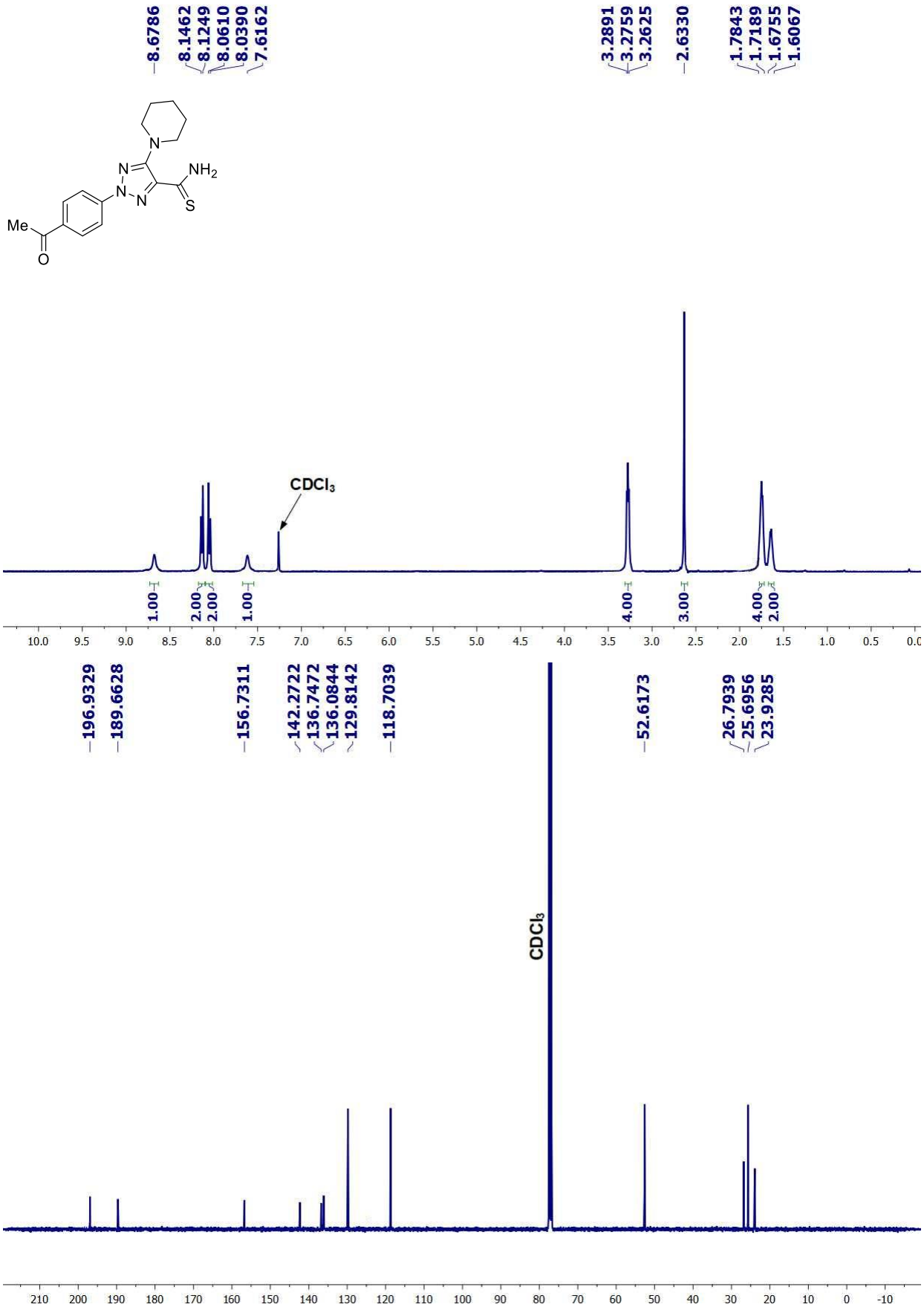

Fig. S3. ^{1}H NMR (400 MHz, $CDCl_3$, TMS) and ^{13}C NMR (100 MHz, $CDCl_3$) spectra of 2-(4-acetylphenyl)-5-(piperidin-1-yl)-2*H*-1,2,3-triazole-4-carbothioamide (**8c**).

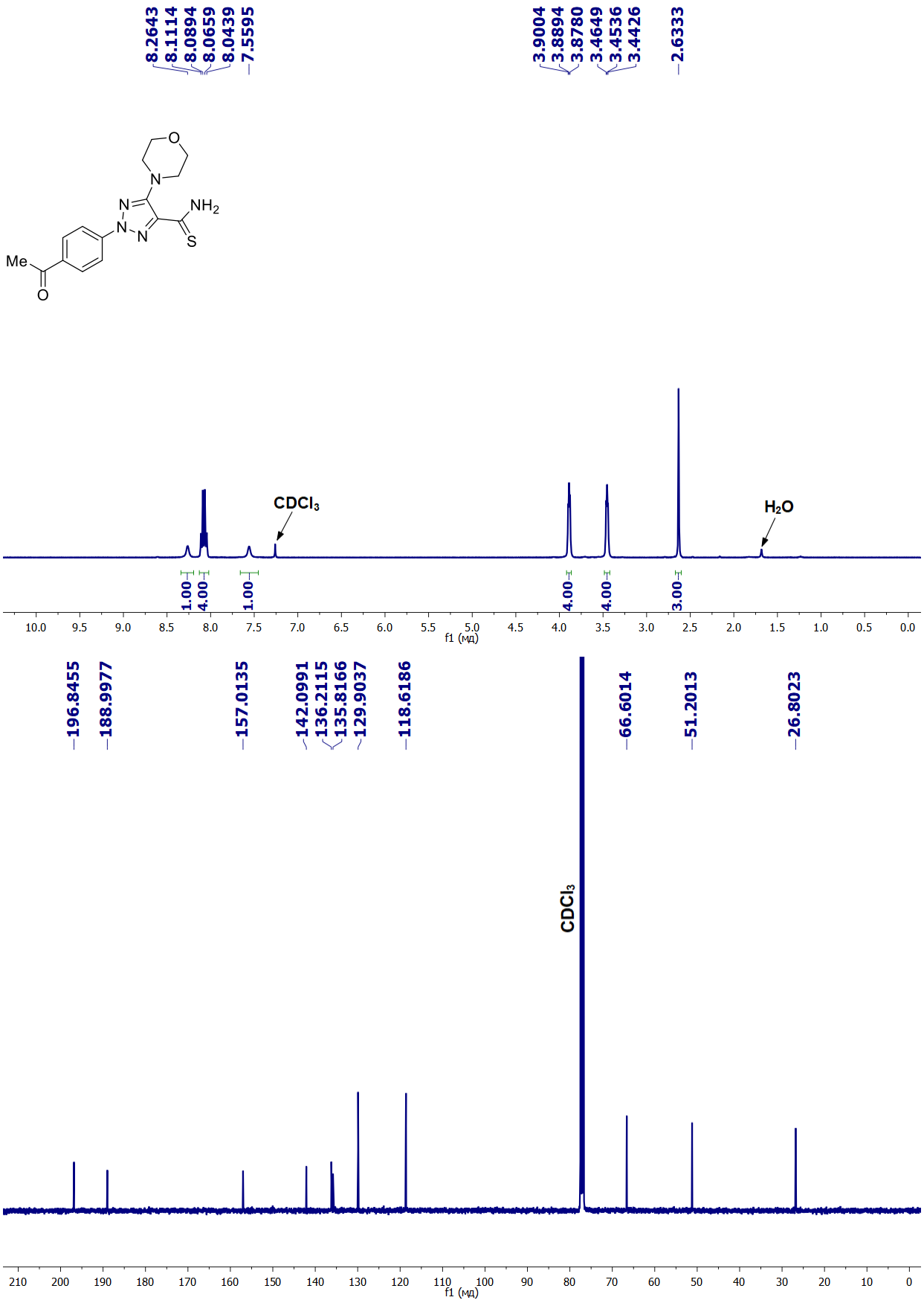

Fig. S4. ^{1}H NMR (400 MHz, $CDCl_3$, TMS) and ^{13}C NMR (100 MHz, $CDCl_3$) spectra of 2-(4-acetylphenyl)-5-morpholino-2*H*-1,2,3-triazole-4-carbothioamide (**8d**).

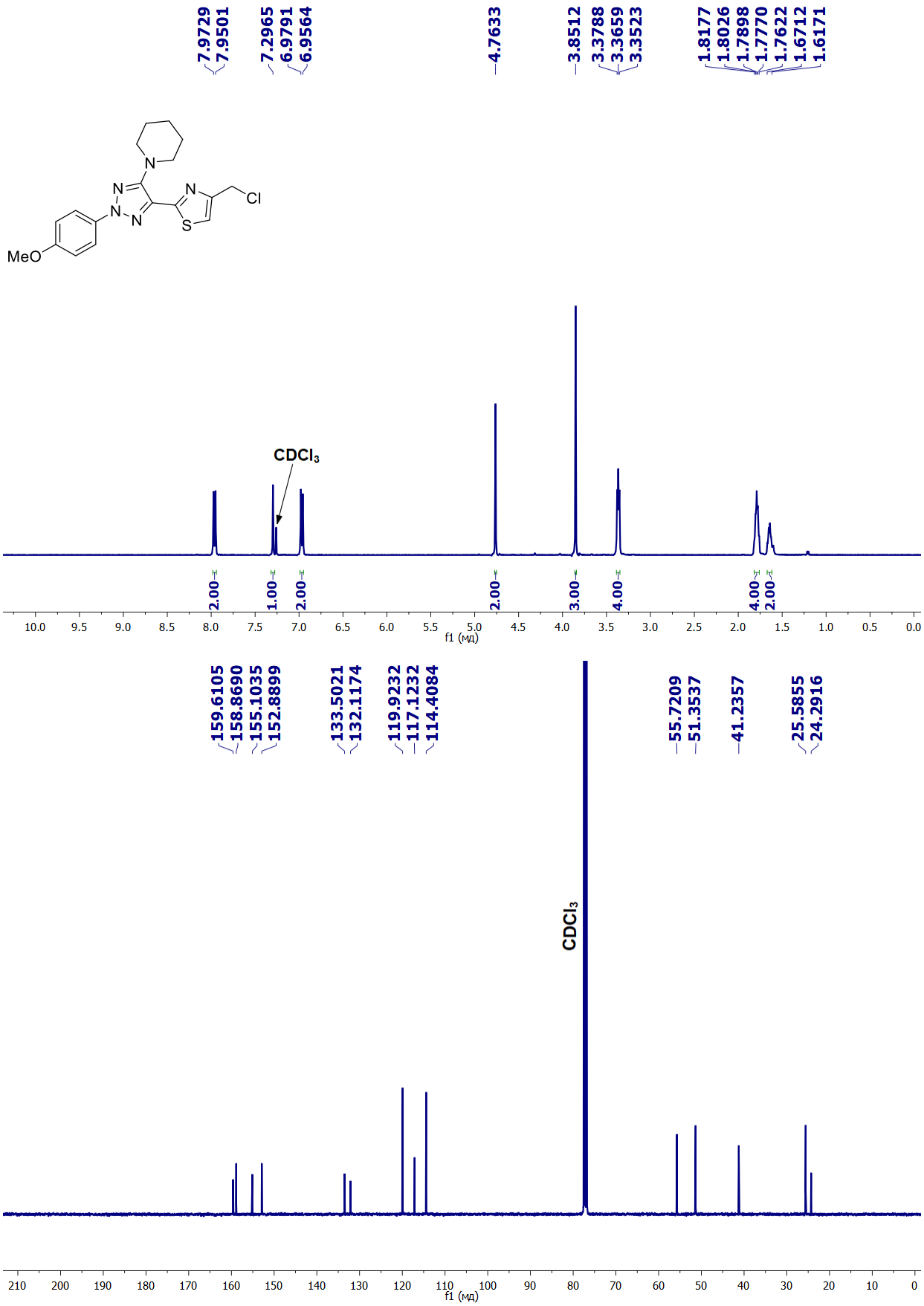

Fig. S5. ^{1}H NMR (400 MHz, $CDCl_3$, TMS) and ^{13}C NMR (100 MHz, $CDCl_3$) spectra of 4-(chloromethyl)-2-(2-(4-methoxyphenyl)-5-(piperidin-1-yl)-2*H*-1,2,3-triazol-4-yl)thiazole (**3a**).

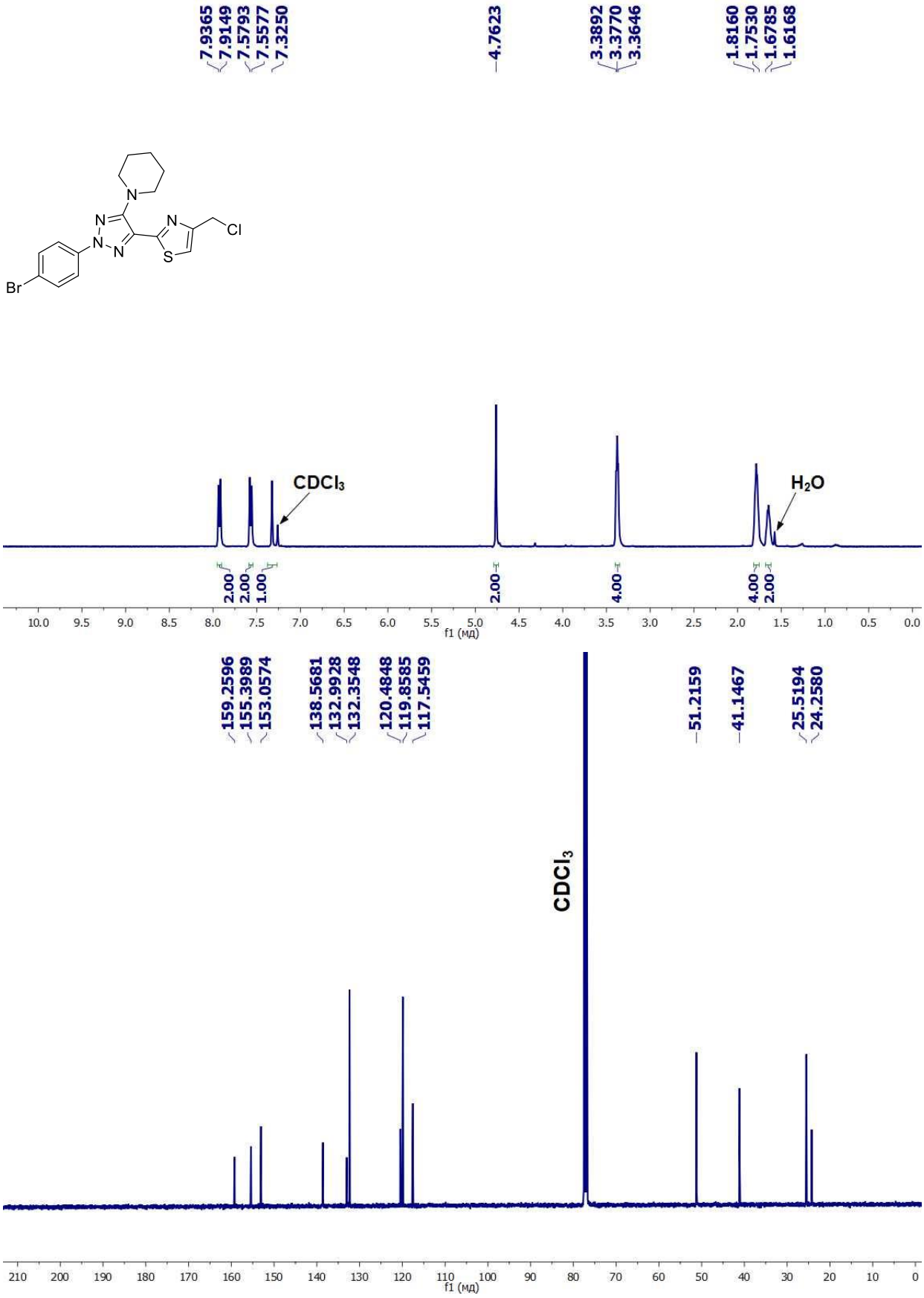

Fig. S6. ^{1}H NMR (400 MHz, $CDCl_3$, TMS) and ^{13}C NMR (100 MHz, $CDCl_3$) spectra of 2-(2-(4-bromophenyl)-5-(piperidin-1-yl)-2*H*-1,2,3-triazol-4-yl)-4-(chloromethyl)thiazole (**3b**).

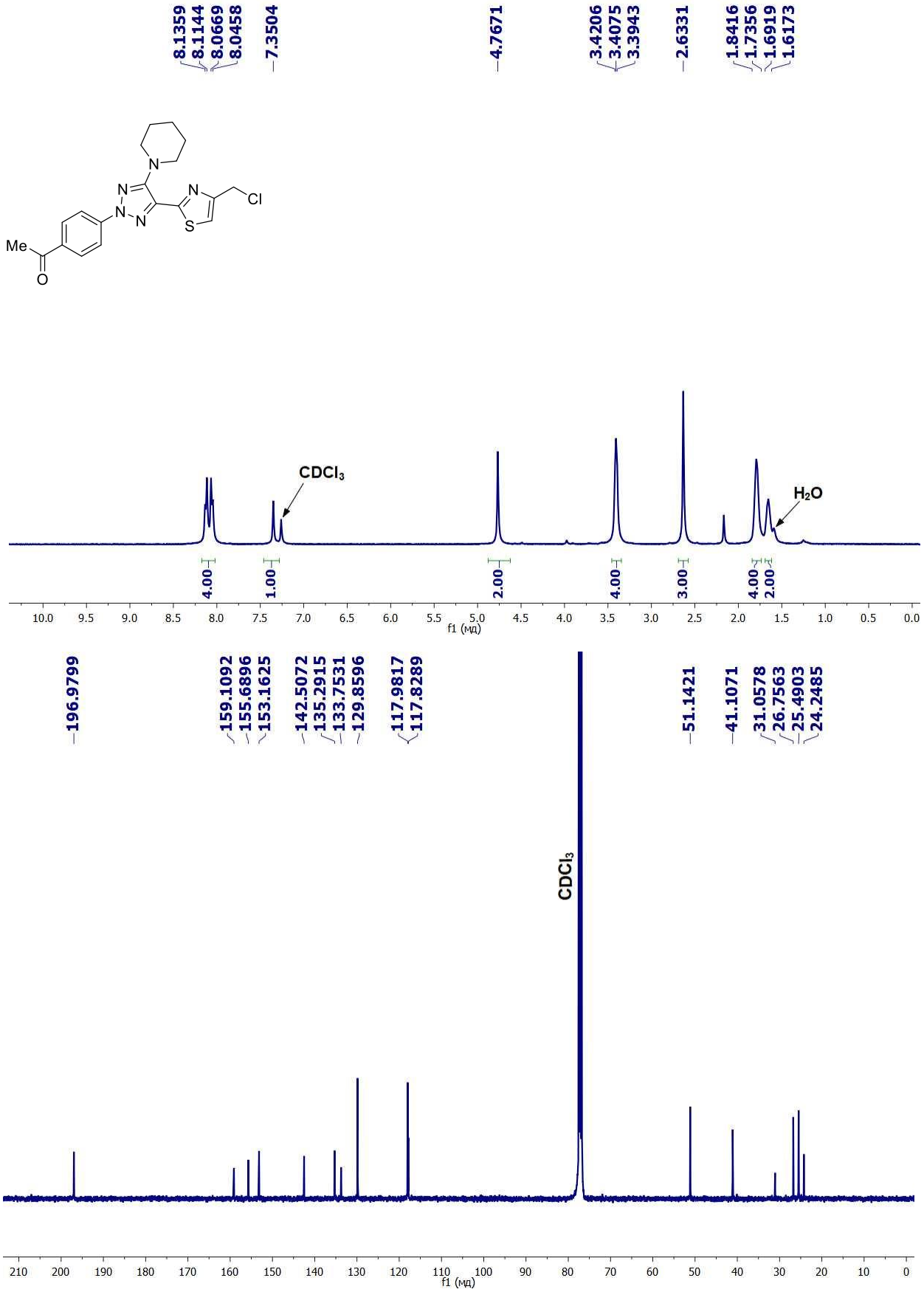

Fig. S7. ^{1}H NMR (400 MHz, $CDCl_3$, TMS) and ^{13}C NMR (100 MHz, $CDCl_3$) spectra of 1-(4-(4-(4-(chloromethyl)thiazol-2-yl)-5-(piperidin-1-yl)-2*H*-1,2,3-triazol-2-yl)phenyl)ethan-1-one (**3c**).

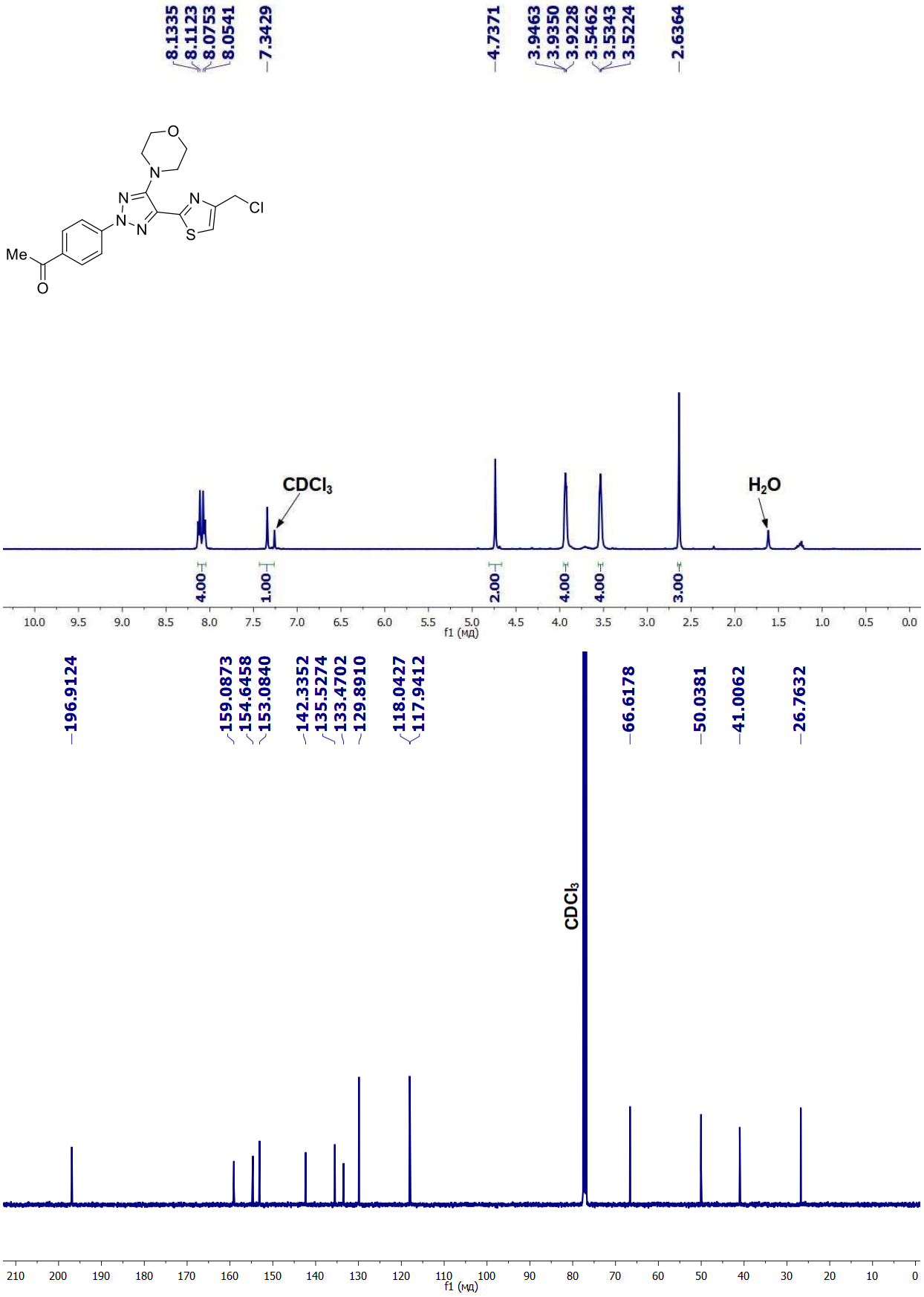

Fig. S8. ^{1}H NMR (400 MHz, $CDCl_3$, TMS) and ^{13}C NMR (100 MHz, $CDCl_3$) spectra of 1-(4-(4-(4-(chloromethyl)thiazol-2-yl)-5-morpholino-2*H*-1,2,3-triazol-2-yl)phenyl)ethan-1-one (**3d**).

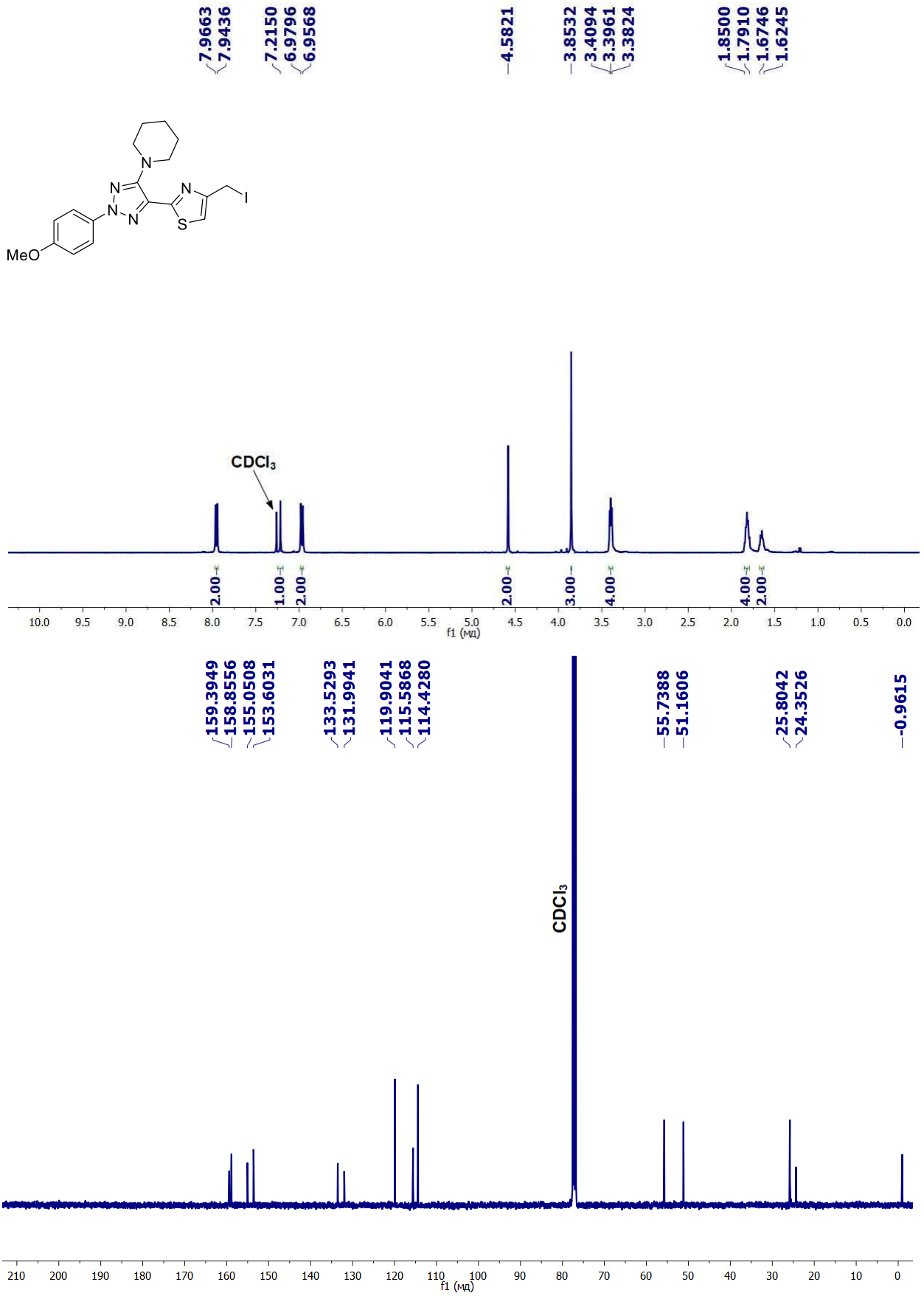

Fig. S9. ^{1}H NMR (400 MHz, $CDCl_3$, TMS) and ^{13}C NMR (100 MHz, $CDCl_3$) spectra of 4-(iodomethyl)-2-(2-(4-methoxyphenyl)-5-(piperidin-1-yl)-2*H*-1,2,3-triazol-4-yl)thiazole (**6a**).

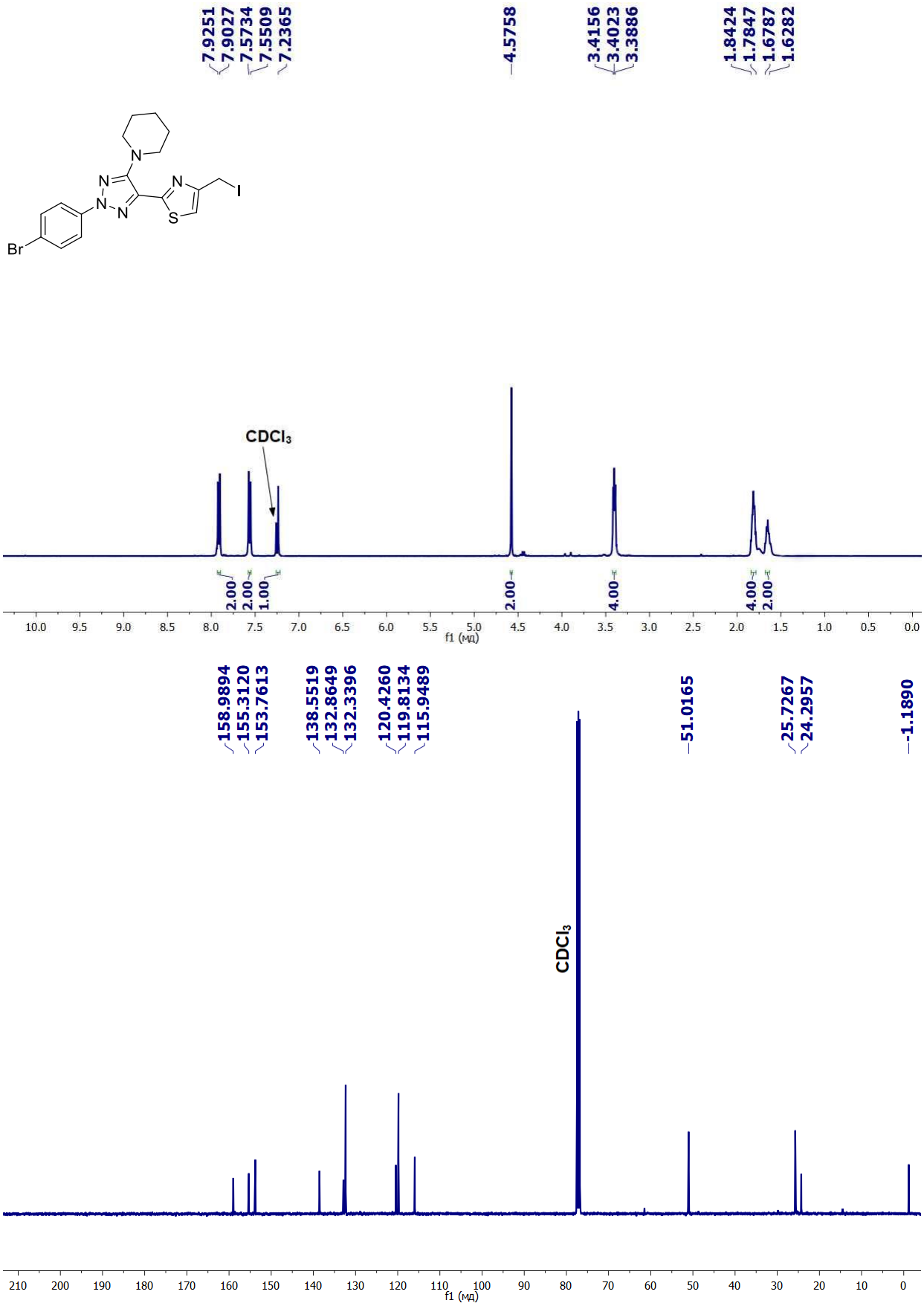

Fig. S10. ^{1}H NMR (400 MHz, $CDCl_3$, TMS) and ^{13}C NMR (100 MHz, $CDCl_3$) spectra of 2-(2-(4-bromophenyl)-5-(piperidin-1-yl)-2*H*-1,2,3-triazol-4-yl)-4-(iodomethyl)thiazole (**6b**).

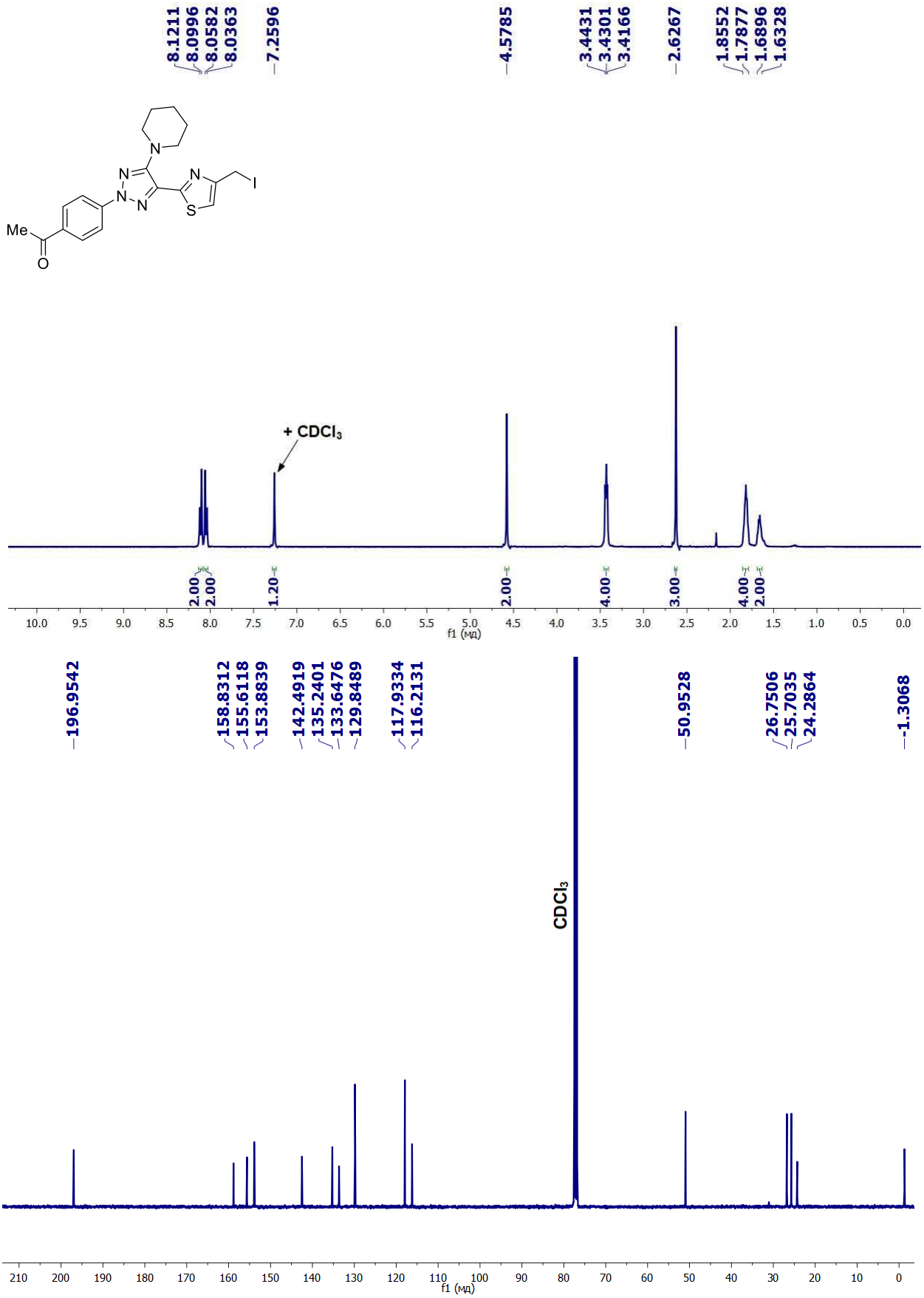

Fig. S11. ^{1}H NMR (400 MHz, $CDCl_3$, TMS) and ^{13}C NMR (100 MHz, $CDCl_3$) spectra of 1-(4-(4-(4-(iodomethyl)thiazol-2-yl)-5-(piperidin-1-yl)-2*H*-1,2,3-triazol-2-yl)phenyl)ethan-1-one (**6c**).

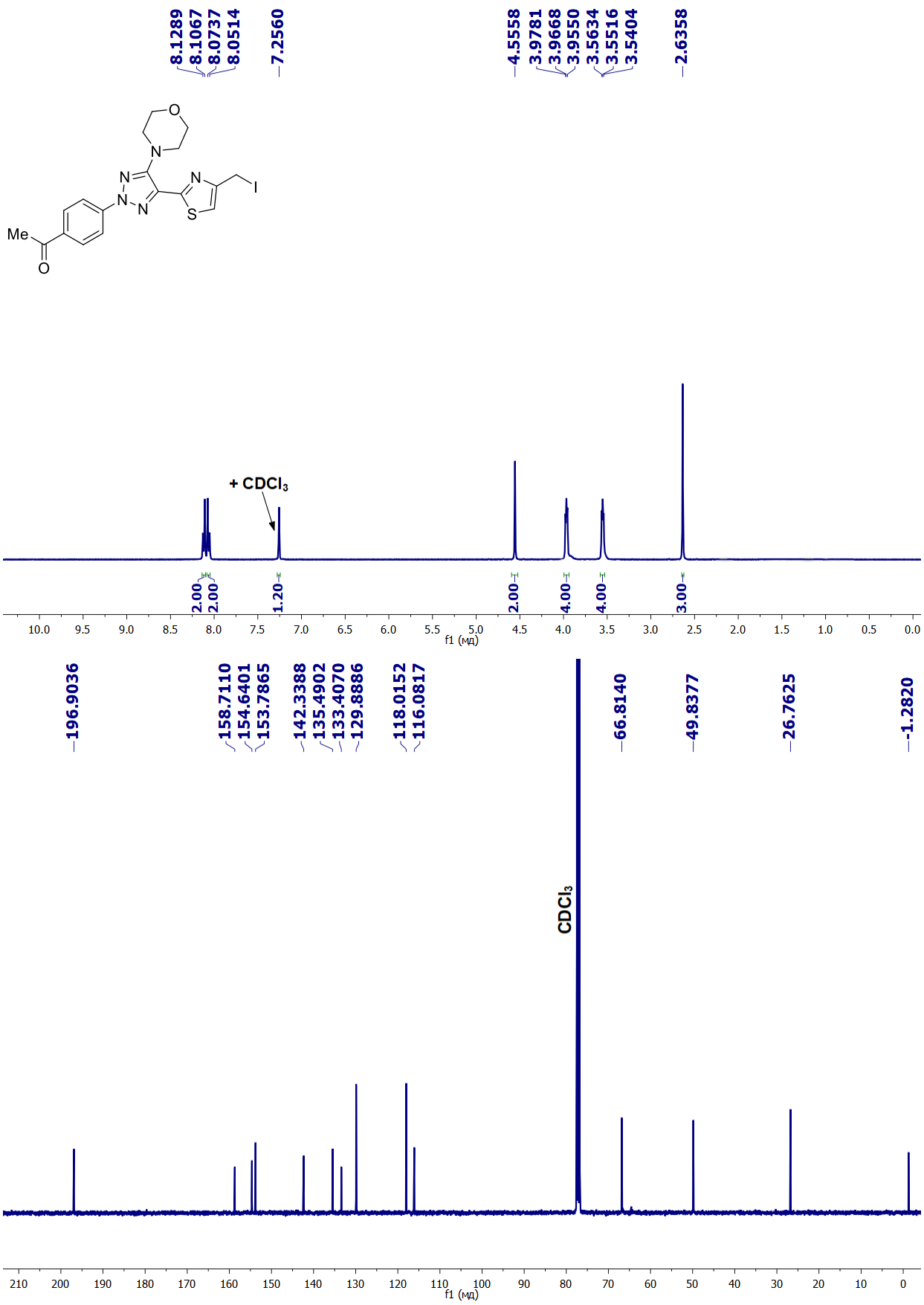

Fig. S12. ^{1}H NMR (400 MHz, $CDCl_3$, TMS) and ^{13}C NMR (100 MHz, $CDCl_3$) spectra of 1-(4-(4-(4-(iodomethyl)thiazol-2-yl)-5-morpholino-2*H*-1,2,3-triazol-2-yl)phenyl)ethan-1-one (**6d**).

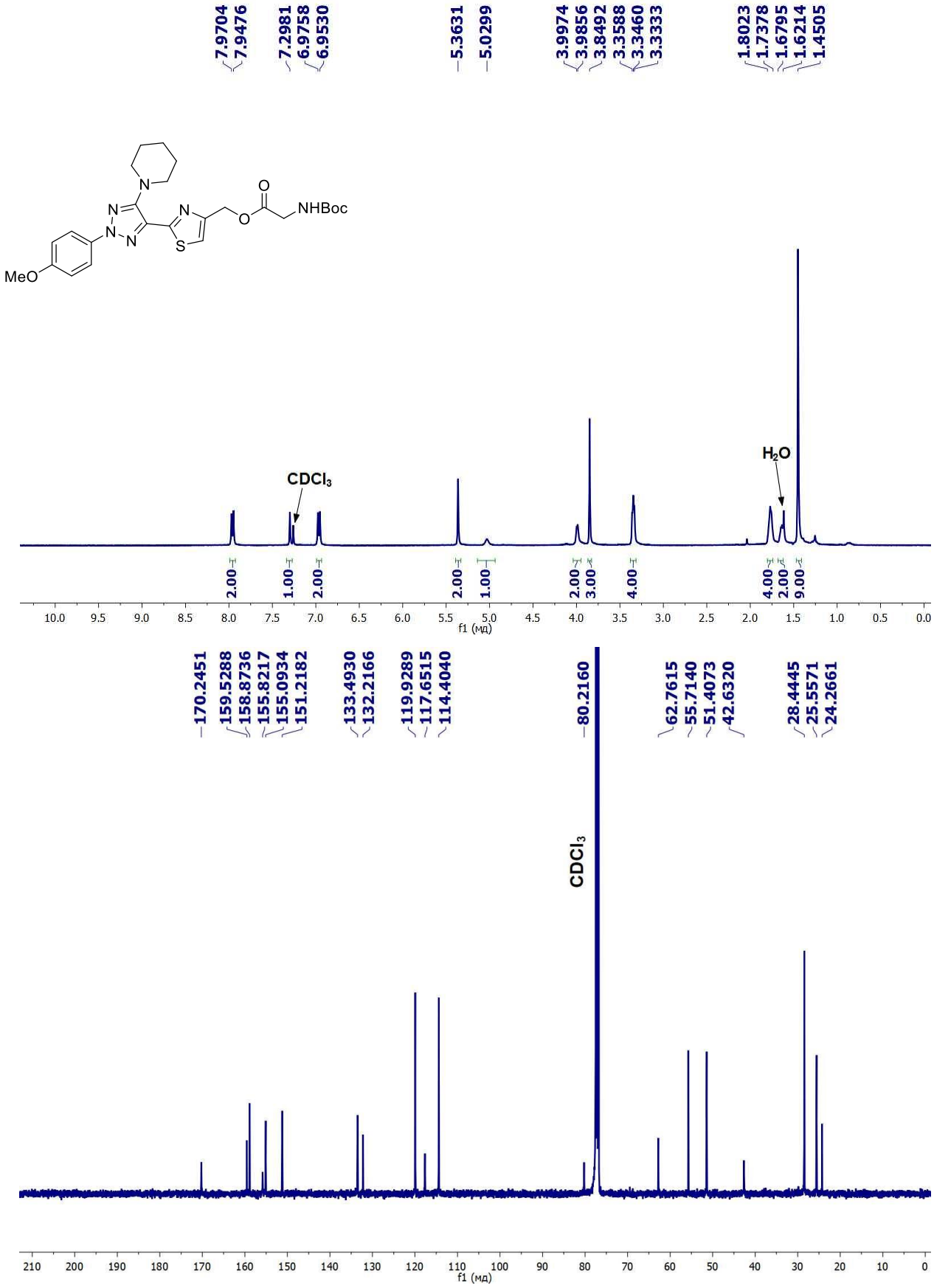

Fig. S13. ^{1}H NMR (400 MHz, $CDCl_3$, TMS) and ^{13}C NMR (100 MHz, $CDCl_3$) spectra of (2-(2-(4-methoxyphenyl)-5-(piperidin-1-yl)-2*H*-1,2,3-triazol-4-yl)thiazol-4-yl)methyl (*tert*-butoxycarbonyl)glycinate (**1a**).

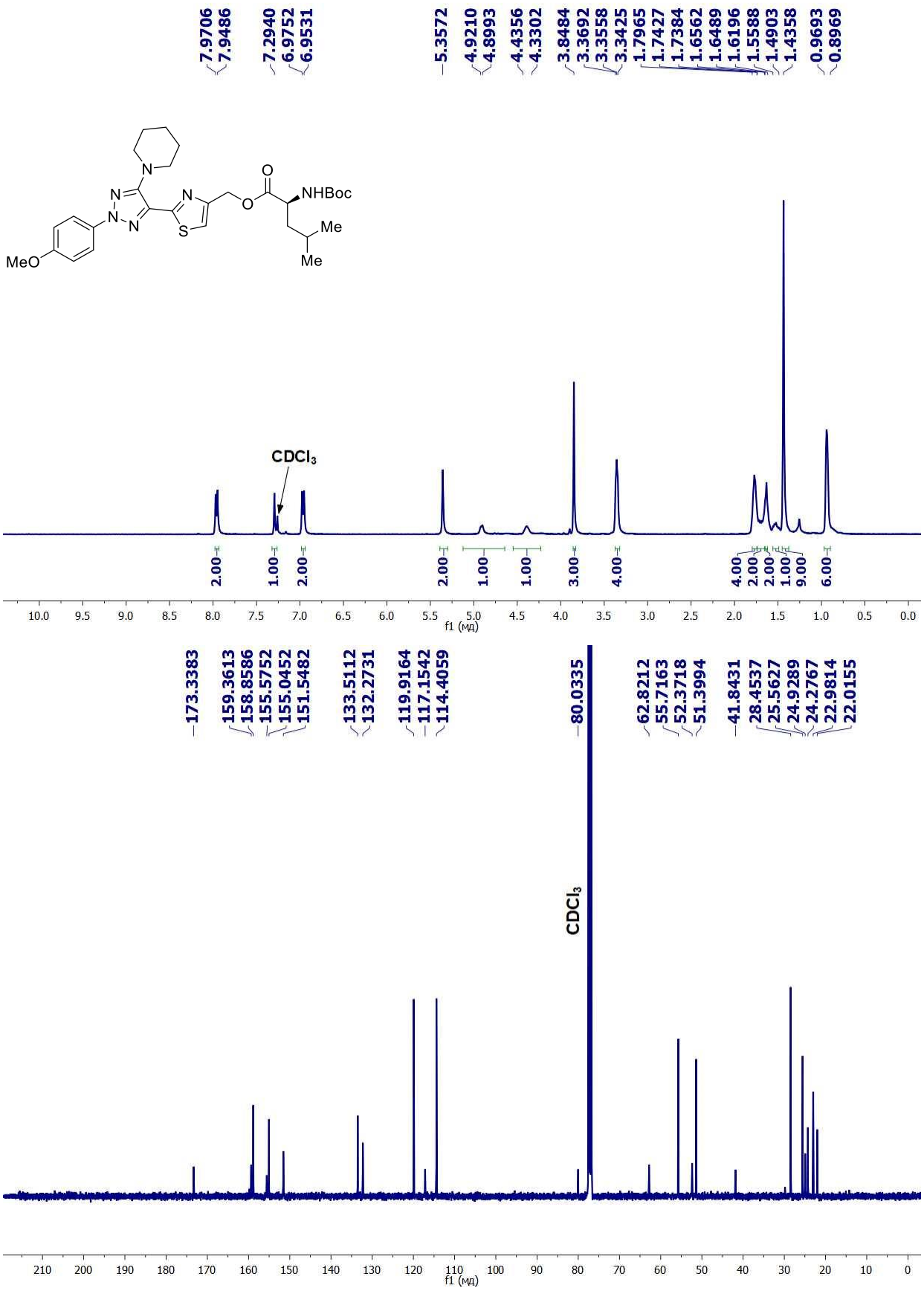

Fig. S14. ^{1}H NMR (400 MHz, $CDCl_3$, TMS) and ^{13}C NMR (100 MHz, $CDCl_3$) spectra of (2-(2-(4-methoxyphenyl)-5-(piperidin-1-yl)-2*H*-1,2,3-triazol-4-yl)thiazol-4-yl)methyl (*tert*-butoxycarbonyl)-*L*-leucinate (**1b**).

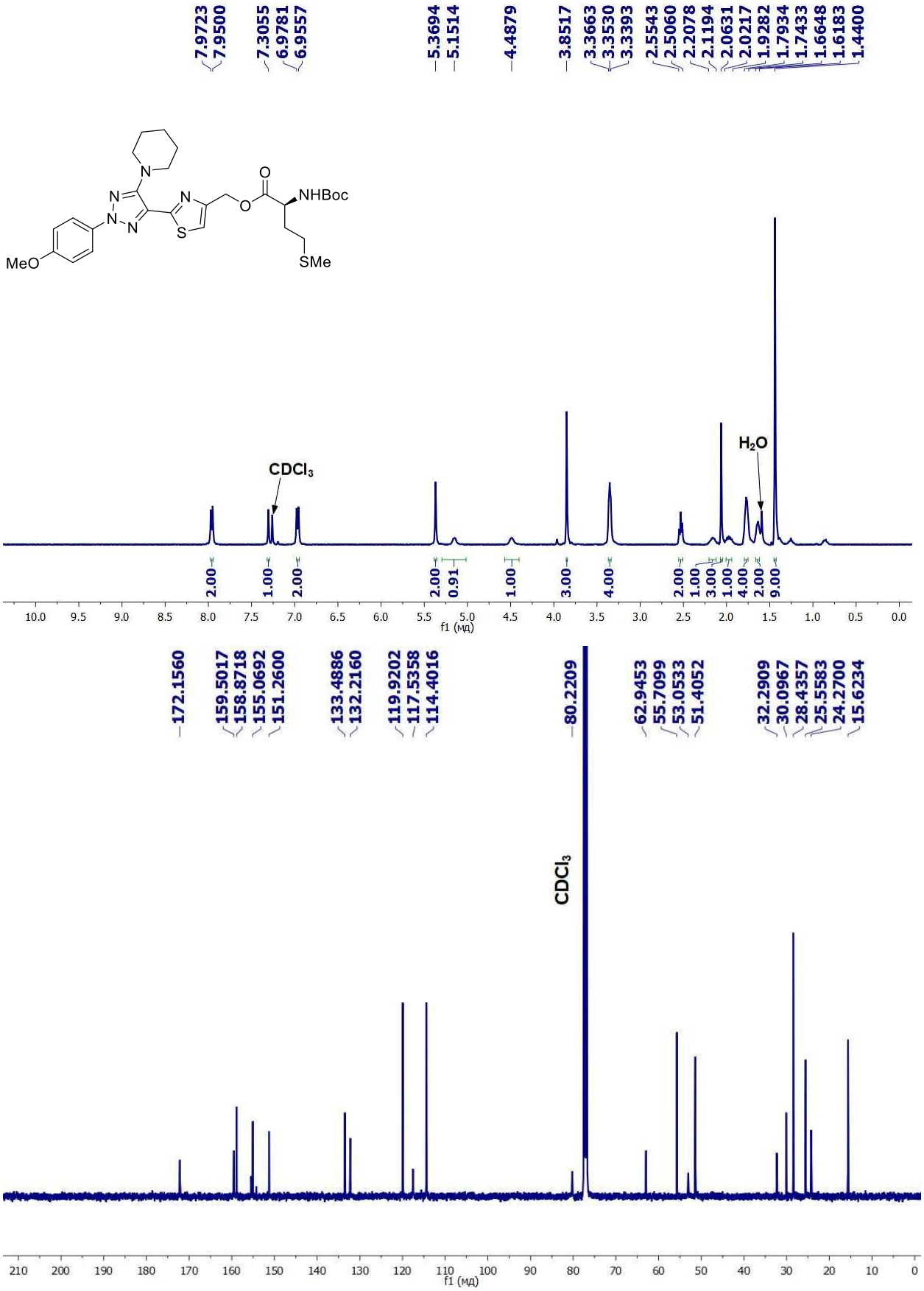

Fig. S15. ^{1}H NMR (400 MHz, $CDCl_3$, TMS) and ^{13}C NMR (100 MHz, $CDCl_3$) spectra of (2-(2-(4-methoxyphenyl)-5-(piperidin-1-yl)-2*H*-1,2,3-triazol-4-yl)thiazol-4-yl)methyl (*tert*-butoxycarbonyl)-*L*-methioninate (**1c**).

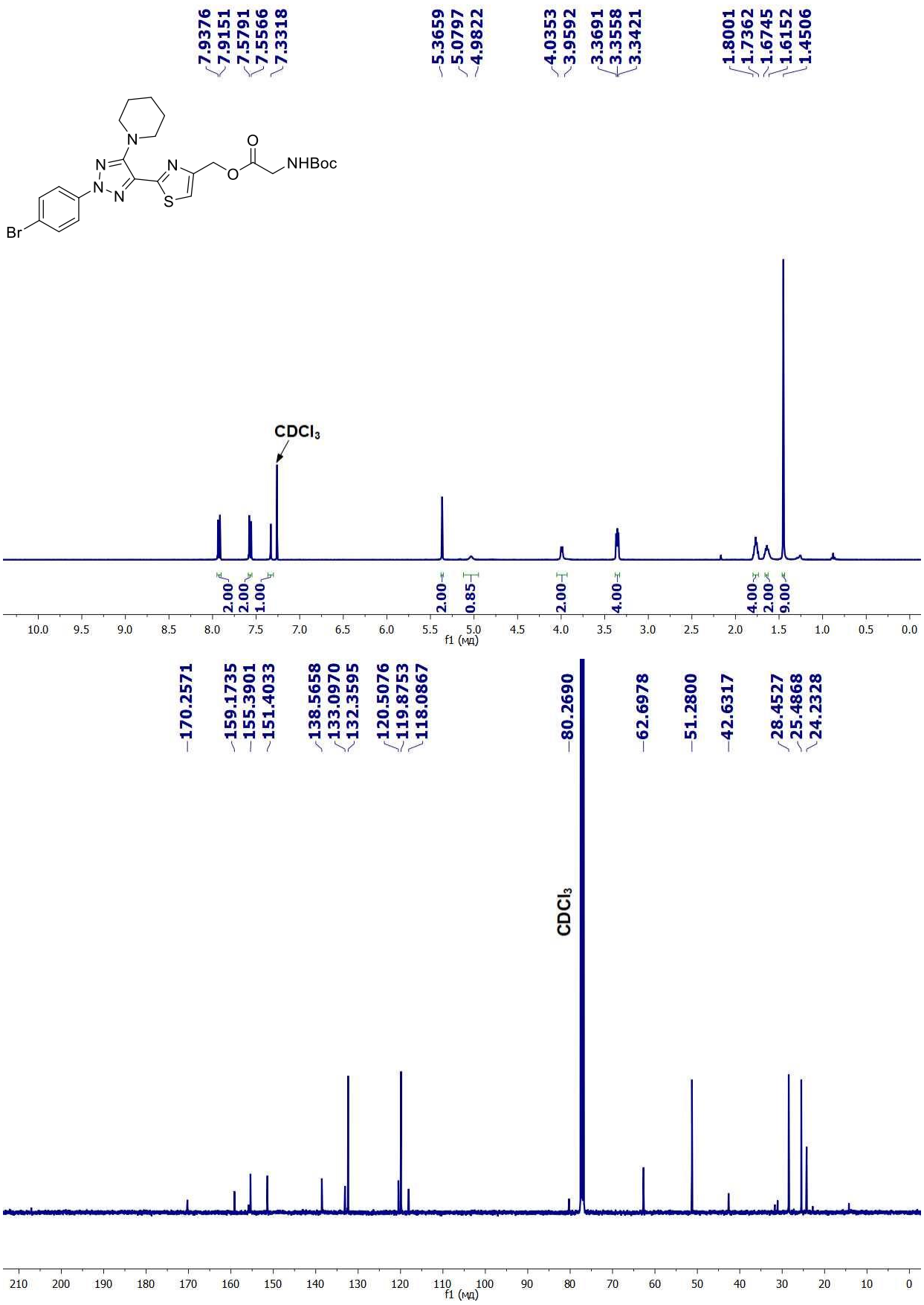

Fig. S16. ^{1}H NMR (400 MHz, $CDCl_3$, TMS) and ^{13}C NMR (100 MHz, $CDCl_3$) spectra of (2-(2-(4-bromophenyl)-5-(piperidin-1-yl)-2*H*-1,2,3-triazol-4-yl)thiazol-4-yl)methyl (*tert*-butoxycarbonyl)glycinate (**1d**).

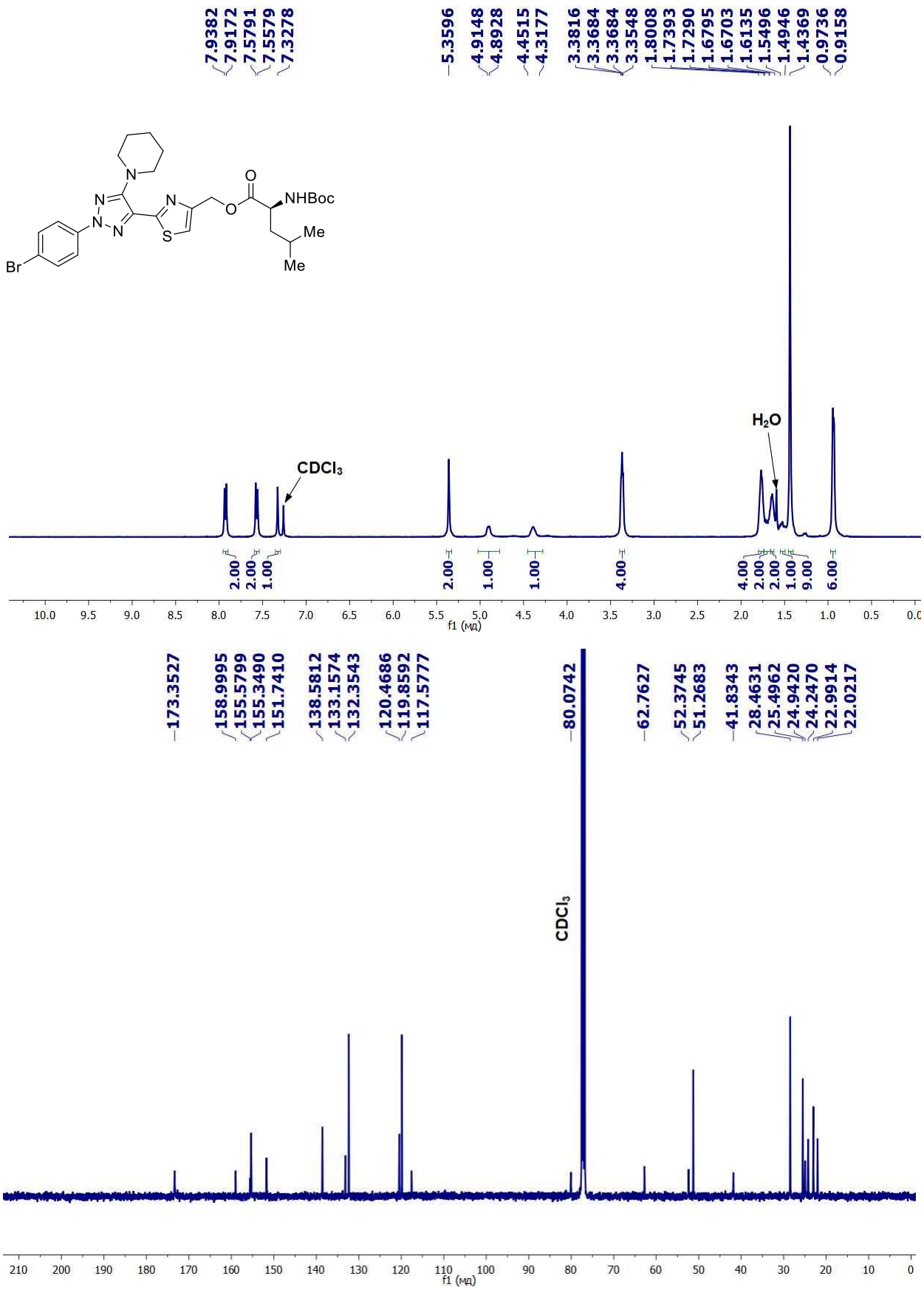

Fig. S17. ^{1}H NMR (400 MHz, $CDCl_3$, TMS) and ^{13}C NMR (100 MHz, $CDCl_3$) spectra of (2-(2-(4-methoxyphenyl)-5-(piperidin-1-yl)-2*H*-1,2,3-triazol-4-yl)thiazol-4-yl)methyl (*tert*-butoxycarbonyl)-*L*-methioninate (**1e**).

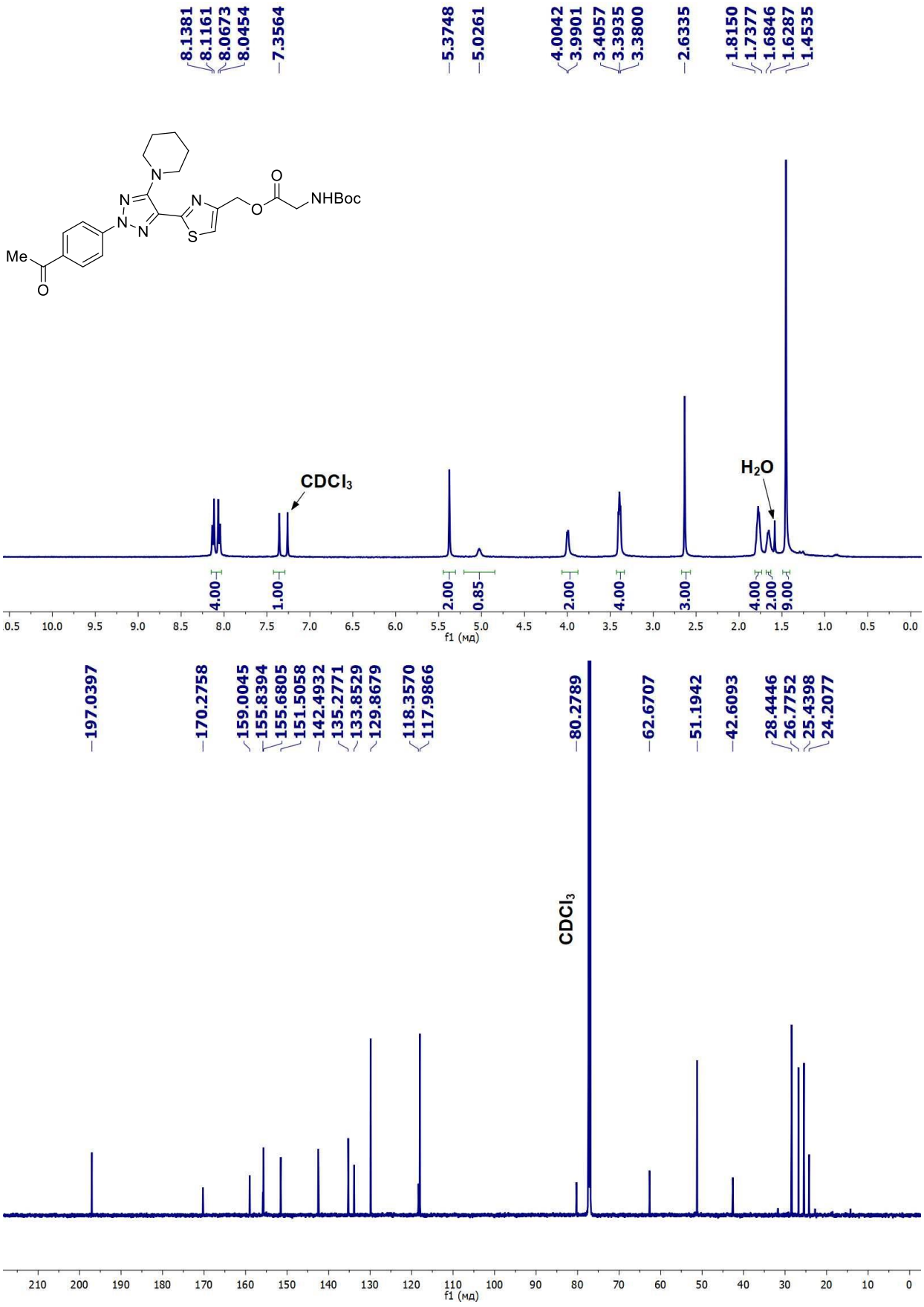

Fig. S18. ^{1}H NMR (400 MHz, $CDCl_3$, TMS) and ^{13}C NMR (150 MHz, $CDCl_3$) spectra of (2-(2-(4-acetylphenyl)-5-(piperidin-1-yl)-2*H*-1,2,3-triazol-4-yl)thiazol-4-yl)methyl (*tert*-butoxycarbonyl)glycinate (**1f**).

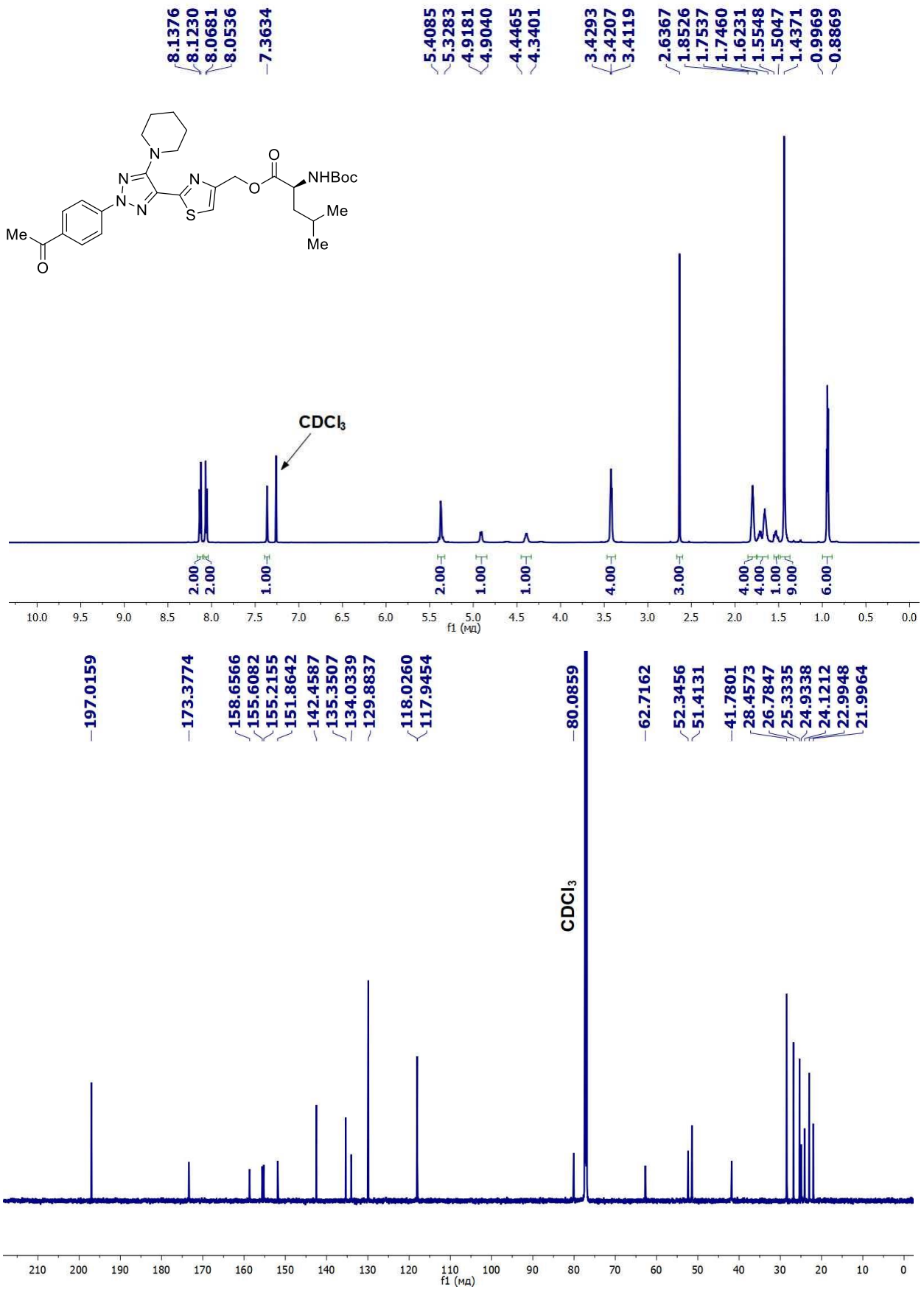

Fig. S19. ^{1}H NMR (600 MHz, $CDCl_3$, TMS) and ^{13}C NMR (150 MHz, $CDCl_3$) spectra of (2-(2-(4-acetylphenyl)-5-(piperidin-1-yl)-2*H*-1,2,3-triazol-4-yl)thiazol-4-yl)methyl (*tert*-butoxycarbonyl)-*L*-leucinate (**1g**).

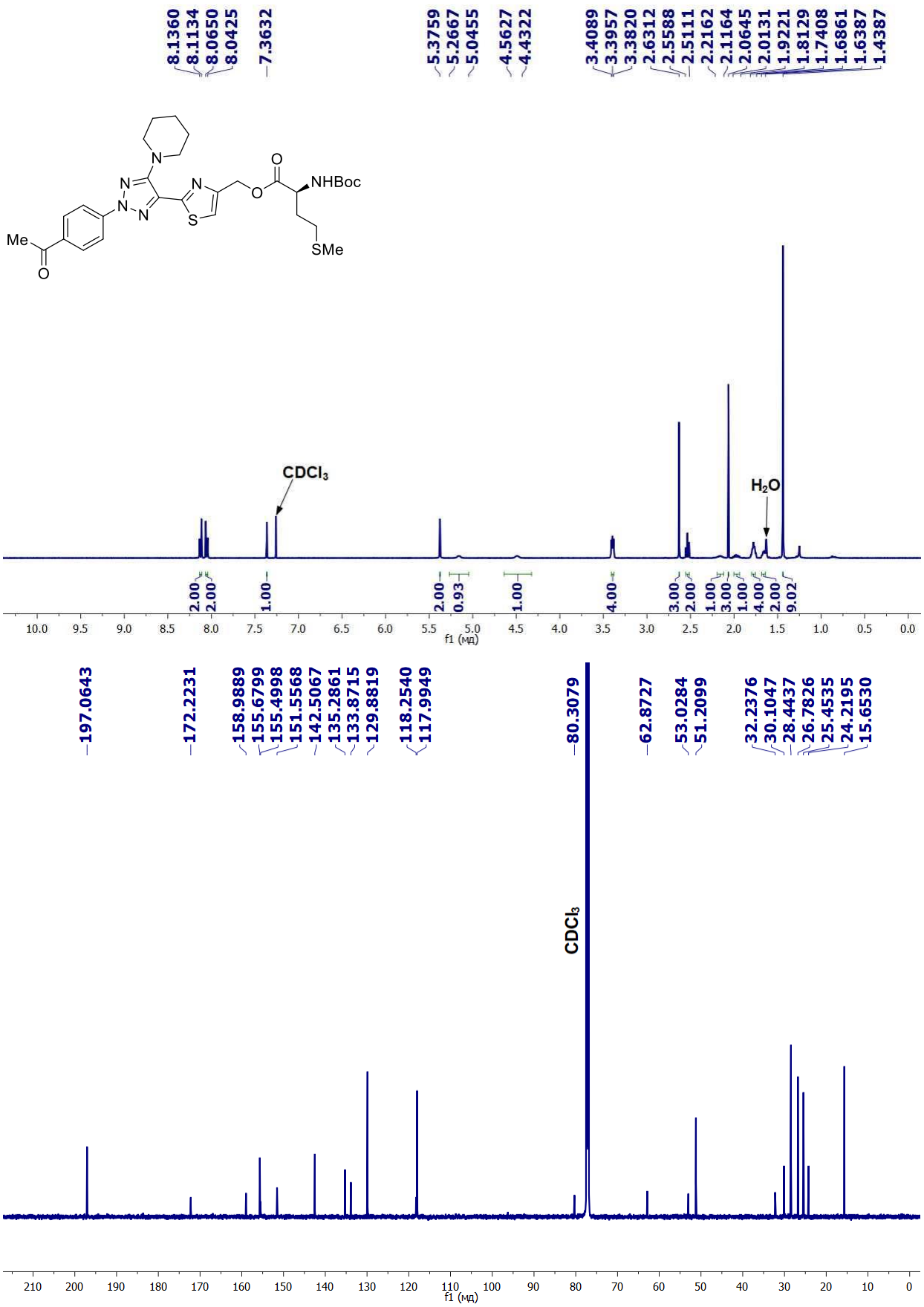

Fig. S20. ^{1}H NMR (400 MHz, $CDCl_3$, TMS) and ^{13}C NMR (150 MHz, $CDCl_3$) spectra of (2-(2-(4-acetylphenyl)-5-(piperidin-1-yl)-2*H*-1,2,3-triazol-4-yl)thiazol-4-yl)methyl (*tert*-butoxycarbonyl)-*L*-methioninate (**1h**).

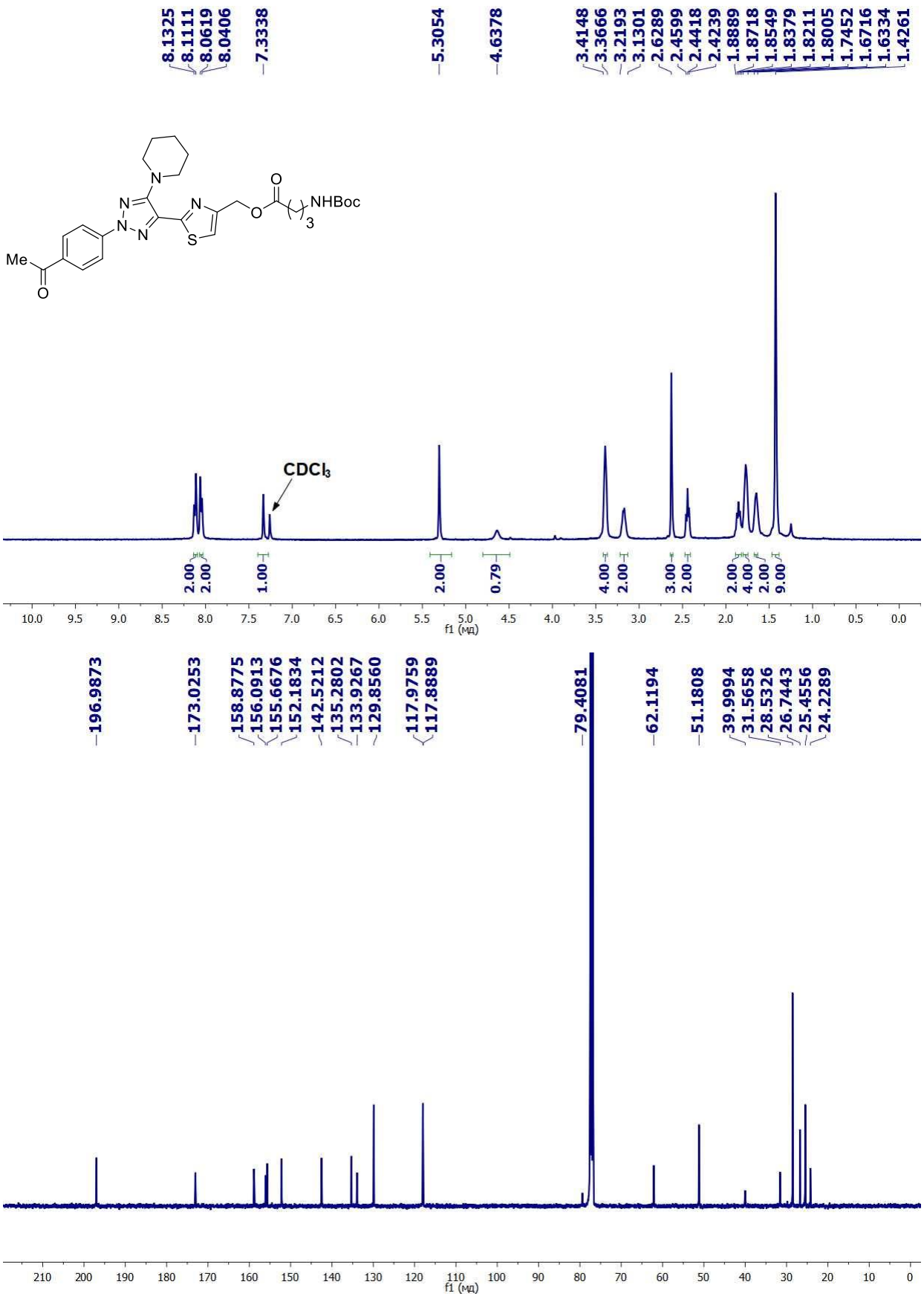

Fig. S21. ^{1}H NMR (400 MHz, $CDCl_3$, TMS) and ^{13}C NMR (100 MHz, $CDCl_3$) spectra of (2-(2-(4-acetylphenyl)-5-(piperidin-1-yl)-2*H*-1,2,3-triazol-4-yl)thiazol-4-yl)methyl 4-((*tert*-butoxycarbonyl)amino)butanoate (**1i**).

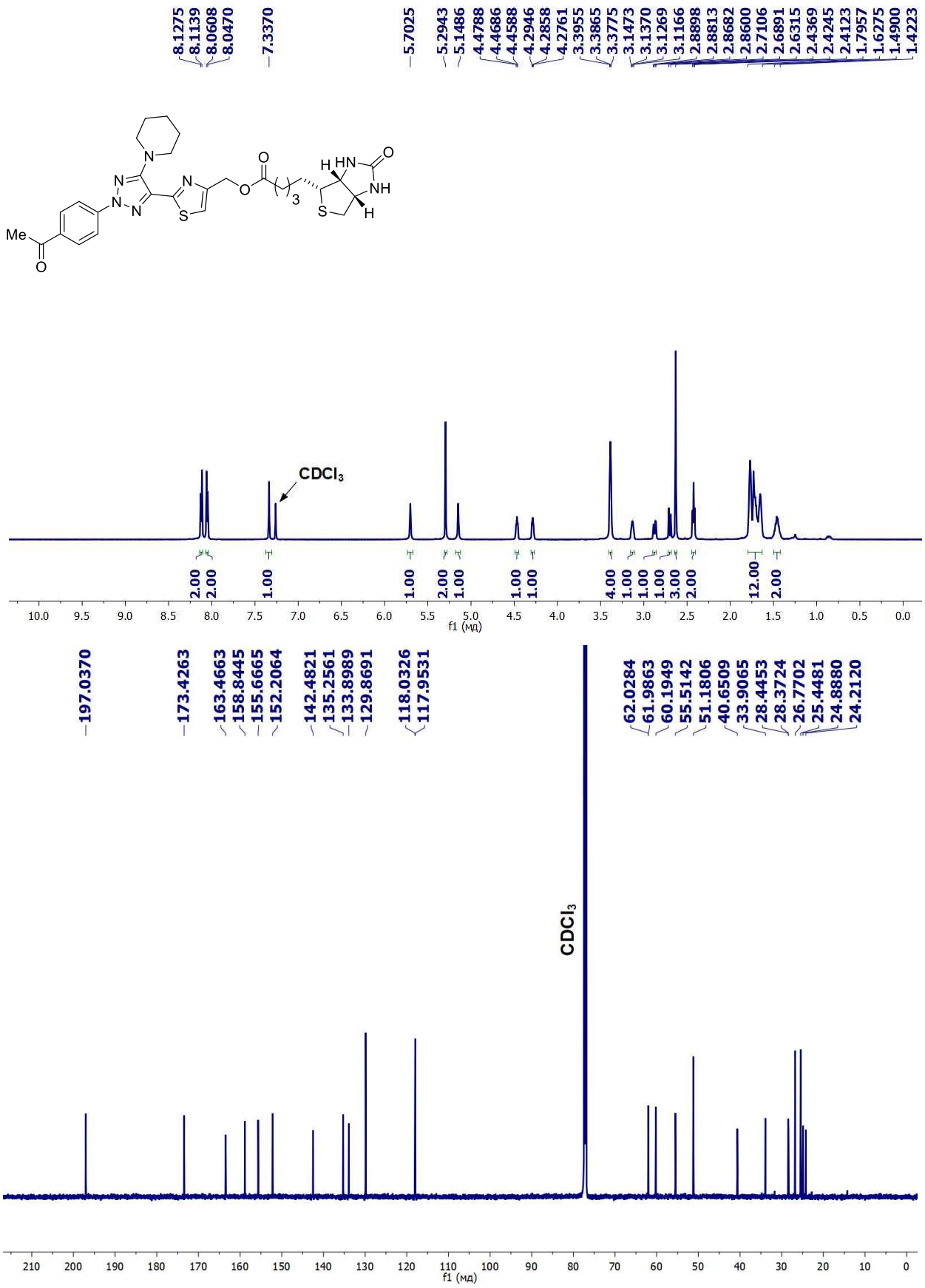

Fig. S22. ^{1}H NMR (600 MHz, $CDCl_3$, TMS) and ^{13}C NMR (150 MHz, $CDCl_3$) spectra of (2-(2-(4-acetylphenyl)-5-(piperidin-1-yl)-2*H*-1,2,3-triazol-4-yl)thiazol-4-yl)methyl 5-((3a*R*,4*R*,6a*S*)-2-oxohexahydro-1*H*-thieno[3,4-*d*]imidazol-4-yl)pentanoate (**1j**).

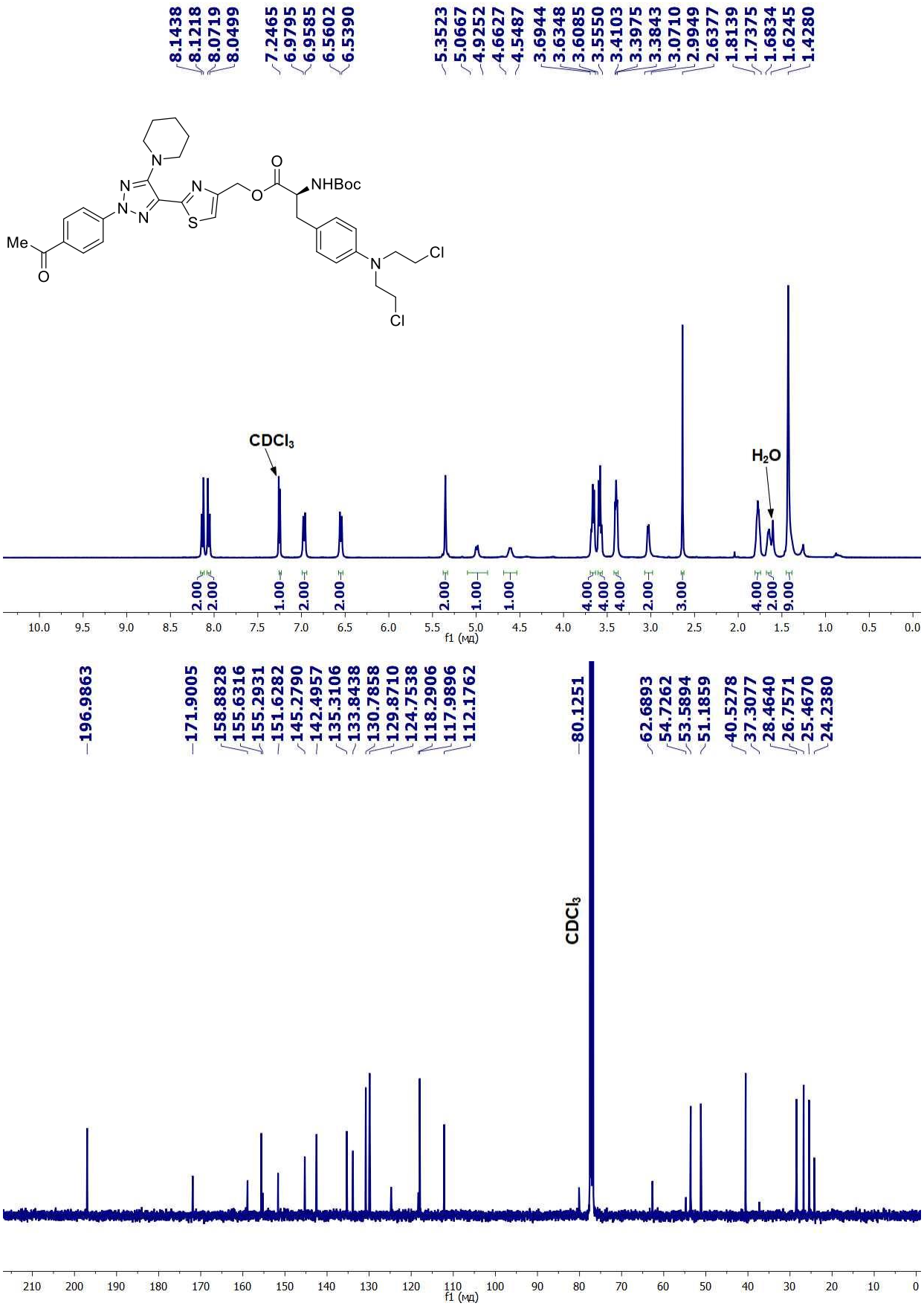

Fig. S23. ^{1}H NMR (400 MHz, $CDCl_3$, TMS) and ^{13}C NMR (100 MHz, $CDCl_3$) spectra of (2-(2-(4-acetylphenyl)-5-(piperidin-1-yl)-2*H*-1,2,3-triazol-4-yl)thiazol-4-yl)methyl (*S*)-3-(4-(bis(2-chloroethyl)amino)phenyl)-2-((*tert*-butoxycarbonyl)amino)propanoate (**1k).**

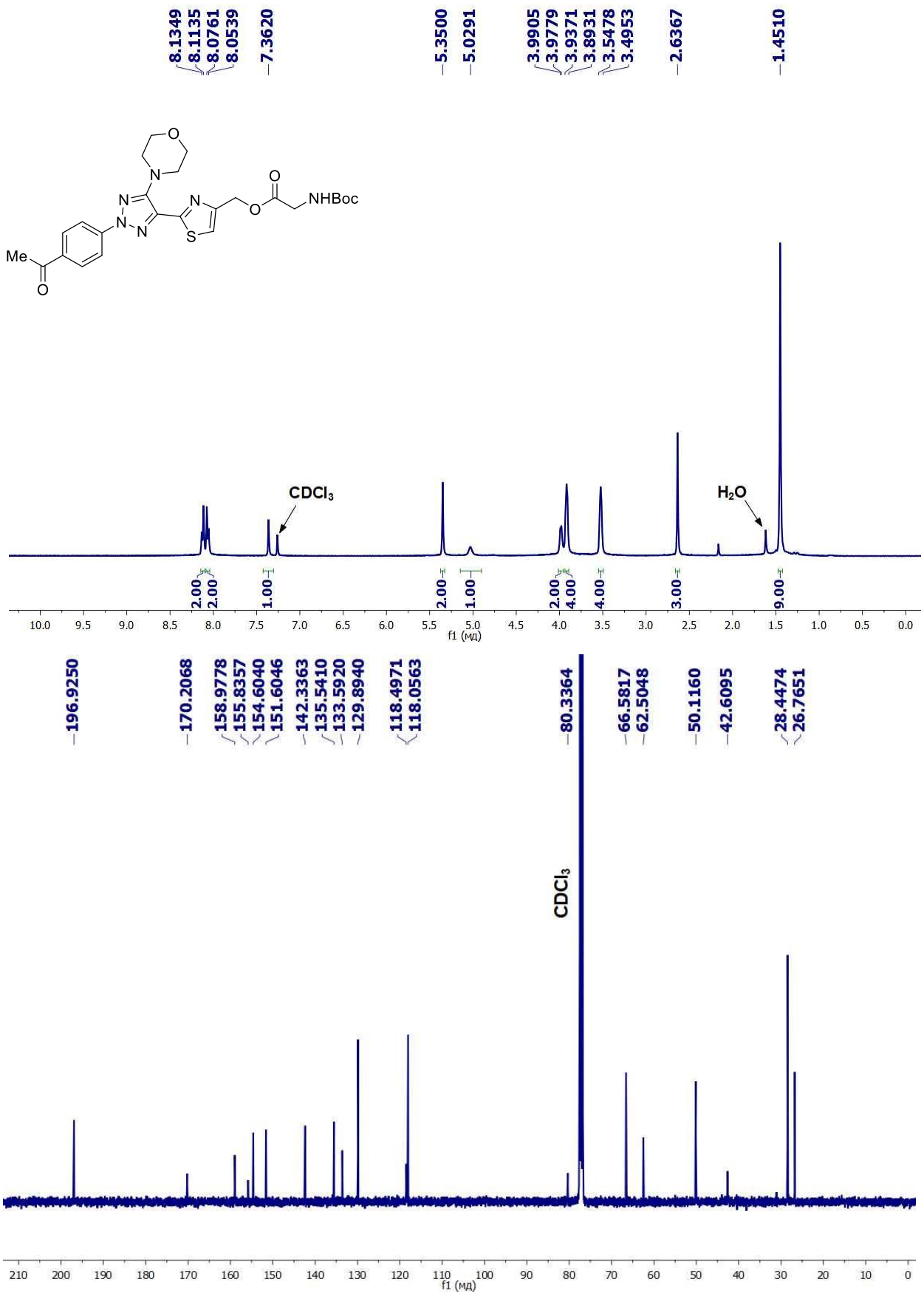

Fig. S24. ^{1}H NMR (400 MHz, $CDCl_3$, TMS) and ^{13}C NMR (100 MHz, $CDCl_3$) spectra of (2-(2-(4-acetylphenyl)-5-morpholino-2*H*-1,2,3-triazol-4-yl)thiazol-4-yl)methyl (*tert*-butoxycarbonyl)glycinate (**1l**).

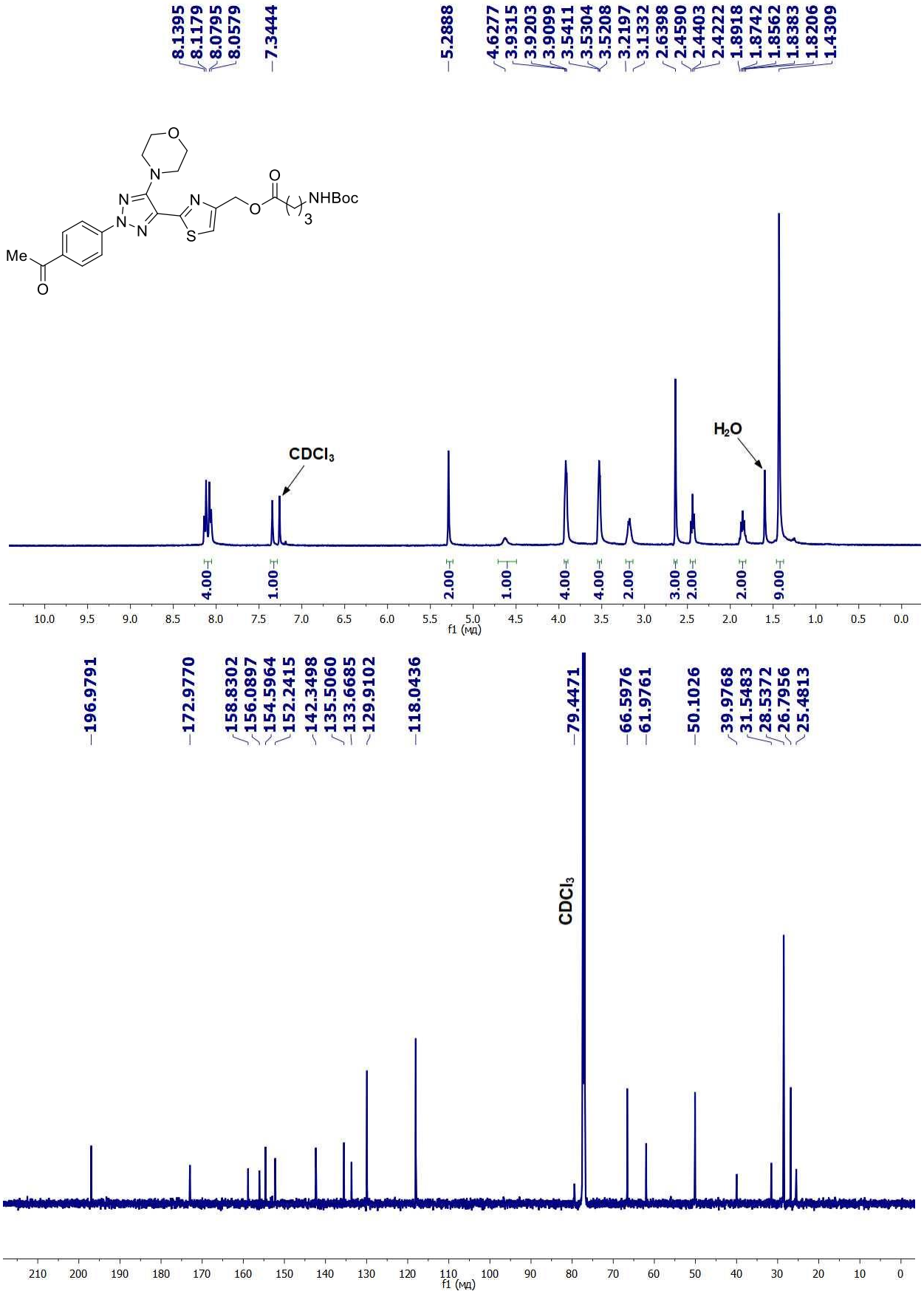

Fig. S25. ^{1}H NMR (400 MHz, $CDCl_3$, TMS) and ^{13}C NMR (150 MHz, $CDCl_3$) spectra of (2-(2-(4-acetylphenyl)-5-morpholino-2*H*-1,2,3-triazol-4-yl)thiazol-4-yl)methyl-4-((*tert*-butoxycarbonyl)amino)butanoate (**1m**).

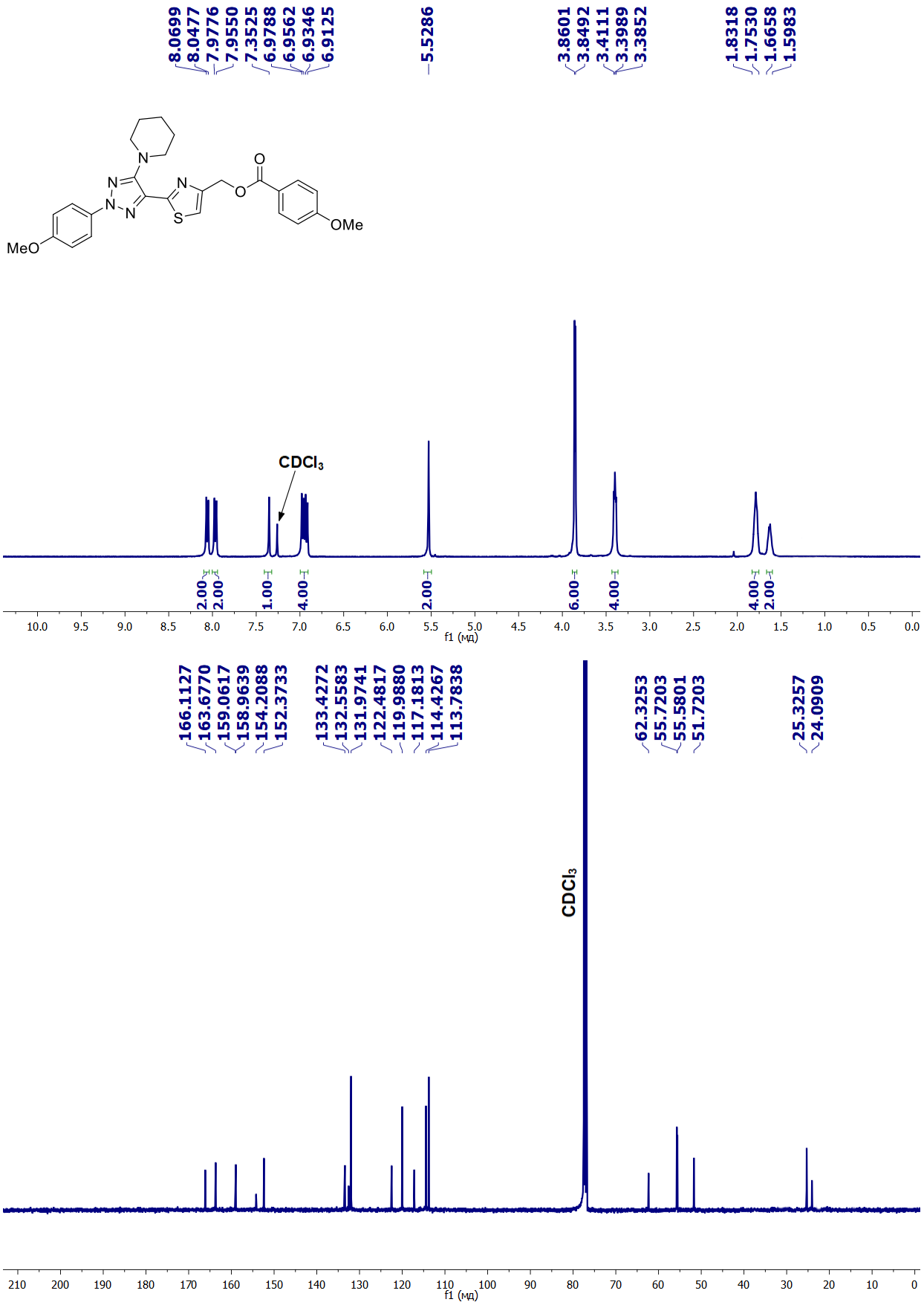

Fig. S26. ^{1}H NMR (400 MHz, $CDCl_3$, TMS) and ^{13}C NMR (100 MHz, $CDCl_3$) spectra of (2-(2-(4-methoxyphenyl)-5-(piperidin-1-yl)-2*H*-1,2,3-triazol-4-yl)thiazol-4-yl)methyl-4-methoxy-benzoate (**1n**).

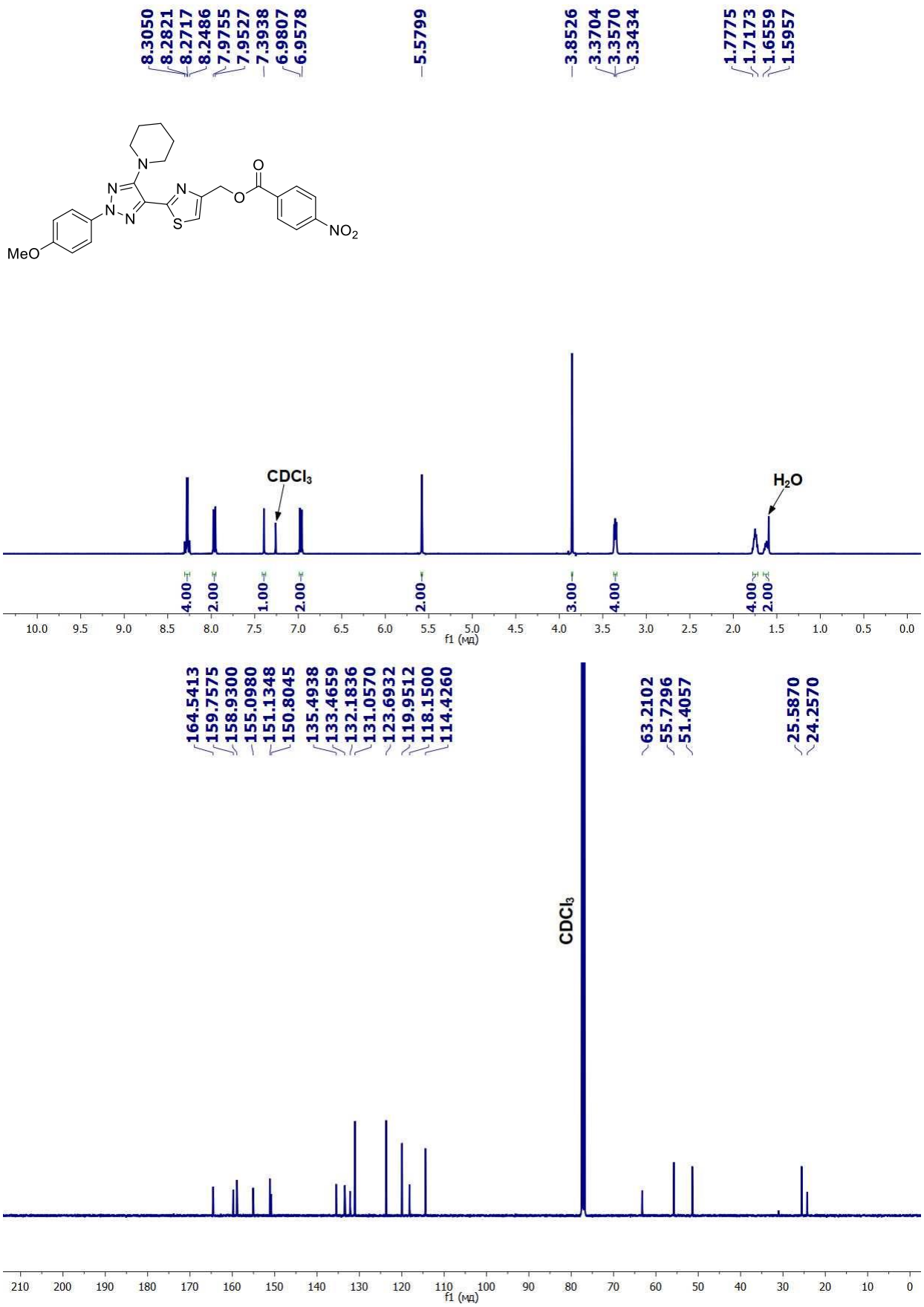

Fig. S27. ^{1}H NMR (400 MHz, $CDCl_3$, TMS) and ^{13}C NMR (100 MHz, $CDCl_3$) spectra of (2-(2-(4-bromophenyl)-5-(piperidin-1-yl)-2*H*-1,2,3-triazol-4-yl)thiazol-4-yl)methyl 4-methoxybenzoate (**1o**).

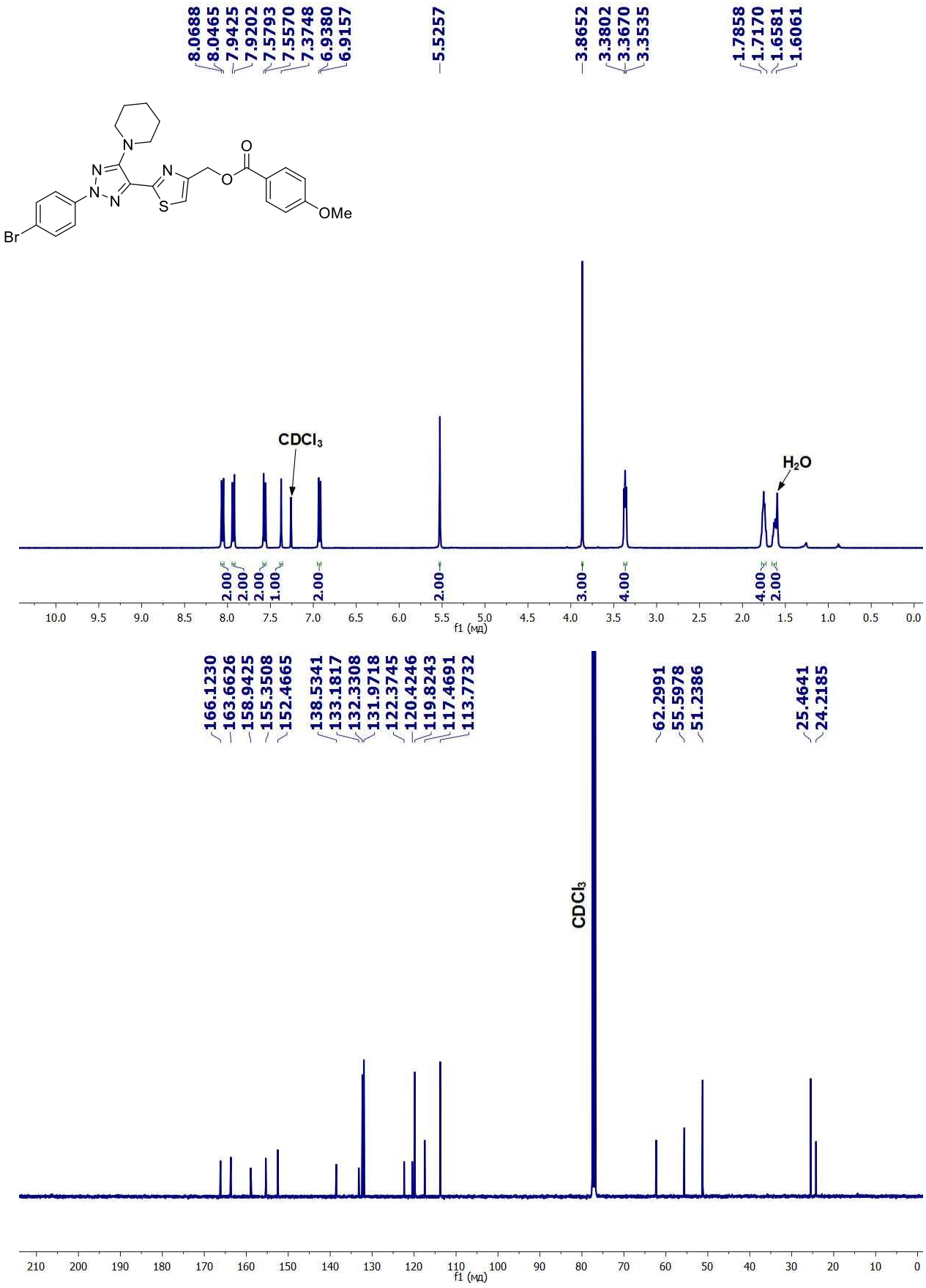

Figure S28. ^{1}H NMR (400 MHz, $CDCl_3$, TMS) and ^{13}C NMR (100 MHz, $CDCl_3$) spectra of (2-(2-(4-bromophenyl)-5-(piperidin-1-yl)-2*H*-1,2,3-triazol-4-yl)thiazol-4-yl)methyl 4-methoxybenzoate (**1p**).

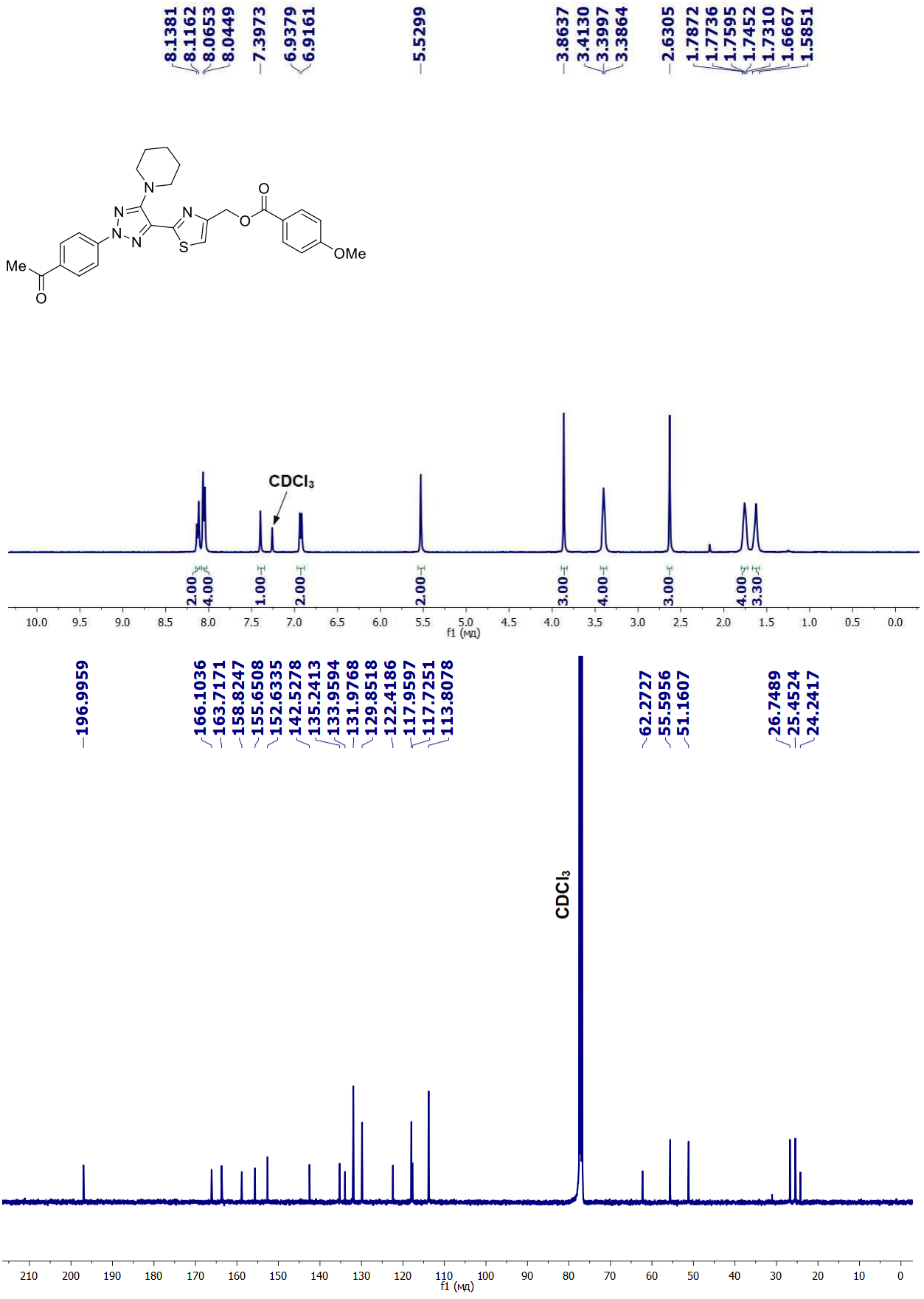

Fig. S29. ^{1}H NMR (400 MHz, $CDCl_3$, TMS) and ^{13}C NMR (100 MHz, $CDCl_3$) spectra of (2-(2-(4-acetylphenyl)-5-(piperidin-1-yl)-2*H*-1,2,3-triazol-4-yl)thiazol-4-yl)methyl 4-methoxybenzoate (**1q**).

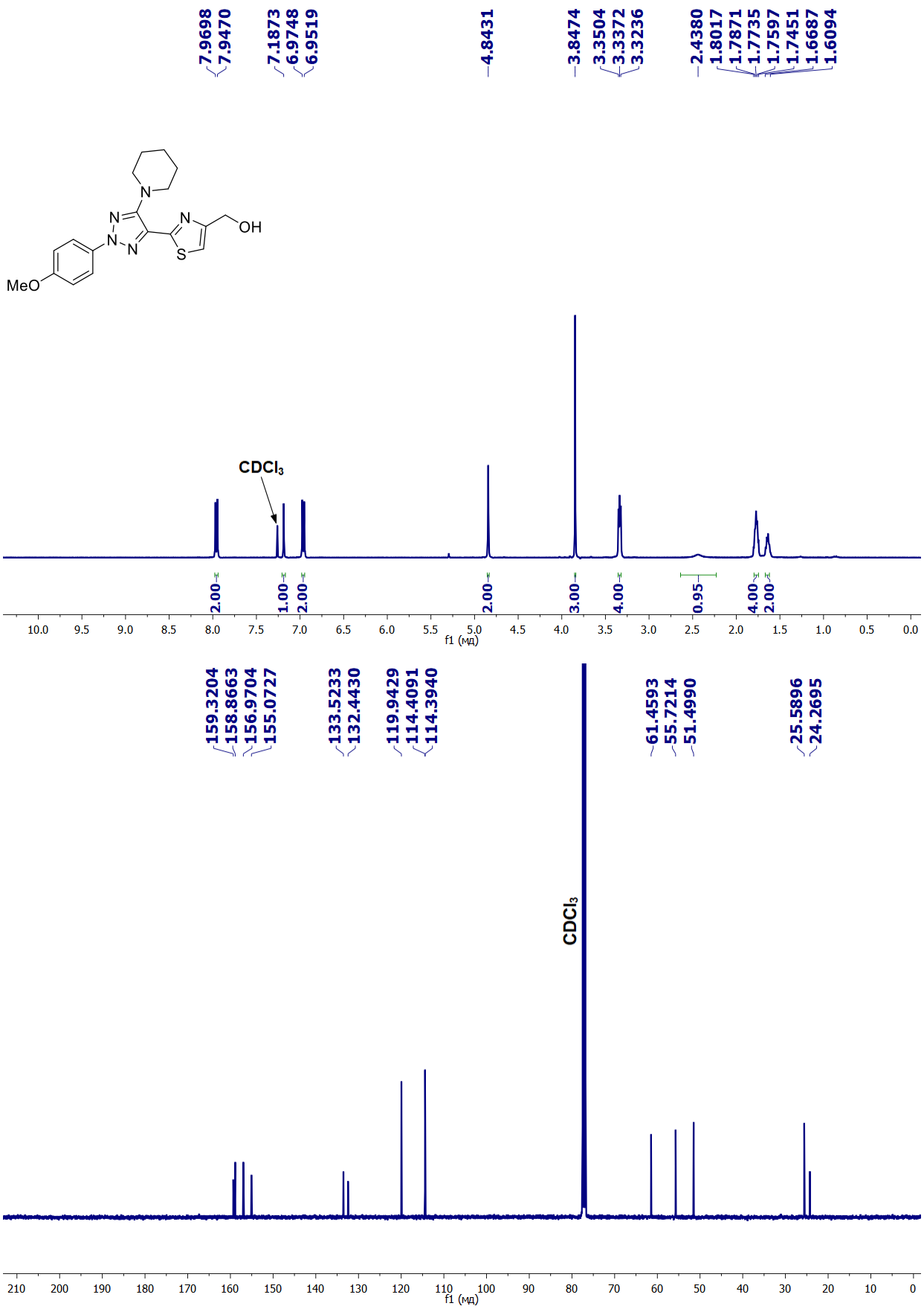

Fig. S30. ^{1}H NMR (400 MHz, $CDCl_3$, TMS) and ^{13}C NMR (100 MHz, $CDCl_3$) spectra of (2-(2-(4-methoxyphenyl)-5-(piperidin-1-yl)-2*H*-1,2,3-triazol-4-yl)thiazol-4-yl)methanol (**7a**).

Fig. S31. ^{1}H NMR (400 MHz, $CDCl_3$, TMS) and ^{13}C NMR (100 MHz, $CDCl_3$) spectra of (2-(2-(4-bromophenyl)-5-(piperidin-1-yl)-2H-1,2,3-triazol-4-yl)thiazol-4-yl)methanol (**7b**).

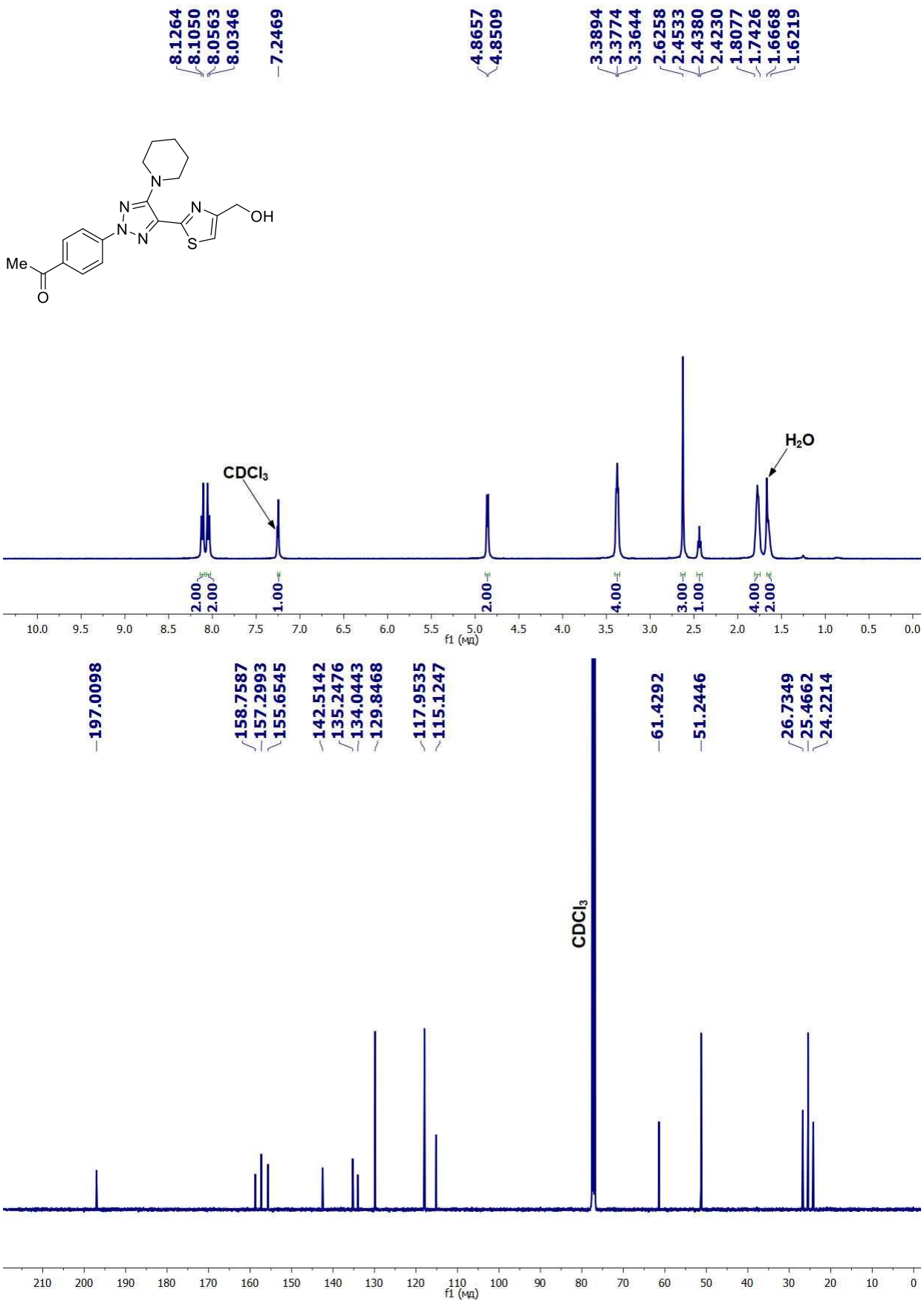

Fig. S32. ^{1}H NMR (400 MHz, $CDCl_3$, TMS) and ^{13}C NMR (100 MHz, $CDCl_3$) spectra of 1-(4-(4-(4-(hydroxymethyl)thiazol-2-yl)-5-(piperidin-1-yl)-2*H*-1,2,3-triazol-2-yl)phenyl)ethan-1-one (**7c**).

3. Photophysical properties of ATTs-CH_2Cl 3a-d and ATTs-CH_2I 6a-d

UV-Vis absorption spectra were recorded on a Shimadzu UV-1800 spectrophotometer (Kyoto, Japan). Fluorescence of the sample solutions was measured using a Hitachi F-7000 spectrophotometer (Tokyo, Japan). The absorption and emission spectra were recorded in Toluene, 1,4-Dioxane, $CHCl_3$, MeOH, Acetone, MeCN, DMSO and DMSO-H_2O (1:9, v/v), DMSO-PBS (1:9, v/v, pH 7.4) mixtures in 10.00 mm quartz cells. The excitation wavelength was at the absorption maxima. Atmospheric oxygen contained in solutions was not removed. Concentration of the compounds in the solution was 5.0×10^{-5} M and 5.0×10^{-6} M for absorption and fluorescence measurements, respectively. The relative fluorescence quantum yields (QY) were determined using quinine sulfate (5×10^{-5} M) in 0.1 M H_2SO_4 as a standard ($\Phi_F = 0.54$).

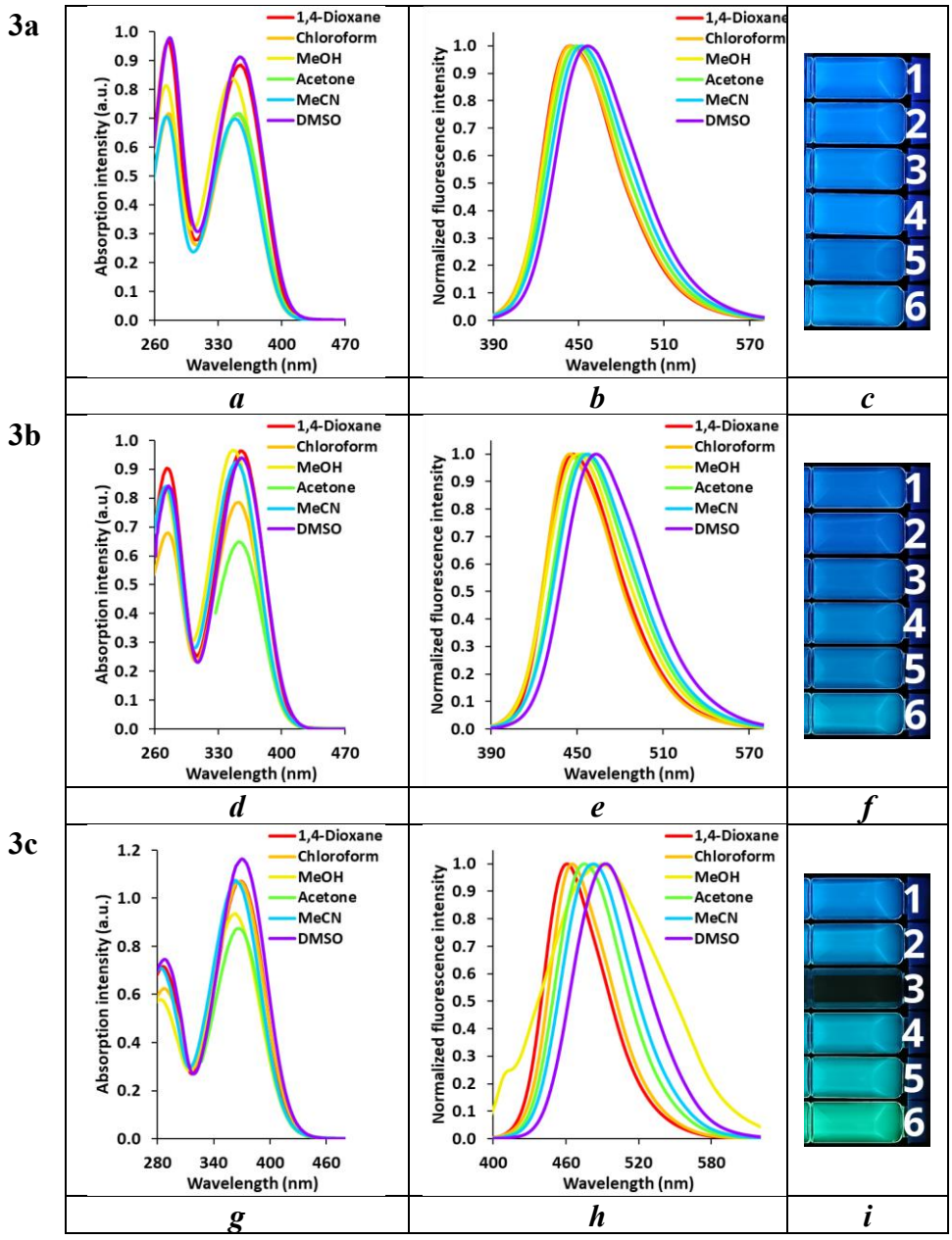

3d

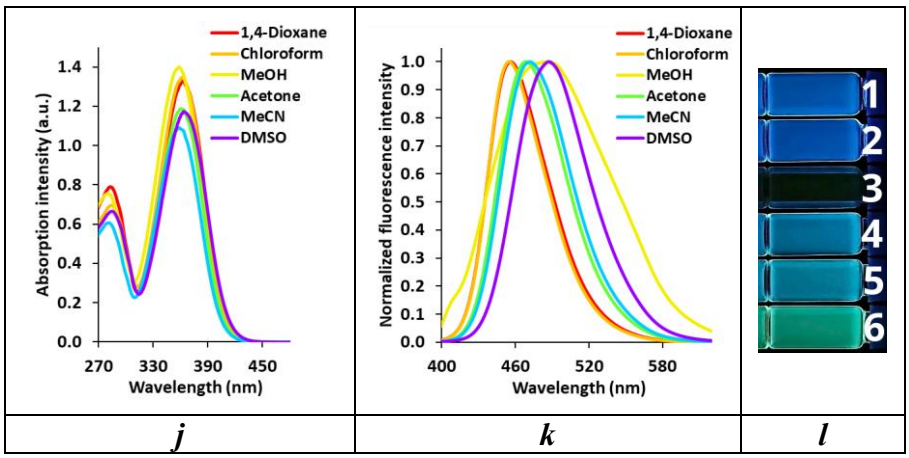

Fig. S33. Absorption (*a*, *d*, *g*, *j*) ($c = 5.0\times10^{-5}$ M) and emission spectra (*b*, *i*, *h*, *k*) ($c = 5.0\times10^{-6}$ M) for ATTs-CH_2Cl **3a** (*a*, *b*), **3b** (*d*, *e*), **3c** (*g*,*h*) and **3d** (*j*, *k*) solutions in different solvents; (*c*, *d*, *g*, *h*, *k*, *l*) photographs of ATTs-CH_2Cl **3a** (*c*), **3b** (*g*), **3c** (*j*) and **3d** (*l*) solutions in (1) 1,4-dioxane, (2) chloroform, (3) methanol, (4) acetone, (5) acetonitrile, (6) DMSO under UV irradiation (λ_{ir} = 365 nm).

Table S2. Characteristics of absorption spectra ($c = 5\times10^{-5}$ M) and emission spectra ($c = 5\times10^{-6}$ M) of thiazole ATTs-CH_2Cl **3a-d** and ATTs-CH_2I **6a-d** solutions in different solvents.

Entry	Compd	Structure	Solvent	λ_{abs}, nm	ε^a, $M^{-1}cm^{-1}$	λ_{em}, nm	QY^b, %	SS, nm/cm^{-1}
1	**3a**	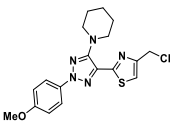	1,4-Dioxane	275, 355	17600	444	68	89/5646
2			$CHCl_3$	275, 351	14200	444	50	93/5968
3			MeOH	273, 345	16600	449	46	104/6714
4			Acetone	352	14300	449	46	97/6137
5			MeCN	273, 349	13900	452	25	103/6529
6			DMSO	277, 354	18300	456	35	102/6319
7	**3b**	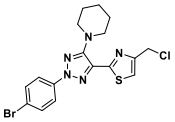	1,4-Dioxane	273, 355	19200	447	74	92/5798
8			$CHCl_3$	275, 353	15700	445	64	92/5857
9			MeOH	271, 347	19300	451	61	104/6645
10			Acetone	354	12900	455	60	101/6271
11			MeCN	272, 349	18400	457	55	108/6771
12			DMSO	275, 358	14200	463	77	105/6335
13	**3c**	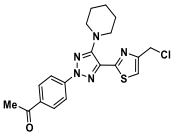	1,4-Dioxane	283, 362	21400	461	72	92/5408
14			$CHCl_3$	285, 362	21400	466	68	99/5789
15			MeOH	281, 358	18700	490	2	127/7140
16			Acetone	361	17500	475	58	110/6345
17			MeCN	284, 364	21500	483	53	119/6769
18			DMSO	288, 370	23300	493	63	123/6743
19	**3d**	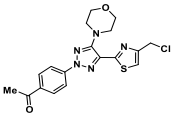	1,4-Dioxane	283, 362	26500	456	76	94/5694
20			$CHCl_3$	285, 362	26900	455	79	93/5646
21			MeOH	281, 358	28000	485	2	127/7314
22			Acetone	361	23700	468	68	107/6333
23			MeCN	282, 359	21800	472	65	113/6669

24			DMSO	285, 364	23500	487	64	123/6939
25			1,4-Dioxane	276, 357	20000	444	11	87/5489
26			$CHCl_3$	276, 355	16100	445	8	90/5697
27	**6a**	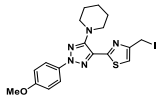	MeOH	273, 349	16500	448	15	99/6332
28			Acetone	354	15600	446	10	92/5827
29			MeCN	274, 351	19200	451	6	100/6317
30			DMSO	277, 357	18600	459	13	102/6225
31			1,4-Dioxane	270, 356	20700	446	13	90/5668
32			$CHCl_3$	270, 353	20000	443	14	90/5755
33	**6b**	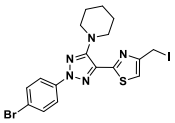	MeOH	267, 349	15400	448	23	99/6332
34			Acetone	356	20300	454	14	98/6063
35			MeCN	269, 353	19400	454	9	101/6302
36			DMSO	272, 358	18700	464	23	106/6381
37			1,4-Dioxane	289, 370	25500	461	17	91/5335
38			$CHCl_3$	290, 372	26100	467	18	95/5468
39	**6c**	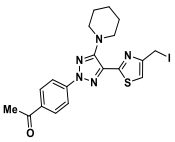	MeOH	286, 363	22900	495	1	132/7346
40			Acetone	370	20800	477	18	107/6063
41			MeCN	287, 367	23900	484	11	117/6587
42			DMSO	289, 372	24900	493	30	121/6598
43			1,4-Dioxane	286, 364	26300	457	16	93/5591
44			$CHCl_3$	287, 364	26100	456	21	92/5543
45	**6d**	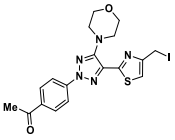	MeOH	282, 361	25700	492	2	131/7376
46			Acetone	364	26100	470	23	106/6196
47			MeCN	284, 362	27500	472	14	110/6438
48			DMSO	285, 367	24500	488	33	121/6756

a – value of the coefficient for the long-wave maximum;

b - Relative QY, determined relative to the standard (quinine sulphate solution; $c = 5.0 \times 10^{-5}$ M in 0.1 M H_2SO_4; $\Phi_F = 54.0$ %).

4. Quantum mechanical calculation data for ATTs-CH_2Cl 3a-c

The molecular geometry of the ground state of all the main rotamers of the investigated molecules was fully optimized in *vacuo* and in implicit solvents (*vide infra*) at the Density Functional Theory (DFT) level, using a combination of the hybrid functionals B3LYP[7] and M06-2X[8] with the triple-ζ basis set 6-311++G**. The D3 version of Grimme's semi-empirical dispersion with Becke-Johnson damping GD3BJ[9] was also included in the case of B3LYP. The optimised geometries were submitted to vibrational analysis. The vibrational frequencies and thermochemical parameters were computed in harmonic approximation at $T = 298.15$ K and $p = 1$ atm, using the same level of theory employed for the optimisation. No imaginary frequencies were found.

Solvent effects were taken into account via the implicit polarizable continuum model in its integral equation formalism (IEF-PCM).[10] For geometry optimisations and frequency calculations, the PCM

molecular cavity was built according to the universal force field (UFF)[11] radii within the value used in the last implementation of the PCM (based on a continuum surface charge formalism). For topological analysis and the evaluation of energetics, SMD parameterisation was employed.[12] The solvent used was dimethylsulphoxide (DMSO). The standard values for dielectric constants and refractive indexes were always assumed. In the case of water, a local micro-explicit solvation about the proton-donor/proton-acceptor centres of the organic molecules was also combined with the implicit model.

The UV-vis absorption spectra for the equilibrium geometries of the rotamers with $\Delta G < 2.5$ kJ·mol^{-1} were calculated at time-dependent density functional theory (TD-DFT) level, accounting for $S_0 \rightarrow S_n$ (n = 1 to 20); the energy of the first 20 triplet states was also computed. The nature of the vertical excited electronic state was analysed both *in vacuo* and in the solvated phase. This investigation was performed by employing the long-range corrected functionals ω-B97X[D][13] and CAM-B3LYP[14] coupled with the 6-311++G** basis set. In the case of the solvated phase, state-specific (SS)[15] treatment of the solvent effects was considered, both within the non-equilibrium (neq) and equilibrium (eq) solvation regimes of all non-dark electronic transitions were also simulated, including the Duschinsky and Herzberg–Teller effects. The first singlet excited state $S(\pi,\pi^*)$ state geometry was optimised using analytical gradients and the first transitions $S_1 \rightarrow S_0$ of the emission. In this case, SS (both eq and neq) treatment of the solvent effects was considered. The properties of the corresponding non-optimised ground state were also computed. Solvent effects were taken into account via IEF-PCM(UFF).

The atomic charge population analysis, electric multiple moments, electronic density, and electrostatic potential were also computed using Mulliken's and the CHELPG procedur[16] for the optimised and vertically de-excited ground state and the vertically excited and relaxed S_1 states.

To investigate the presence and nature of possible intramolecular H-bonding interactions, two different approaches were used: first on one hand, topological analysis based on Bader's atoms in molecules (AIM) theory[17] was used, and second, the -covalent interaction (NCI) index combined with the second derivative of the reduced density gradient along the second main axis of variation were employed.[18] These procedures were applied both to the ground and first singlet excited states.

The different photo-reaction pathways were investigated by means of a relaxed scan of the ground state potential energy surface along with the selected internal coordinates (interatomic distances). Each coordinate was elongated of + 3 Å (step 0.1 Å) starting from the equilibrium value. For each point, the electronic energy of the ground state and the singlet and triplet excited states was computed at TD-DFT level.

The self-consistent field (SCF) algorithm used was the quadratically convergent procedure designed by Bacskay,[19] a method that is acknowledged to be slower but more reliable than the regular

SCF with DIIS extrapolation. For all calculations, the integration grid for the electronic density was set to 250 radial shells and 974 angular points for all the atomic species. The accuracy for the two-electron integrals and their derivatives was set to 10^{-14} a.u.. The convergence criteria for the SCF were set to 10^{-12} for a root mean square (RMS) change in the density matrix and 10^{-10} for a maximum change in the density matrix. The convergence criteria for geometry optimizations were set to 2×10^{-6} a.u. for a maximum force, 1×10^{-6} a.u. for an RMS force, 6×10^{-6} a.u. for a maximum displacement and 4×10^{-6} a.u. for an RMS displacement. For the AIM analysis, the number of paths in each interbasin surface was set equal to 500, the number of points in each interbasin surface path as well as the max number of points of a path equal to 1000, the stepsize 1×10^{-4} bohr, the maximal number of interactions to 512, the criterion for gradient-norm (displacement) convergence to 1×10^{-7} a.u. (1×10^{-8} a.u.), and the minimal distance between CPs to 1×10^{-3} bohr. The search of the CPs was made staring from the nuclear positions, the midpoint of each atom pairs, the centre of any triangle defined by three atoms and tetrahaedron defined by four atoms

The location of BCPs and subsequent calculation of SF values were performed using a modified version of the PROAIMV program.[20] All the other calculations were performed using the GAUSSIAN G169.C01 software package.[21] The calculation of the NCI was performed using homemade code.

Table S3. Thermochemical characteristics of ATT-CH_2Cl **3a-c** rotamers in DMSO *(Energy differences at T = 298.15 K and p = 1.00 atm (in kJ/mol))*

Compound		ΔH/(kJ/mol)	ΔG/(kJ/mol)
3a	A	0.0	0.0
	B	0.1	0.1
	C	6.4	6.1
	D	6.5	6.4
3b	A	0.0	0.0
	C	6.6	5.6
3c	A	0.0	0.0
	B	0.1	1.9
	C	6.9	7.2
	D	6.8	5.1

Table S4. Theoretical and experimental values of maxima absorption and emission of ATT-CH_2Cl **3a-c** in DMSO.

Entry	Comp	λ_{abs}, nm		λ_{em}, nm	
		Exp	Calc	Exp	Calc
1	**3a**	354	356	456	457
2	**3b**	358	372	463	464
3	**3c**	370	360	493	497

Compd	S_0		S_{1r}	
3a	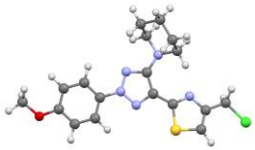	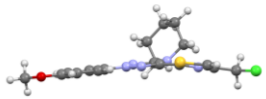	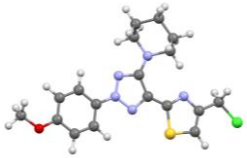	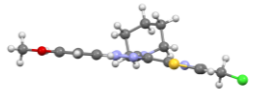
3b	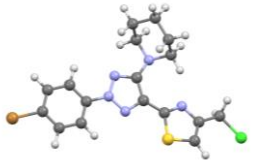	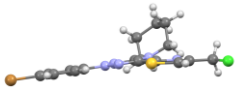	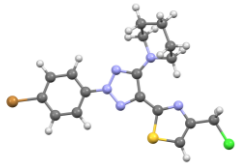	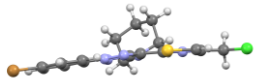
3c	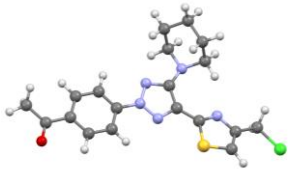	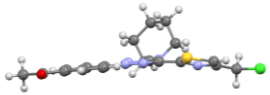	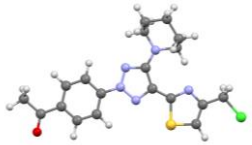	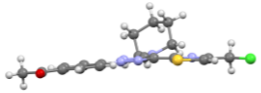

Fig. S34. Optimized geometries of the ATTs-CH_2Cl **3a, b, c** in their *GS* and *ES* in DMSO, depicted from two orthogonal viewpoints. Level of theory: DFT/IEF-PCM(UFF). Legend of colours: white (H), grey (C), lilac (N), green (Cl), yellow (S), red (O), and brown (Br).

Table S5. Selected bonds lengths (in Å) torsion (°) for the *GS* (S_0) optimized geometries of ATTs **3a, b, c** in DMSO

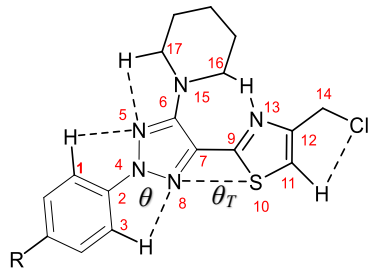

Entry	Compd	C2-C4	N4-N5	N5-C6	C6-C7	N8-C7	N4-N8	C6-N15	C7-C9	C9-S10	S10-C11	C11-C12	C12-N13	C9-N13	C12-C14	θ_{Ar}	θ_T
1	**3a**	1.418	1.346	1.343	1.437	1.345	1.321	1.371	1.448	1.763	1.735	1.365	1.379	1.312	1.501	2.95	11.25
2	**3b**	1.413	1.347	1.342	1.441	1.341	1.324	1.375	1.449	1.762	1.734	1.367	1.373	1.312	1.504	1.79	14.98
3	**3c**	1.409	1.350	1.340	1.444	1.338	1.327	1.373	1.450	1.781	1.738	1.367	1.379	1.312	1.501	1.73	16.05

Table S6. Selected bonds lengths (in Å) torsion (°) for the *ES* (S_1) optimized geometries of ATTs **3a, b, c** in DMSO

Entry	Compd	C2-C4	N4-N5	N5-C6	C7-C6	N8-C7	N4-N8	C6-N15	C7-C9	C9-S10	S10-C11	C11-C12	C12-N13	C9-N13	C12-C14	θ_{Ar}	θ_T
1	**3a**	1.369	1.344	1.333	1.484	1.359	1.367	1.346	1.408	1.777	1.725	1.378	1.361	1.341	1.509	2.01	0.30
2	**3b**	1.370	1.339	1.335	1.485	1.359	1.358	1.342	1.407	1.778	1.722	1.376	1.362	1.338	1.509	0.98	0.69
3	**3c**	1.368	1.337	1.333	1.485	1.353	1.363	1.339	1.413	1.789	1.719	1.374	1.366	1.361	1.499	0.62	0.10

Table S7. Selected lengths (in Å) for noncovalet interaction for the *GS* (S_0) and *ES* (S_1) optimized geometries of ATTs **3a**, **b, c** in DMSO[a]

		S_0						S_1					
Entry	Compd	C1H-N5	C3H-N8	N8-S10	C17-N5	C16H-N13	C11H-Cl	C1H-N5	C3H-N8	N8-S10	C17-N5	C16H-N13	C11H-Cl
1	**3a**	2.495	2.514	3.032	2.514	2.275	2.860	2.489	2.452	2.903	2.489	2.118	2.831
2	**3b**	2.481	2.503	3.036	2.478	2.289	2.859	2.481	2.448	2.889	2.385	2.084	2.827
3	**3c**	2.480	2.500	3.070	2.480	2.288	2.868	2.479	2.452	2.888	2.302	2.064	2.828

a - Van der Wals radii: R_H = 1.2 Å; R_C = 1.85 Å; R_N = 1.50 Å; R_O = 1.40 Å; R_{Cl} = 1.80 Å; R_S = 1.85 Å.

Table S8. Computed electronic, dipole, and electrostatic properties, the parameters[a] for absorption and fluorescence spectra of ATTs-CH_2Cl **3a-c** in DMSO.

Compd	$c_{(HL)}$	ΔE_{01}	f_{01}	$c_{(LH)}$	ΔE_{10}	f_{10}	μ_{0r}	μ_{1v}	μ_{1r}	μ_{0v}	$\theta_{0\text{-}1v}$	$\theta_{0\text{-}1r}$	θ_{0v}
3a	0.6682	3.486	0.887	-0.691	2.713	0.9086	5.4	10.0	9.7	5.3	9.1	9.5	9.5
3b	0.6871	3.450	0.862	0.692	2.673	0.864/7	3.4	7.8	8.7	4.0	14.2	15.5	15.5
3c	0.6861	0.668	1.003	-0.683	2.673	0.9727	6.9	12.8	13.7	7.7	14.5	8.2	8.2

a - $c_{(HL)}$ and $c_{(LH)}$ – transition coefficient; ΔE_{01} and ΔE_{01} eV - HOMO and LUMO energies gap; λ_{01}, nm - absorption wavelength and oscillator strength (f_{01}); emission wavelength (λ_{10}, nm) and oscillator strength (f_{10}); modulus of the electric dipole moments of the GS (μ_0, D), of the vertical FC ES (μ_{1v}, D), and of the relaxed ES (μ_{1r}, D), and angles formed by the directions of the electric dipole moment vectors ($\theta_{0,1v}$, deg) and $\theta_{0,1r}$, deg)).

5. Photophysical properties for the ATT-PCs 1a-q

Table S9. Photophysical data for the ATT-PC **1g** in solvents with different polarities (for absorption: $c = 5 \times 10^{-5}$ M and for emission: $c = 5 \times 10^{-6}$ M).

Entry	Solvents	λ_{max}[a], nm	ε, $M^{-1}cm^{-1}$	λ_{em}, nm	QY,[b] %	SS, nm/cm^{-1}	f[c]
1	Toluene	373	24800	456	96.3	83/4880	0.697
2	1,4-Dioxane	369	23700	461	84.8	92/5408	0.482
3	$CHCl_3$	368	19500	465	97.5	97/5667	0.734
4	EtOH	364	29700	496	9.8	132/7311	1.108
5	MeOH	364	30100	492	1.8	128/7147	1.246
6	AcOEt	364	25400	465	91.2	100/5921	0.946
7	DMF	370	25000	485	84.4	115/6408	0.856
8	MeCN	364	22800	483	79.7	119/6769	0.877
9	DMSO	371	22100	493	62.6	122/6670	0.793

a – long-wave maximum.
b – Relative QY, determined relative to the standard (quinine sulphate solution; $c = 5.0 \times 10^{-5}$ M in 0.1 M H_2SO_4; $\Phi_F = 54.0$ %).
c – Experimental value of the oscillator strength

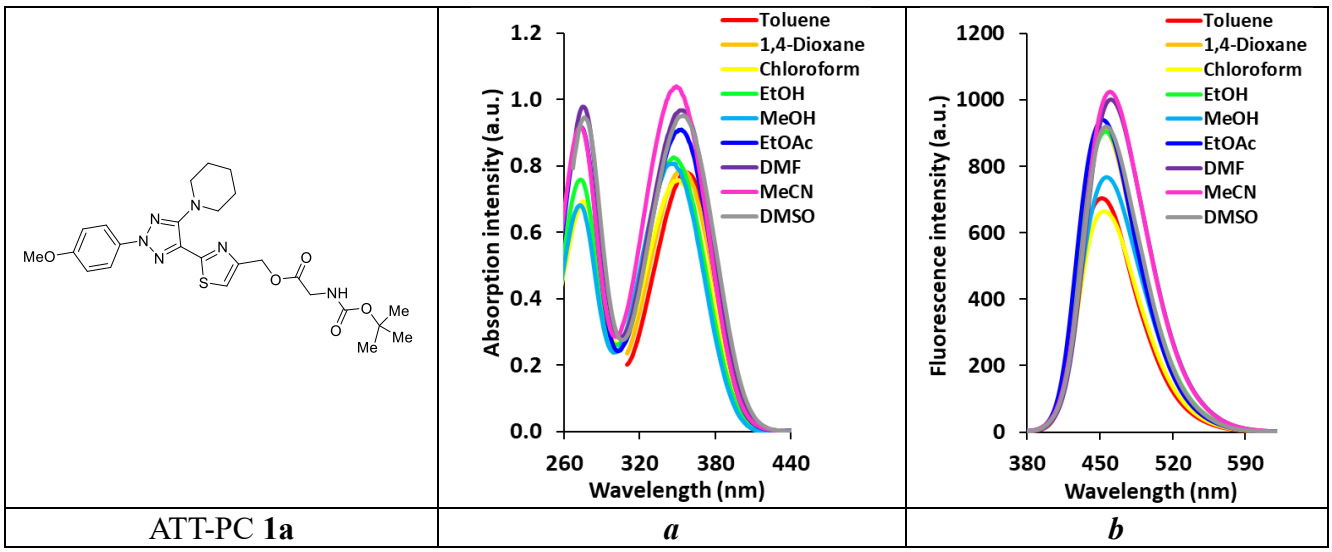

ATT-PC **1a**	***a***	***b***

Fig. S35. (*a*) Absorption (c = 5.0 × 10^{-5} M) and (*b*) fluorescence (c = 5.0 × 10^{-6} M) spectra of ATT-PC **1a** in different solvents.

Table S10. Characteristics of absorption spectra (c = 5×10^{-5} M) and emission spectra (c = 5×10^{-6} M) of ATT-PCs **1a** in different solvents

Entry	Solvents	λ_{max}[a], nm	ε, M^{-1} cm^{-1}	λ_{em}, nm	QY,[b] %	SS, nm/cm^{-1}	*f*[c]
1	Toluene	356	15600	452	69.6	96/5966	0.471
2	1,4-Dioxane	354	15820	453	84.4	99/6174	0.698
3	$CHCl_3$	350	15160	454	72.8	104/6545	0.679
4	EtOH	347	16500	455	74.6	108/6840	0.339
5	MeOH	348	16140	456	61.8	108/6806	0.665
6	EtOAc	353	18180	453	71.9	100/6254	0.966
7	DMF	352	19340	460	77.7	108/6670	0.723
8	MeCN	349	20800	460	66.2	111/6914	0.879
9	DMSO	355	19100	456	73.4	101/6239	0.783

a – long-wave maximum.
b – Relative QY, determined relative to the standard (quinine sulphate solution; c = 5.0 × 10^{-5} M in 0.1 M H_2SO_4; Φ_F = 54.0 %).
c – Experimental value of the oscillator strength

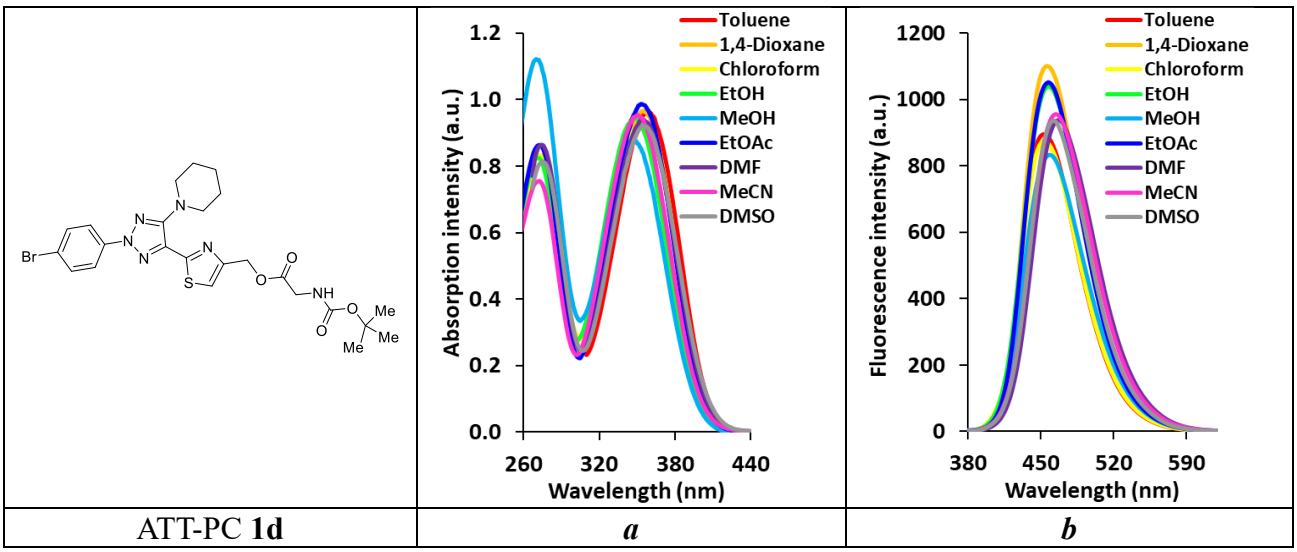

ATT-PC **1d**	***a***	***b***

Fig. S36. (*a*) Absorption (c = 5.0 × 10^{-5} M) and (*b*) fluorescence (c = 5.0 × 10^{-6} M) spectra of ATT-PC **1d** in different solvents.

Table S11. Characteristics of absorption spectra (c = 5×10^{-5} M) and emission spectra (c = 5×10^{-6} M) of ATT-PC **1d** in different solvents.

Entry	Solvents	λ_{max}[a], nm	ε, M^{-1} cm^{-1}	λ_{em}, nm	QY[b], %	SS, nm/cm^{-1}	*f*[c]
1	Toluene	359	19300	453	69.3	94/5780	0.531
2	1,4-Dioxane	354	19300	456	82.8	102/6319	1.018
3	$CHCl_3$	350	18400	453	72.9	103/6496	0.856
4	EtOH	349	18900	458	69.6	109/6819	0.850
5	MeOH	347	17600	459	60.7	112/7032	0.979
6	EtOAc	353	19700	457	69.7	104/6447	1.016
7	DMF	355	18800	467	76.5	112/6756	0.729
8	MeCN	351	19100	465	66.4	114/6985	0.819
9	DMSO	355	18400	463	75.5	108/6571	0.722

a – long-wave maximum.
b – Relative QY, determined relative to the standard (quinine sulphate solution; c = 5.0 × 10^{-5} M in 0.1 M H_2SO_4; Φ_F = 54.0 %).
c – Experimental value of the oscillator strength

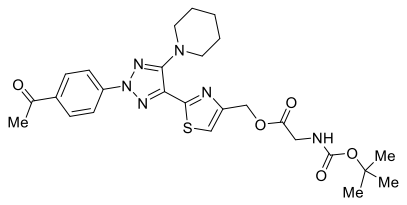	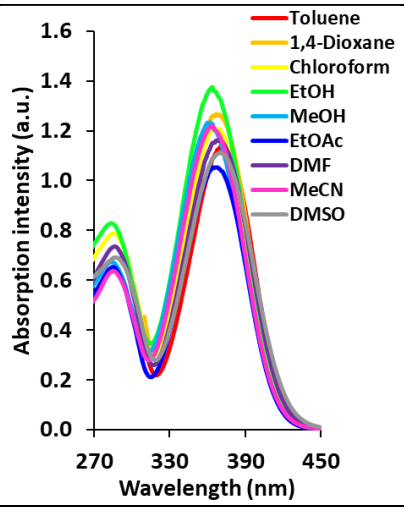	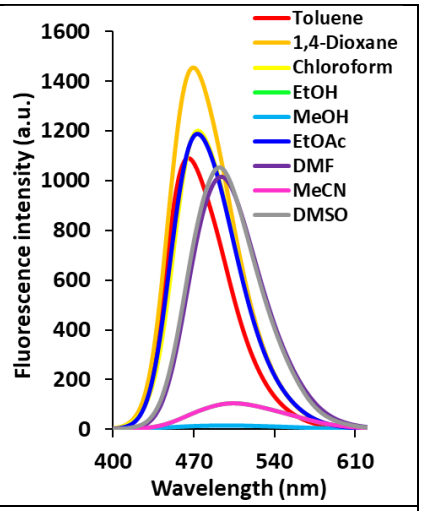
ATT-PC **1f**	***a***	***b***

Fig. S37. (*a*) Absorption (c = 5.0 × 10^{-5} M) and (*b*) fluorescence (c = 5.0 × 10^{-6} M) spectra of ATT-PC **1f** in different solvents.

Table S12. Characteristics of absorption spectra (c = 5×10^{-5} M) and emission spectra (c = 5×10^{-6} M) of ATT-PC **1f** in different solvents.

Entry	Solvents	λ_{max}[a], nm	ε, M^{-1} cm^{-1}	λ_{em}, nm	QY, %	SS[b], nm/cm^{-1}	*f* [c]
	Toluene	373	22800	465	70.9	92/5304	0.635
2	1,4-Dioxane	367	25300	470	81.2	103/5971	1.346
3	$CHCl_3$	364	24200	474	75.2	110/6375	1.030
4	EtOH	364	27500	504	7.5	140/7631	1.129
5	MeOH	362	24700	498	1.4	136/7544	0.955
6	EtOAc	364	21100	473	71.7	109/6331	0.781
7	DMF	369	23200	494	67.3	125/6857	0.797
8	MeCN	363	24400	491	27.9	128/7182	0.920
9	DMSO	370	22300	493	76.4	123/6743	0.821

a – long-wave maximum.
b – Relative QY, determined relative to the standard (quinine sulphate solution; c = 5.0 × 10^{-5} M in 0.1 M H_2SO_4; Φ_F = 54.0 %).
c – Experimental value of the oscillator strength

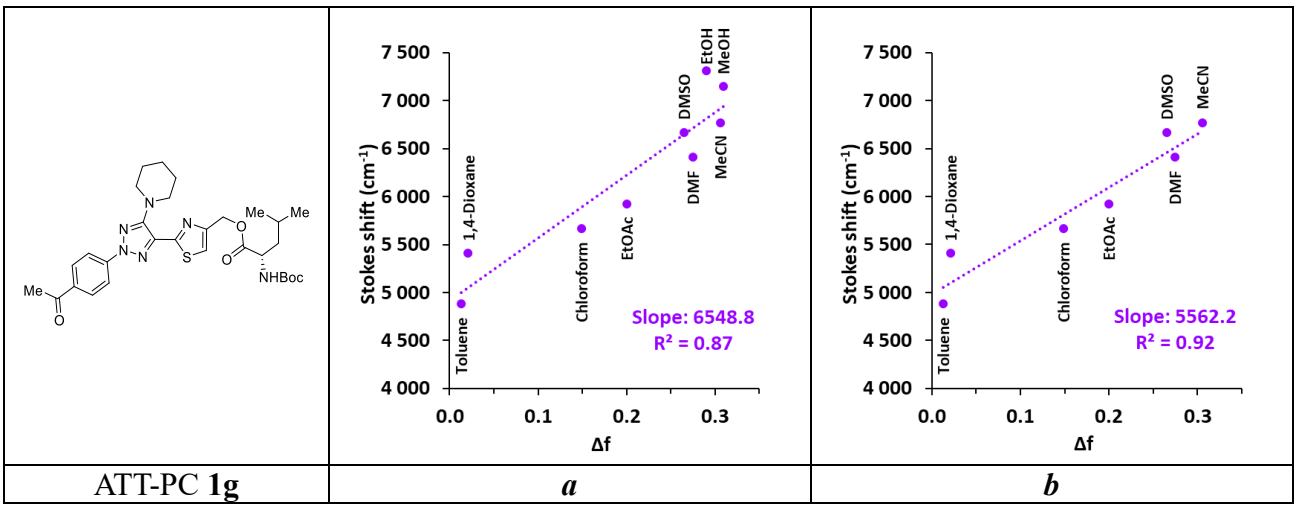

ATT-PC **1g**	***a***	***b***

Fig. 38. Solvent dependence of the Stokes shift for ATT-PC **1g** against the solvent orientation polarizability (Δf) (The Lippert-Mataga plot). Solvents used: (*a*) Toluene, 1,4-Dioxane, $CHCl_3$, EtOAc, DMSO, DMF, EtOH, MeCN, MeOH. (*b*) Toluene, 1,4-Dioxane, $CHCl_3$, EtOAc, DMSO, DMF, MeCN.

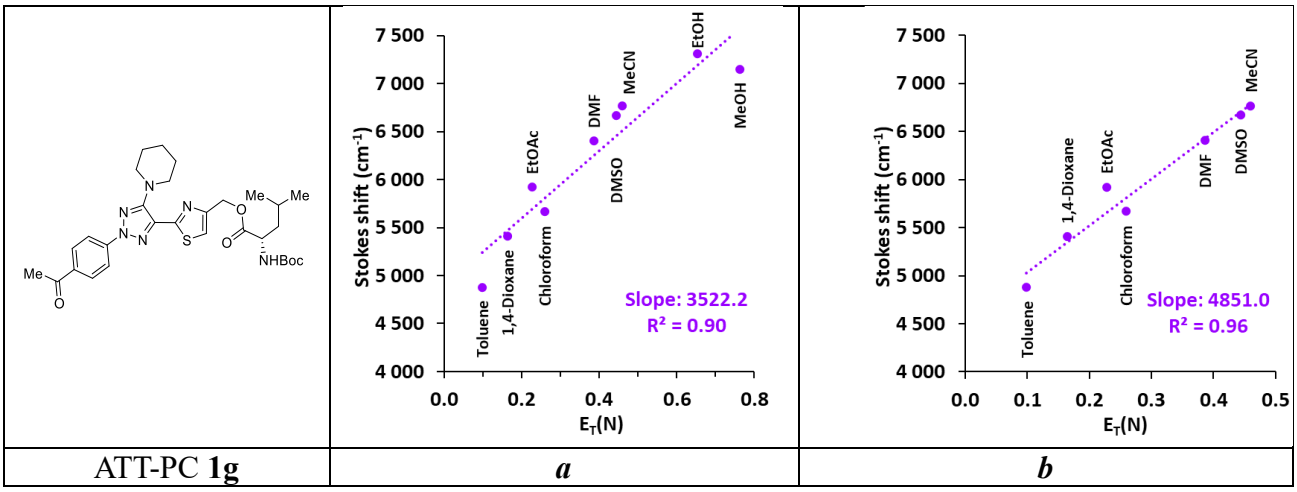

ATT-PC **1g**	***a***	***b***

Fig. S39. Solvent dependence of the Stokes shift for fluorophores **1g** against the macroscopic polarity solvent function (Dimrot-Reichart plots**)**. Solvents used: (*a*) Toluene, 1,4-Dioxane, EtOAc, $CHCl_3$, DMF, DMSO, MeCN, EtOH, MeOH. (*b*) Toluene, 1,4-Dioxane, EtOAc, $CHCl_3$, DMF, DMSO, MeCN.

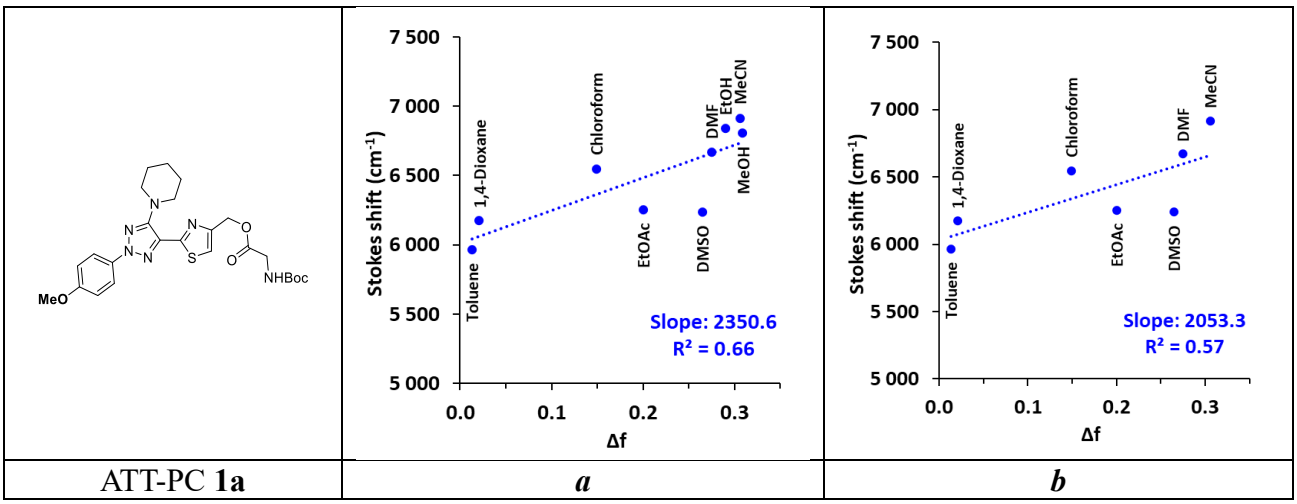

ATT-PC **1a**	***a***	***b***

Fig. S40. Solvent dependence of the Stokes shift for ATT-PC **1a** against the solvent orientation polarizability (Δf) (The Lippert-Mataga plot). Solvents used: (*a*) Toluene, 1,4-Dioxane, $CHCl_3$, EtOAc, DMSO, DMF, EtOH, MeCN, MeOH. (*b*) Toluene, 1,4-Dioxane, $CHCl_3$, EtOAc, DMSO, DMF, MeCN.

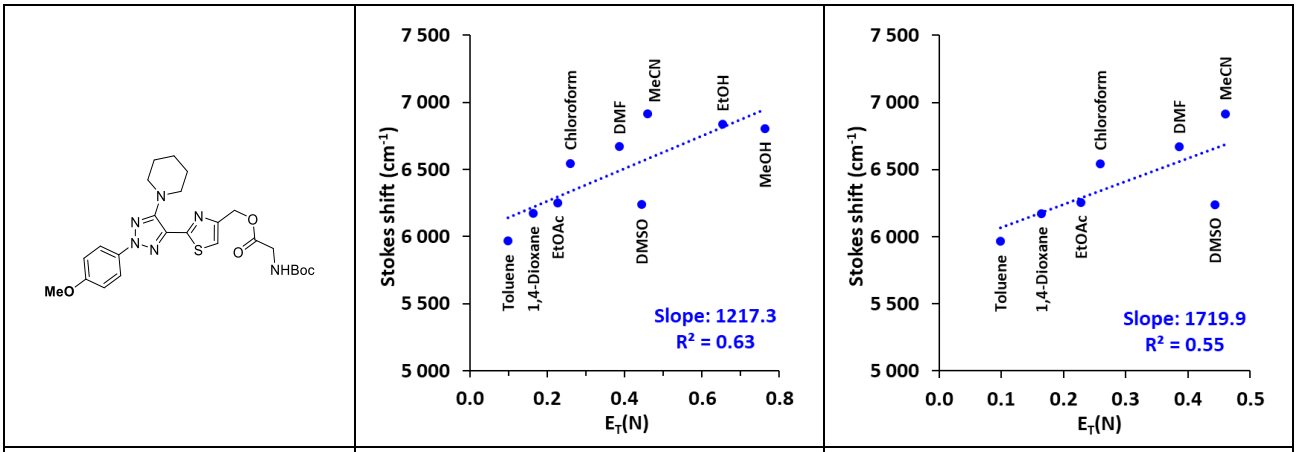

ATT-PC **1a**	***a***	***b***

Fig. S41. Solvent dependence of the Stokes shift for ATT-PC **1a** against the macroscopic polarity solvent function (Dimrot-Reichart plots**)**. Solvents used: (*a*) Toluene, 1,4-Dioxane, EtOAc, $CHCl_3$, DMF, DMSO, MeCN, EtOH, MeOH. (*b*) Toluene, 1,4-Dioxane, EtOAc, $CHCl_3$, DMF, DMSO, MeCN.

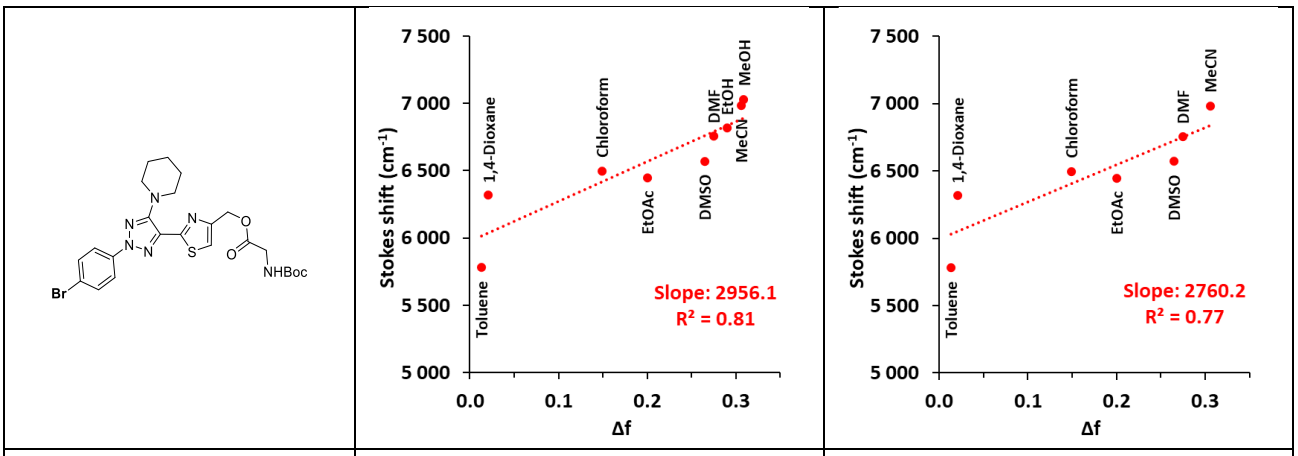

ATT-PC **1d**	***a***	***b***

Fig. S42. Solvent dependence of the Stokes shift for ATT-PC **1d** against the solvent orientation polarizability (Δf) (The Lippert-Mataga plot). Solvents used: (*a*) Toluene, 1,4-Dioxane, $CHCl_3$, EtOAc, DMSO, DMF, EtOH, MeCN, MeOH. (*b*) Toluene, 1,4-Dioxane, $CHCl_3$, EtOAc, DMSO, DMF, MeCN.

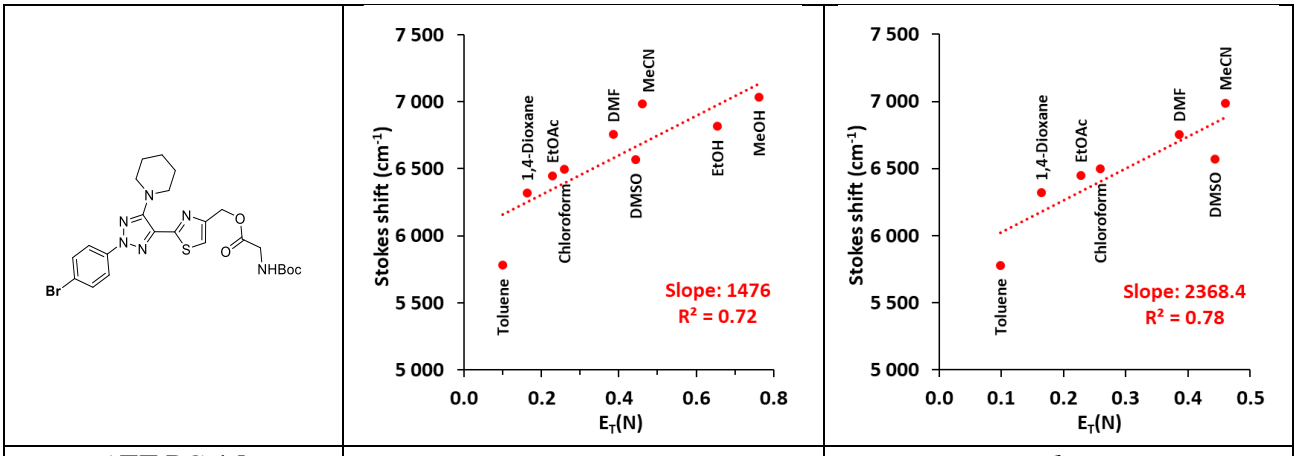

ATT-PC **1d**	***a***	***b***

Fig. S43. Solvent dependence of the Stokes shift for ATT-PC **1d** against the macroscopic polarity solvent function (Dimrot-Reichart plots). Solvents used: (*a*) Toluene, 1,4-Dioxane, EtOAc, $CHCl_3$, DMF, DMSO, MeCN, EtOH, MeOH. (*b*) Toluene, 1,4-Dioxane, EtOAc, $CHCl_3$, DMF, DMSO, MeCN.

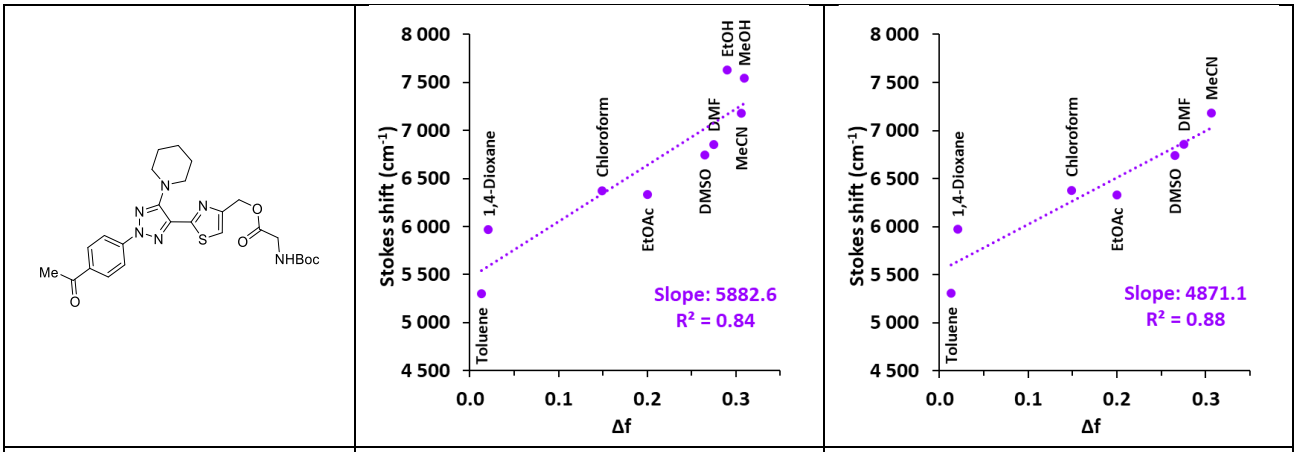

ATT-PC **1f**	***a***	***b***

Fig. S44. Solvent dependence of the Stokes shift for ATT-PC **1f** against the solvent orientation polarizability (Δf) (The Lippert-Mataga plot). Solvents used: (*a*) Toluene, 1,4-Dioxane, $CHCl_3$, EtOAc, DMSO, DMF, EtOH, MeCN, MeOH. (*b*) Toluene, 1,4-Dioxane, $CHCl_3$, EtOAc, DMSO, DMF, MeCN.

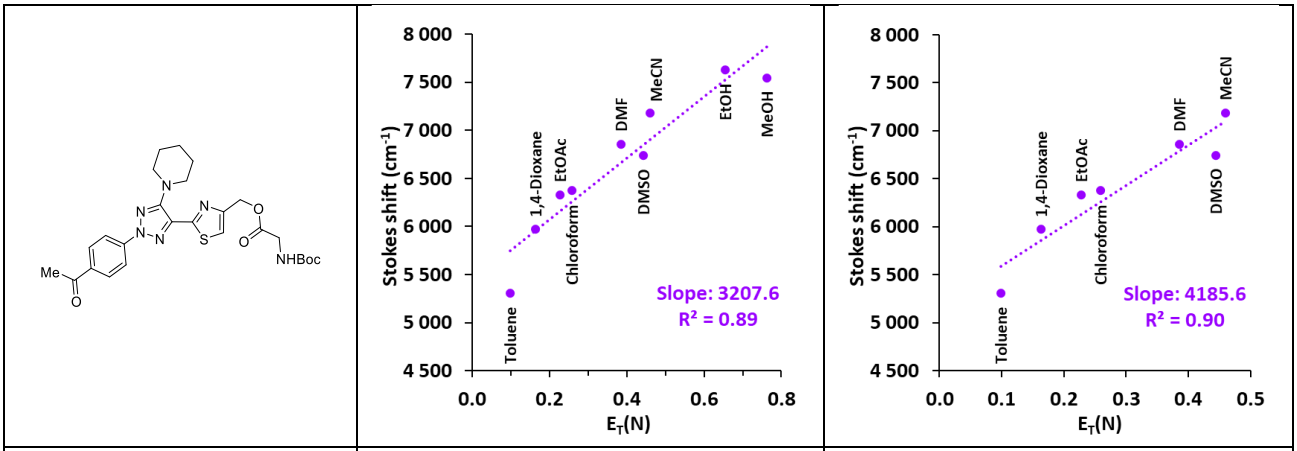

ATT-PC **1f**	***a***	***b***

Fig. S45. Solvent dependence of the Stokes shift for ATT-PC **1f** against the macroscopic polarity solvent function (Dimrot-Reichart plots). Solvents used: (*a*) Toluene, 1,4-Dioxane, EtOAc, $CHCl_3$, DMF, DMSO, MeCN, EtOH, MeOH. (*b*) Toluene, 1,4-Dioxane, EtOAc, $CHCl_3$, DMF, DMSO, MeCN.

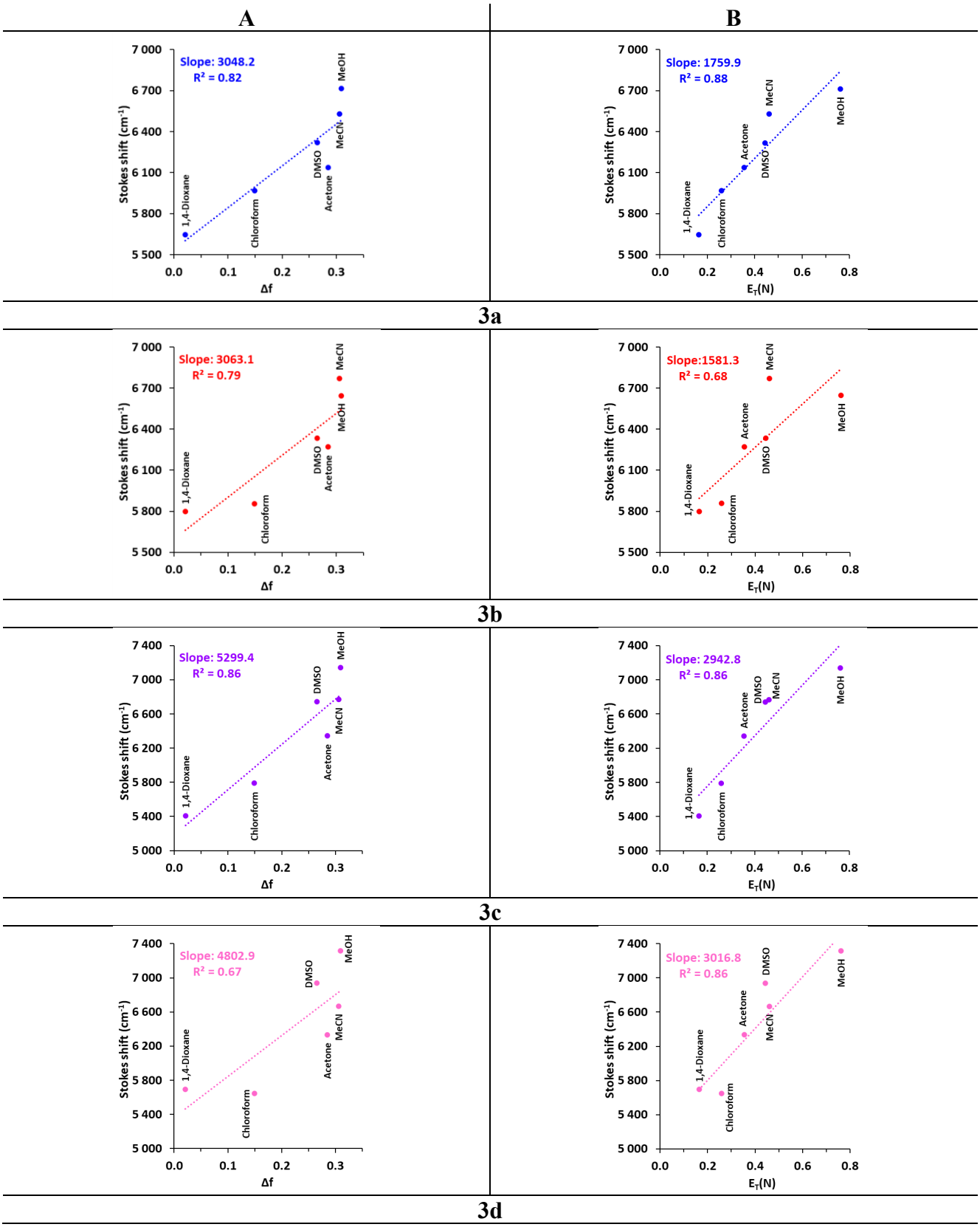

Fig. S46. Solvent dependence of the Stokes shift for ATTs-CH_2Cl **3a-d** against (A) the solvent orientation polarizability (Δf) (The Lippert-Mataga plot) and (B) the macroscopic polarity solvent function (Dimrot-Reichart plots). Solvents used: 1,4-Dioxane, $CHCl_3$, DMSO, Acetone, MeCN, MeOH.

Table S13. Photophysical data for the ATT-PCs **1a-q** in DMSO, DMSO-H_2O (1:9, v/v), DMSO-PBS (1/9, v/v, pH 7.4) mixtures with ($c = 5 \times 10^{-5}$ M for absorption and $c = 5 \times 10^{-6}$ M for emission).

Entry	Compd	Structure	Solvent	λ_{max}, nm	ε, $M^{-1}cm^{-1}$	λ_{em}, nm	QY[a], %	SS, nm/cm^{-1}
1	**1a**	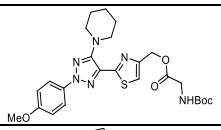	DMSO	276, 355	19100	456	73.4	101/6239
2			DMSO-H_2O	278, 355	17600	456	41.9	101/6239
3			DMSO-PBS	285, 376	16600	454	27.2	78/4569
4	**1b**	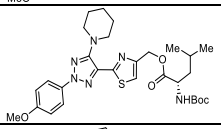	DMSO	280, 359	14700	455	89.1	96/5877
5			DMSO-H_2O	276, 354	16500	450	37.5	96/6026
6			DMSO-PBS	283, 371	16900	449	18.4	78/4682
7	**1c**	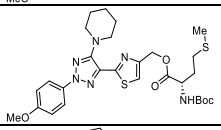	DMSO	276, 355	18700	456	74.6	101/6239
8			DMSO-H_2O	280, 354	17100	452	34.0	98/6125
9			DMSO-PBS	286, 379	17100	451	35.4	72/4212
10	**1d**	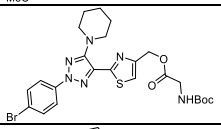	DMSO	276, 355	18400	463	75.5	108/6571
11			DMSO-H_2O	276, 355	16600	453	25.9	98/6094
12			DMSO-PBS	280, 364	16800	453	17.5	89/5397
13	**1e**	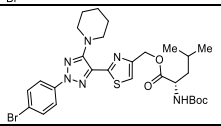	DMSO	278, 359	18500	462	85.8	103/6210
14			DMSO-H_2O	276, 355	16800	449	59.6	94/5897
15			DMSO-PBS	280, 362	17200	447	13.0	85/5253
16	**1f**	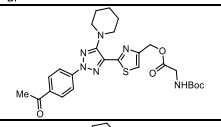	DMSO	287, 370	22300	493	76.4	123/6743
17			DMSO-H_2O	290, 368	18300	484	13.0	116/6513
18			DMSO-PBS	297, 392	15300	484	5.3	92/4849
19	**1g**	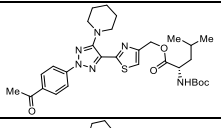	DMSO	288, 371	22100	493	62.6	122/6670
20			DMSO-H_2O	290, 369	20100	478	28.0	109/6180
21			DMSO-PBS	298, 393	16700	476	43.2	83/4437
22	**1h**	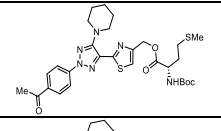	DMSO	287, 370	23300	493	77.0	122/6702
23			DMSO-H_2O	290, 370	20000	482	23.8	112/6280
24			DMSO-PBS	294, 385	19600	483	7.7	98/5270
25	**1i**	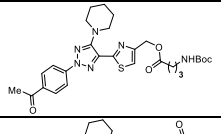	DMSO	288, 370	24800	493	76.3	123/6743
26			DMSO-H_2O	290, 368	20700	483	22.5	115/6470
27			DMSO-PBS	299, 398	17600	483	9.4	85/4422
28	**1j**	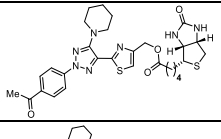	DMSO	288, 371	23900	492	69.0	121/6629
29			DMSO-H_2O	265, 368	20200	492	12.8	124/6849
30			DMSO-PBS	292, 377	19400	488	12.8	111/6033
31	**1k**	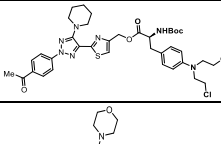	DMSO	288, 371	23800	492	35.5	121/6629
32			DMSO-H_2O	262, 372	21600	477	23.8	105/5917
33			DMSO-PBS	264, 376	21500	476	26.5	100/5587
34	**1l**	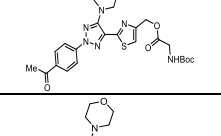	DMSO	285, 364	25400	488	80.6	124/6981
35			DMSO-H_2O	287, 362	20500	482	0.6	120/6877
36			DMSO-PBS	290, 367	18300	463	0.5	96/5650
37	**1m**	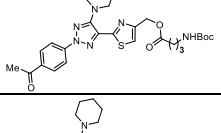	DMSO	285, 364	23800	485	80.2	121/6854
38			DMSO-H_2O	274, 364	19900	480	1.2	116/6639
39			DMSO-PBS	290, 390	13700	472	1.8	82/4455
40	**1n**	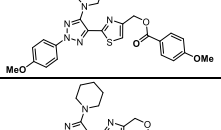	DMSO	268, 354	16800	457	75.2	103/6367
41			DMSO-H_2O	262, 355	14600	455	29.2	100/6191
42			DMSO-PBS	284, 380	16400	453	24.8	73/4241
43	**1o**	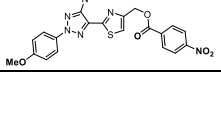	DMSO	274, 355	18500	464	0.7	109/6617
44			DMSO-H_2O	273, 358	16500	407	0.1	49/3363
45			DMSO-PBS	283, 376	17500	417	0.1	41/2615

46	**1p**	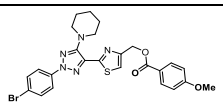	DMSO	268, 356	16200	463	75.9	107/6492
47			DMSO-H_2O	260, 356	13300	452	30.9	96/5966
48			DMSO-PBS	279, 378	15600	449	24.1	71/4183
49	**1q**	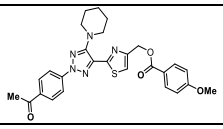	DMSO	262, 371	21500	493	68.1	122/6670
50			DMSO-H_2O	259, 371	17800	481	27.0	110/6164
51			DMSO-PBS	269, 397	16800	479	27.5	82/4312

a –The molar extinction coefficient for the long-wave maximum is given.
b – Relative QY, determined relative to the standard (quinine sulphate solution; c = 5.0 × 10^{-5} M in 0.1 M H_2SO_4; Φ_F = 54.0 %).

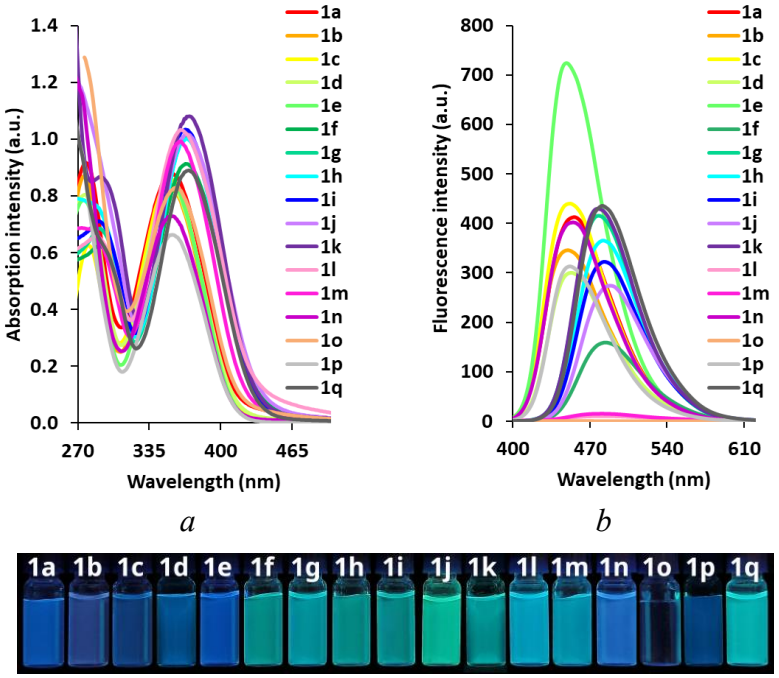

Fig. S47. Spectra (*a*) of absorption (c = 5 × 10^{-5} M), (*b*) of emission (c = 5 × 10^{-6} M) of ATT-PCs **1a-q** in DMSO-H_2O (1:9, v/v) and (c) photographs of solutions upon UV irradiation (λ = 365 nm).

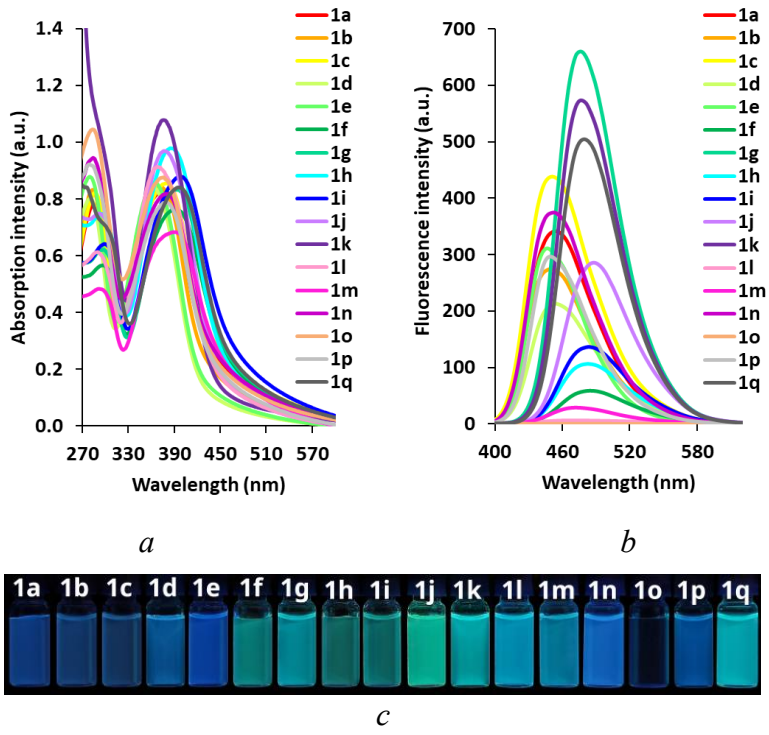

Fig. S48. Spectra (*a*) of absorption (c = 5 × 10^{-5} M), (*b*) of emission (c = 5 × 10^{-6} M) of ATT-PCs **1a-q** in DMSO-PBS (1:9, v/v, pH 7.4) and (*c*) photographs of solutions upon UV irradiation (λ = 365 nm).

6. Quantum Mechanical Calculation data for ATT-PCs 1a, d, f

Table S14. Thermochemical characteristics of ATT-PCs **1a, d, f** rotamers in DMSO
(Energy differences at T = 298.15 K and p = 1.00 atm (in kJ/mol))

Compd	Rotamer	ΔH/(kJ/mol)	ΔG/(kJ/mol)
1a	A	0.0	1.2
	B	0.1	0.0
1d	A	-	-
1f	A	0.0	0.0
	B	0.1	0.6

Compd	S_0		S_{1r}	
1a	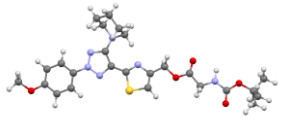	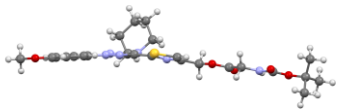	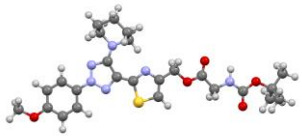	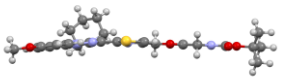
1d	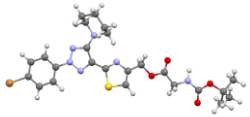	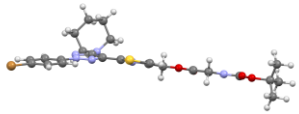	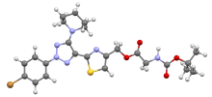	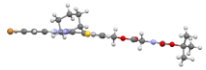
1f	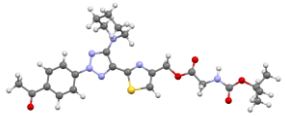	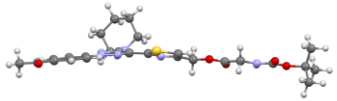	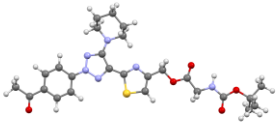	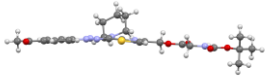

Fig. S49. Optimized geometries of compounds **1a**, **d** and **f** in their *GS* and *ES* in DMSO, depicted from two orthogonal viewpoints. Level of theory: DFT/IEF-PCM(UFF). Legend of colours: white (H), grey (C), lilac (N), yellow (S), red (O), and brown (Br).

Table S15. Selected bonds lengths (in Å) torsion (°) for the *GS* (S_0) optimized geometries of ATT-PCs **1a, d, f** in DMSO

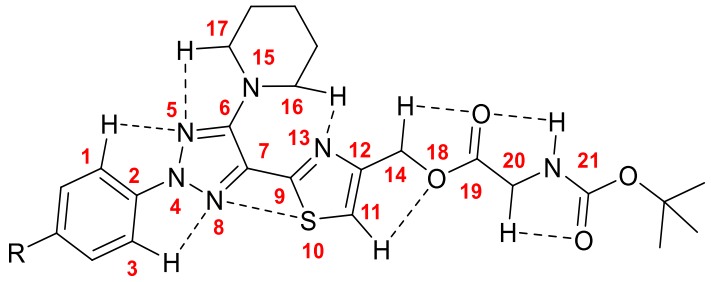

Entry	Compd	C2-C4	N4-N5	N5-C6	C6-C7	N8-C7	N4-N8	C6-N15	C7-C9	C9-S10	S10-C11	C11-C12	C12-N13	C9-N13	C12-C14	C14-O18	θ_{Ar}	θ_T	θ
1	**1a**	1.418	1.346	1.343	1.437	1.345	1.321	1.377	1.448	1.763	1.735	1.367	1.377	1.313	1.498	1.444	3.75	14.03	0.18
2	**1d**	1.413	1.348	1.342	1.441	1.341	1.324	1.375	1.449	1.762	1.734	1.367	1.377	1.312	1.498	1.443	1.63	14.47	0.27
3	**1f**	1.409	1.350	1.340	1.444	1.338	1.326	1.374	1.450	1.761	1.734	1.367	1.367	1.312	1.498	1.443	2.25	16.97	0.23

Table S16. Selected bonds lengths (in Å) torsion (°) for the *ES* (S_1) optimized geometries of ATT-PCs **1a, d, f** in DMSO

Entry	Compd	C2-C4	N4-N5	N5-C6	C6-C7	N8-C7	N4-N8	C6-N15	C7-C9	C9-S10	S10-C11	C11-C12	C12-N13	C9-N13	C12-C14	C14-O18	θ_{Ar}	θ_T	θ
1	**1a**	1.369	1.344	1.333	1.465	1.339	1.353	1.339	1.413	1.770	1.719	1.367	1.377	1.313	1.498	1.444	0.50	1.87	1.46
2	**1d**	1.370	1.339	1.336	1.466	1.339	1.355	1.342	1.407	1.776	1.722	1.376	1.360	1.339	1.495	1.496	1.01	3.36	1.37
3	**1f**	1.368	1.337	1.339	1.485	1.338	1.354	1.339	1.413	1.770	1.719	1.374	1.363	1.332	1.495	1.434	0.10	0.41	3.44

Table S17. Selected lengths (in Å) for noncovalet interaction for the *GS* (S_0) optimized geometries of ATT-PCs **1a**, **d**, **f** in DMSO[a]

Entry	Compd	C1H-N5	C3H-N8	N8-S10	C17-N5	C16H-N13	C11H-O18	C14H-O19	C19O-N21H	C20H-C21O
1	**1a**	2.495	2.512	3.035	2.484	2.277	2.615	2.667	2.294	2.824
2	**1d**	2.482	2.502	3.036	2.480	2.278	2.614	2.651	2.295	2.831
3	**1f**	2.481	2.499	3.042	2.477	2.278	2.615	2.656	2.295	2.835

a - Van der Wals radii: R_H = 1.2 Å; R_C = 1.85 Å; R_N = 1.50 Å; R_O = 1.40 Å; R_{Cl} = 1.80 Å; R_S = 1.85

Table S18. Selected lengths (in Å) for noncovalet interaction for the *ES* (S_1) optimized geometries of ATT-PCs **1a**, **d**, **f** in DMSO[a]

Entry	Compd	C1H-N5	C3H-N8	N8-S10	C17-N5	C16H-N13	C11H-O18	C14H-O19	C19O-N21H	C20H-C21O
1	**1a**	2.486	2.455	2.690	2.355	2.115	2.577	2.622	2.278	2.813
2	**1d**	2.461	2.446	2.886	2.321	2.080	2.572	2.631	2.281	2.813
3	**1f**	2.479	2.451	2.887	2.301	2.061	2.578	2.625	2.281	2.811

a - Van der Wals radii: R_H = 1.2 Å; R_C = 1.85 Å; R_N = 1.50 Å; R_O = 1.40 Å; R_{Cl} = 1.80 Å; R_S = 1.85

Table S19. Computed photophysical characteristics of ATT-conjugates **1a**, **d**, **f** in DMSO[a].

Compd	$c_{(HL)}$	ΔE_{01}	f_{01}	$c_{(LH)}$	ΔE_{10}	f_{10}	μ_0	μ_{1v}	μ_{1r}	μ_{0v}	$\theta_{0\text{-}1v}$	$\theta_{0\text{-}1vr}$	$\theta_{0\text{-}1v}$
1a	0.6860	3.4937	0.8888	-0.6908	2.7099	0.9110	4.6	9.2	9.0	4.6	8.7	11.3	8.8
1d	0.6680	3.4462	0.8674	-0.6923	2.6823	0.9873	3.3	7.5	8.1	3.8	18.7	25.0	21.3
1f	0.6681	3.3437	1.0054	0.68300	2.2504	0.9747	6.7	12.8	13.7	7.6	11.5	10.4	5.1

a - absorption wavelength (λ_{01}, nm) and oscillator strength (f_{01}), emission wavelength (λ_{10}, nm) and oscillator strength (f_{10}), modulus of the electric dipole moments of the ground state (μ_0, D), of the vertical FC excited state (μ_{1v}, D), and of the relaxed excited state (μ_{1r}, D), and angles formed by the directions of the electric dipole moment vectors (($\theta_{0,1v}$, deg) and ($\theta_{0,1r}$, deg)).

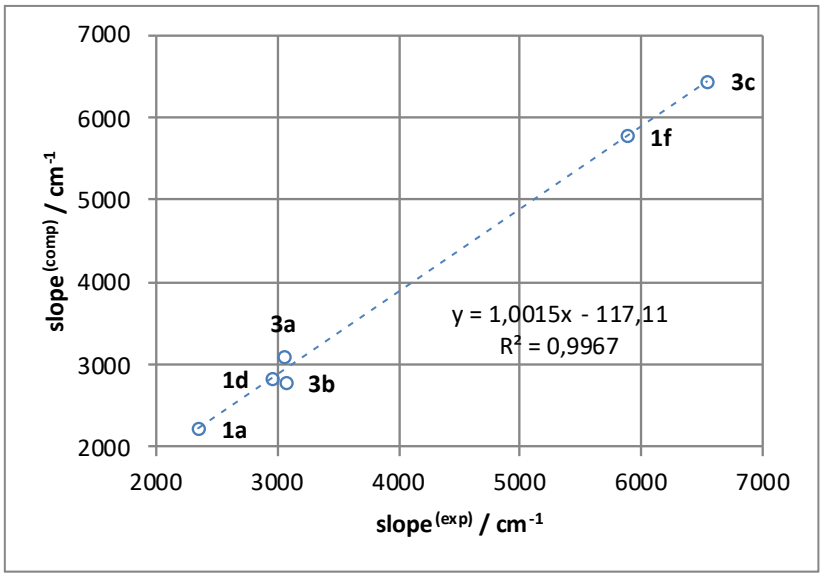

Fig. 50. Computed and experimental values of the slopes for the selected systems.

7. Photodissociation of ATT-PCs 1a-q

Photorelease investigations were performed on a reactor Acceled, Penn Photon Devices, LLC 1055 Mensch Dam Road Pennsburg, PA 18073, USA equipped with LED (365 and 420 nm). The photon flux ($q_{n,p}$) was determined using potassium ferrioxalate actinometry. The measured values were:

1) $q_{n,p} = 1.404 \times 10^{-7}$ einstein·s^{-1} (radiant power (P_{LED}) is 0.046 W) for λ = 365 nm at 10% of the LED's maximum output power (I_{ir} = 10%);
2) $q_{n,p} = 2.793 \times 10^{-7}$ einstein·s^{-1} (P_{LED} = 0.092 W) for λ = 365 nm at I_{ir} = 20%;
3) $q_{n,p} = 2.046 \times 10^{-7}$ einstein·s^{-1} (P_{LED} = 0.058 W) for λ = 420 nm at I_{ir} = 20%.

The photodissociation quantum yields (Q_U) were calculated based on these photon flux values.

The rate constant (k) was determined using the derived equation: $\ln(I_0 - I_\infty)/(I_t - I_\infty) = kt$; where I_0 is the initial intensity of sample solution, I_∞ is the intensity of this solution at the end of the transformation, and I_t is intensity of the sample at time t. The observed rate constant (k) and standard deviation were determined from three kinetic experiments for each sample.

HPLC-HRMS analysis of the photodissociacion of compounds 1b, 1e, 1g, 1i and 1j.

General procedure for photolysis of 1b, 1e, 1g, 1i** and **1j.

Compound **1** (2 mg) was dissolved in a quartz tube in MeCN-H_2O (1:9, v/v) (20 ml). The solution was irradiated in a photoreactor at a wavelength of 365 nm or 420 nm and a light intensity of 10, 20 and 50%. At regular interval of time, an 1 mL aliquots were taken and injected into Agilent 6545 Q-TOF (Agilent Technologies Inc., Santa Clara, CA, USA) with LC/MS system. HPLC-HRMS analysis of the photodissociation of compounds **1b**, **1e**, **1g, 1i** and **1j** was performed on an Agilent 1290 Infinity II HPLC system connected with a quadrupole time-of-flight (Q-TOF) accurate mass detector (Agilent 6545 Q-TOF LC-MS, Agilent Technologies, Santa Clara, USA). Chromatographic separations were performed using a "Zorbax Eclipse Plus C18" (2.1 mm × 50 mm, 1.8 μm, Agilent Technologies, p/n 959757-902) column with an additional 5 mm guard column. The column thermostat temperature was 35°C and the injected volume was 1 μL. The mobile phase was prepared from solvent A, containing 0.1% (v/v) formic acid in water and solvent B, containing 0.1% formic acid (v/v) in acetonitrile. Gradient elution was carried out according to the following program: the concentration of solvent B changed linearly over 15 min from 5% to 100%, which was kept for 2 min. Flow rate was kept 0.4 mL/min. The Q-TOF instrument was operated with an electrospray source in positive and negative ion modes using the following conditions: drying gas temperature, 350 °C (nitrogen, 10 L/min); nebulizer pressure, 40 psi; capillary voltage, 3500 V; and fragmentor voltage, 90 V. Ions were scanned in the m/z range of 100–1700 and the acquisition rate was 1.5 spectra/s. The elemental composition of the detected compounds was confirmed by measuring the accurate mass with an error of no more than 5 ppm and the nature of the isotopic distribution. Determination of the yield of L-leucine in the course of reactions was carried out by LC-HRMS on an Agilent 1290 Infinity II HPLC system connected with a Q-TOF accurate mass spectrometer Agilent 6545 Q-TOF LC-MS (Agilent Technologies, USA) under the analysis conditions used to study the reaction progress.

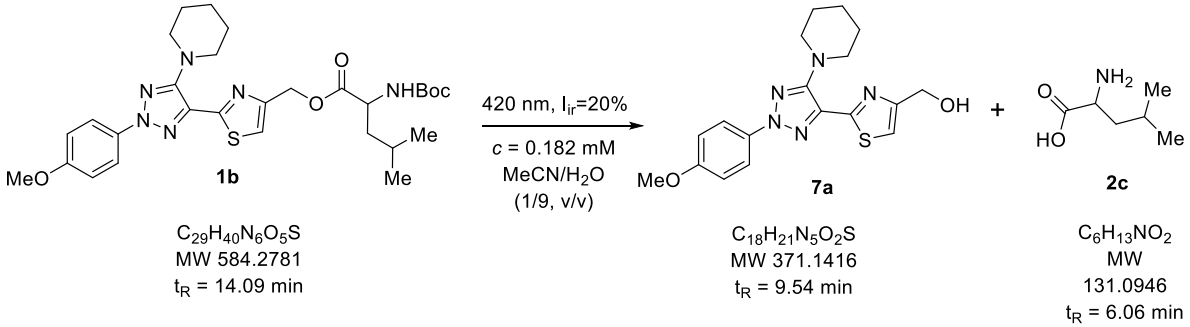

Scheme S8. Photodissociation of ATT-PC **1b**.

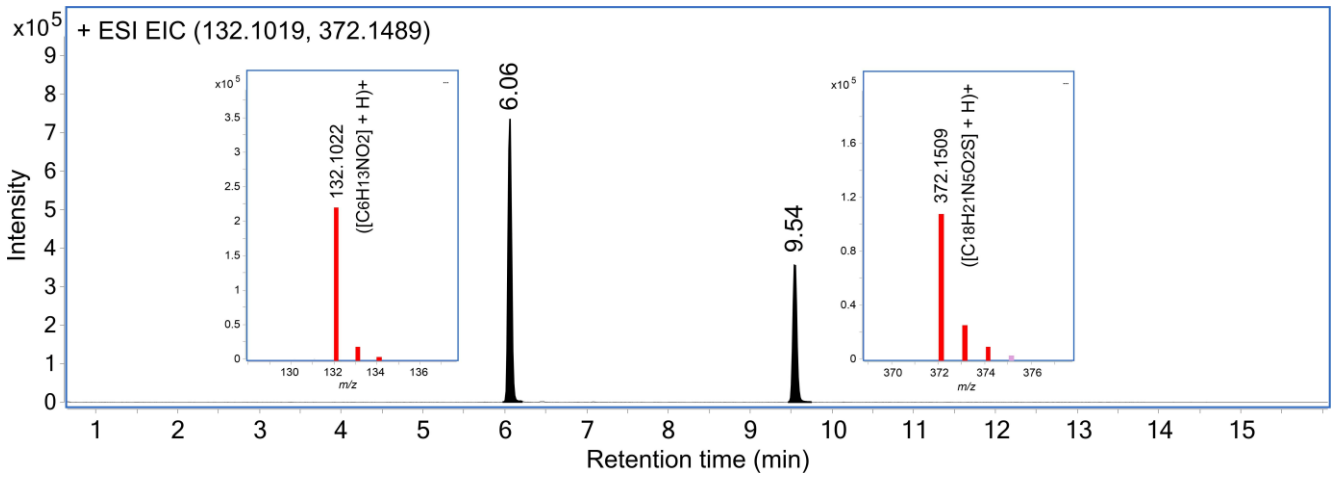

Fig. S51. Extracted ion chromatograms at t_R = 6.06 min and 9.54 min, and the corresponding mass spectra at the end of the experiment, obtained upon irradiation (λ_{ir} = 420 nm, 20% power) of an ATT-PC **1b** solution in MeCN-H_2O (1:9, v/v). The observed peaks correspond to photodissociation products **7a** and **2c**. (It should be noted that the intensity of the peaks depends on the ionization efficiency and therefore it is not correct to relate it to the amount of substance).

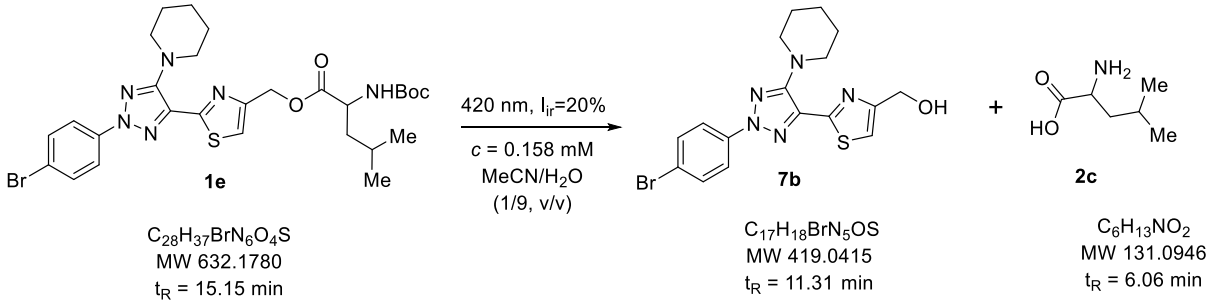

Scheme S9. Photodissociation of ATT-PC **1e**.

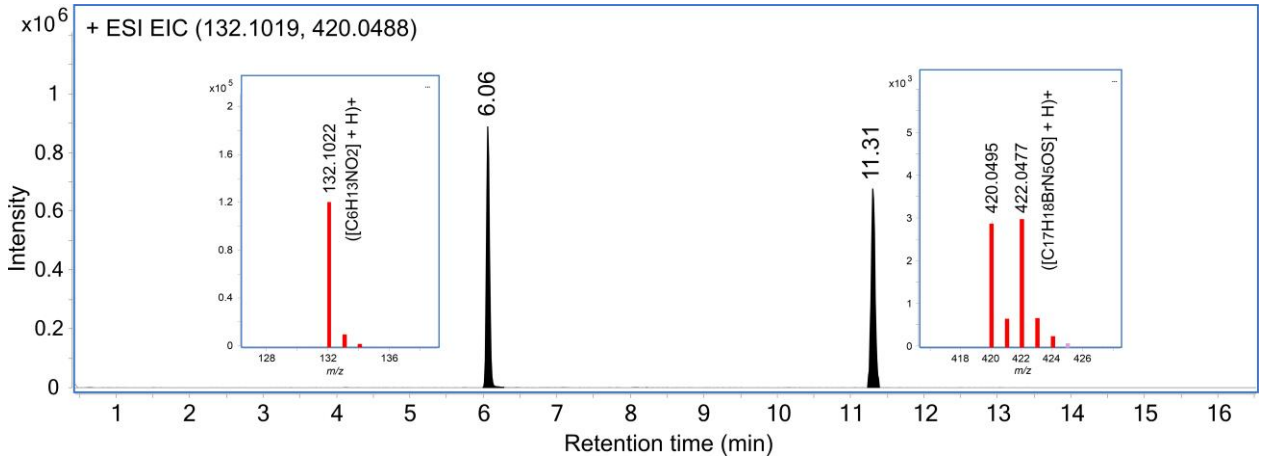

Fig. S52. Extracted ion chromatograms at t_R = 6.06 min and 11.31 min, and the corresponding mass spectra at the end of the experiment, obtained upon irradiation (λ_{ir} = 420 nm, 20% power) of an ATT-PC **1e** solution in MeCN-H_2O (1:9, v/v). The observed peaks correspond to photodissociation products **7b** and **2c**. (It should be noted that the intensity of the peaks depends on the ionization efficiency and therefore it is not correct to relate it to the amount of substance)

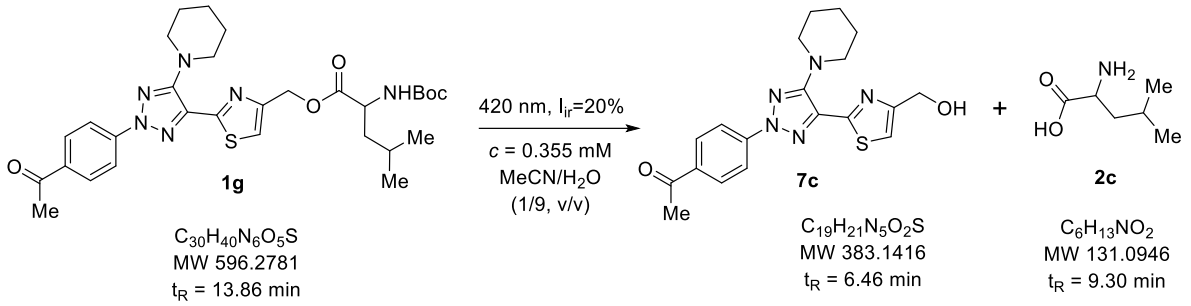

Scheme S10. Photodissociation of ATT-PC **1g.**

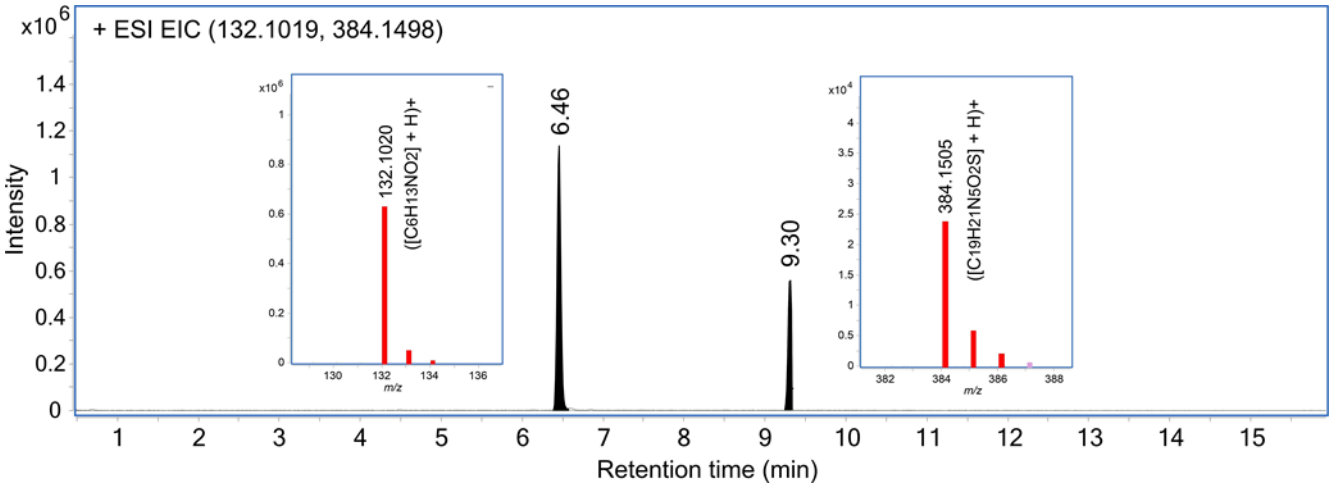

Fig. S53. Extracted ion chromatograms at t_R = 6.45 min and 9.29 min, and the corresponding mass spectra at the end of the experiment, obtained upon irradiation (λ_{ir} = 420 nm, 20% power) of an ATT-PC **1g** solution in MeCN-H_2O (1:9, v/v). The observed peaks correspond to photodissociation products **7c** and **2c**. (It should be noted that the intensity of the peaks depends on the ionization efficiency and therefore it is not correct to relate it to the amount of substance).

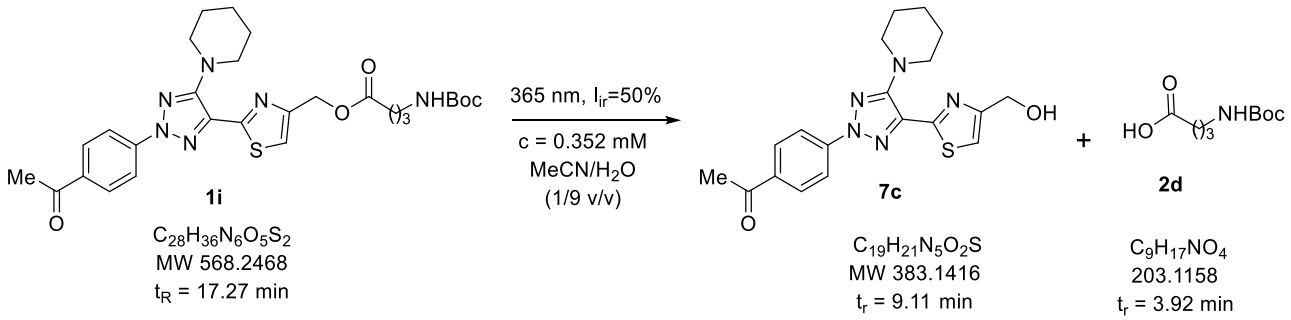

Scheme S11. Photodissociation of ATT-PC **1i.**

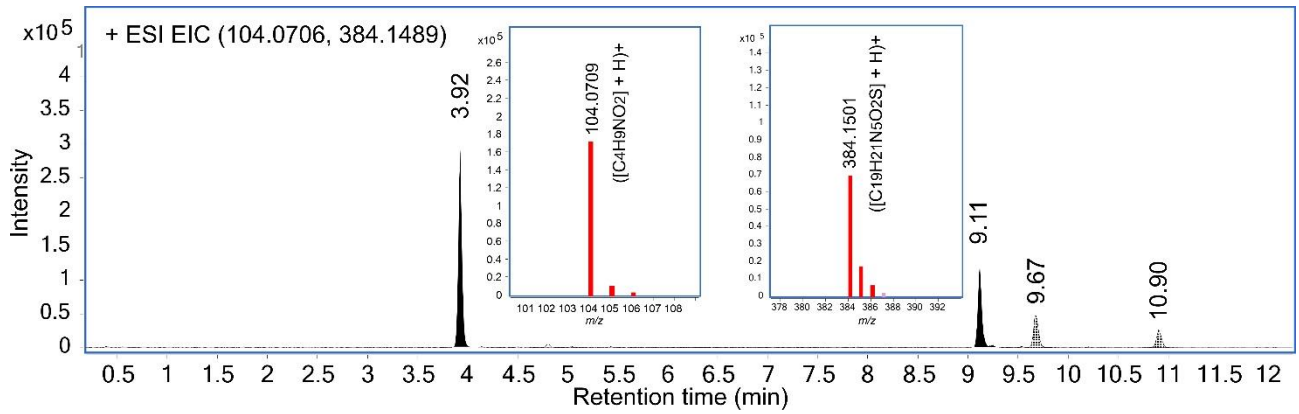

Fig. S54. Extracted ion chromatograms at t_R = 3.92 min and 9.11 min, and the corresponding mass spectra at the end of the experiment, obtained upon irradiation (λ_{ir} = 365 nm, 50% power) of an ATT-PC **1i** solution in MeCN-H_2O (1:9, v/v). The observed peaks correspond to photodissociation products **7c** and **2d**. (It should be noted that the intensity of the peaks depends on the ionization efficiency and therefore it is not correct to relate it to the amount of substance).

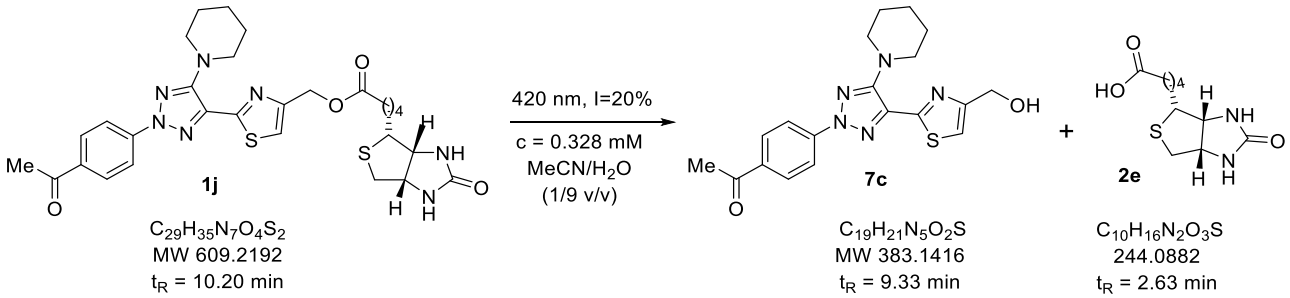

Scheme S12. Photodissociation of ATT-PC **1j** in MeCN/H_2O.

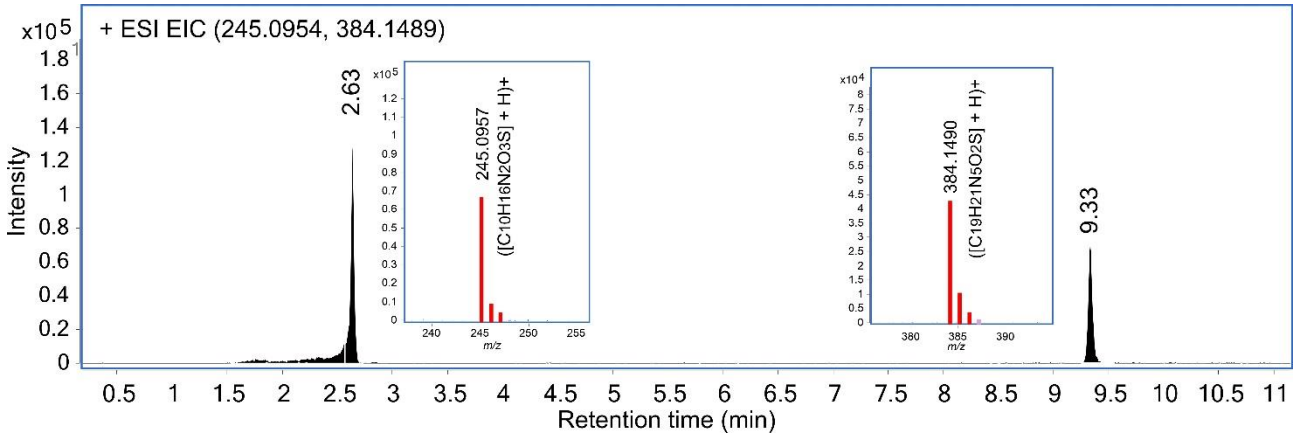

Fig. S55. Extracted ion chromatograms at t_R = 2.63 min and 9.33 min, and the corresponding mass spectra at the end of the experiment, obtained upon irradiation (λ_{ir} = 420 nm, 20% power, argon atmosphere) of an ATT-PC **1j** solution in MeCN-H_2O (1:9, v/v). The observed peaks correspond to photodissociation products **7c** and **2e**. (It should be noted that the intensity of the peaks depends on the ionization efficiency and therefore it is not correct to relate it to the amount of substance).

Table S20. Photophysical data for the ATT-CH_2OH **7a-c** in DMSO, DMSO-H_2O (1:9, v/v) and DMSO-PBS (1:9, v/v; pH 7.4) with a concentration of $c = 5 \times 10^{-5}$ M for absorption and $c = 5 \times 10^{-6}$ M for emission.

Entry	Compd	Structure	Solvent	λ_{max}, nm	ε, $M^{-1}cm^{-1}$	λ_{em}, nm	QY[a], %	SS, nm/cm^{-1}
1			DMSO	353	17900	451	91	98/6156
2	**7a**	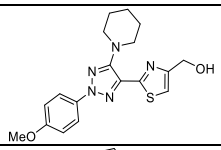	DMSO-H_2O	340	14500	460	70	120/7673
3			DMSO-PBS	340	15000	461	68	121/7720
4			DMSO	354	18900	458	32	104/6415
5	**7b**	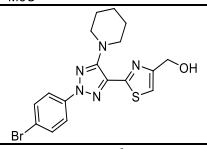	DMSO-H_2O	350	16200	462	26	112/6926
6			DMSO-PBS	363	14800	463	26	100/5950
7			DMSO	370	23400	492	56	122/6702
8	**7c**	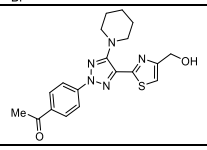	DMSO-H_2O	360	16500	495	1	135/7576
9			DMSO-PBS	363	16300	487	1	124/7014

a – Relative QY, determined relative to the standard (quinine sulphate solution; c = 5.0×10^{-5} M in 0.1 M H_2SO_4; $\Phi_F = 54.0$ %).

Table S21. Time-dependent release of *N*-Boc-Leu (**2c**) during photodissociation of photocage **1g** (c = 0.084 mM) in MeCN-H_2O (1:9, v/v) mixture upon irradiation (λ_{ir} = 420 нм, I_{ir} = 20%, with/without argon atmosphere), with sampling at varying time intervals (ranging from 5 to 40 minutes).

Entry	Time, min.	Air	Ar
		Yield of *N-Boc*-Leu **2c**, %	Yield of *N-Boc*-Leu **2c**, %
1	10	9.1	-
2	15	-	18.9
3	30	22.7	29.7
4	50	24.4	33.6
5	80	25.9	36.2
6	120	23.2	39.6
7	150	-	40.1

1a in DMSO/PBS (pH 7.4) (1/9, v/v), λ_{ir} = 420 nm, I_{ir} = 20%

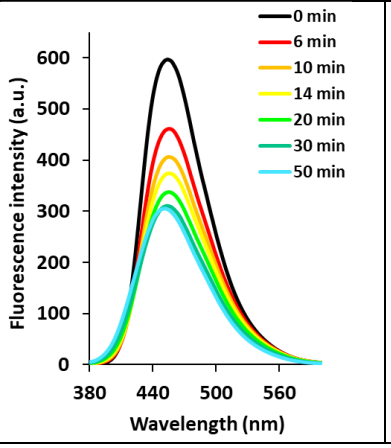

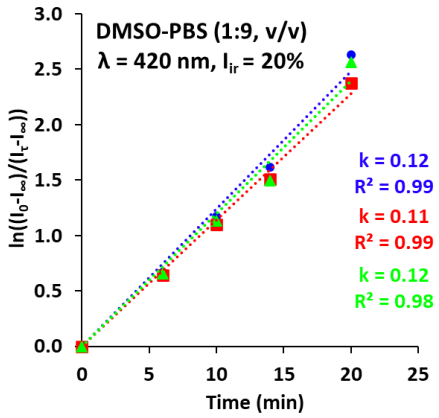

1b in DMSO-PBS (pH 7.4) (1:9, v/v), λ_{ir} = 420 nm, I_{ir} = 20%

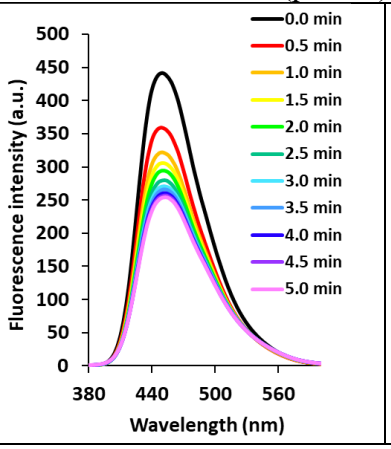

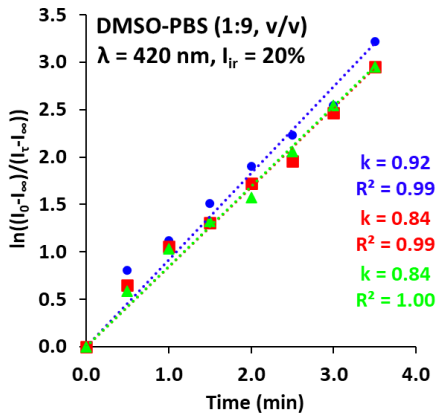

1d in DMSO-PBS (pH 7.4) (1:9, v/v), λ_{ir} = 420 nm, I_{ir} = 20%

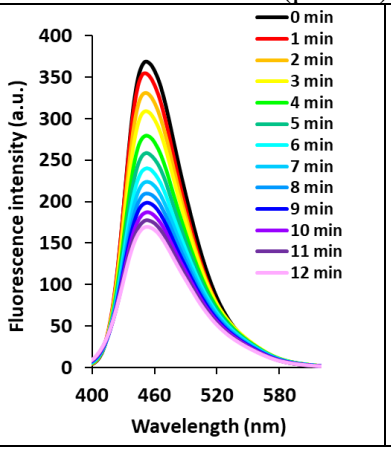

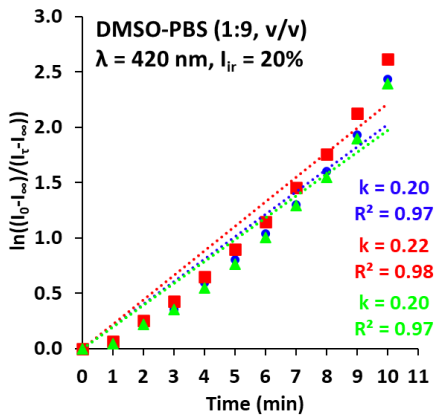

1e in DMSO-PBS (pH 7.4) (1/9, v/v), λ_{ir} = 420 nm, I_{ir} = 20%

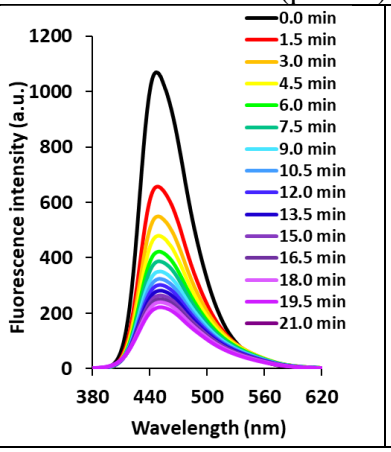

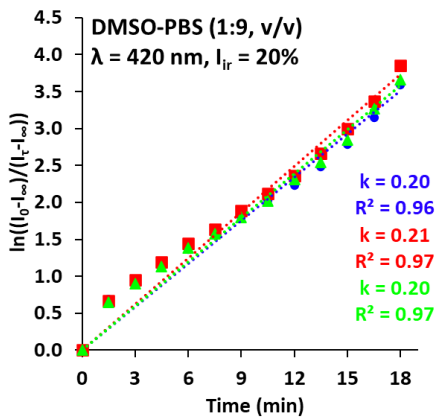

1f in DMSO-PBS (pH 7.4) (1:9, v/v), λ_{ir} = 420 nm, I_{ir} = 20%

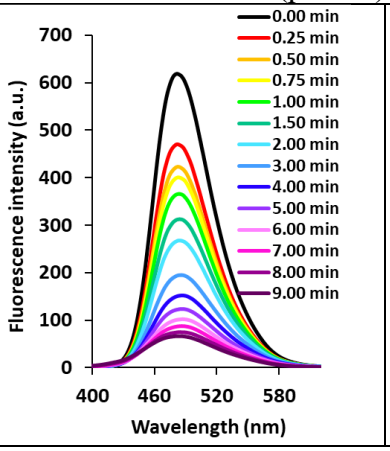

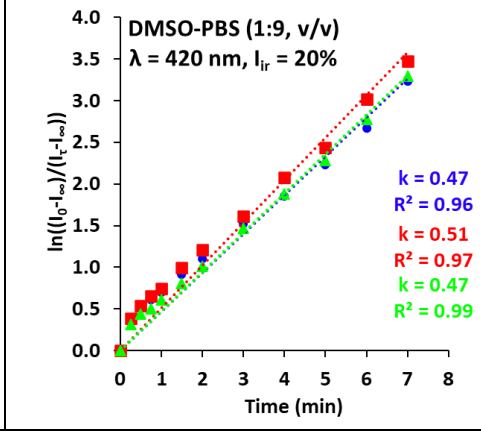

1f in MeCN-H_2O (1:9, v/v), λ_{ir} = 420 nm, I_{ir} = 20%

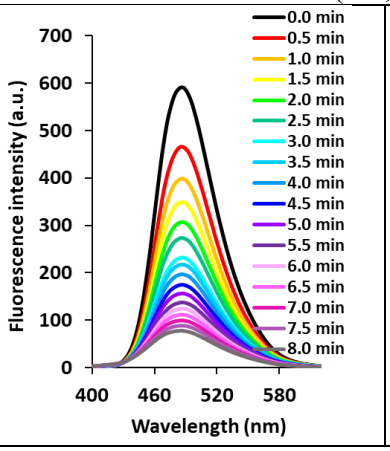

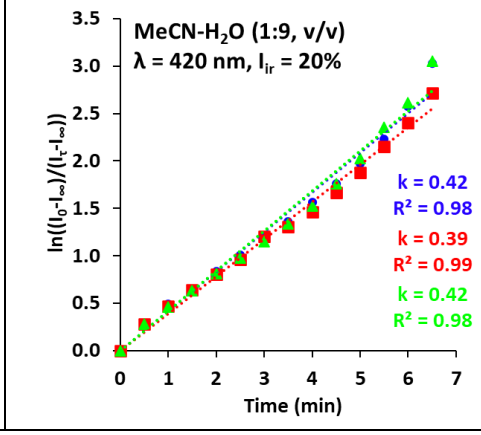

1f in Acetone-H_2O (1:9, v/v), λ_{ir} = 420 nm, I_{ir} = 20%

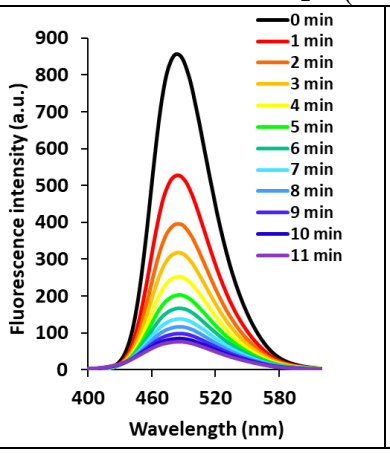

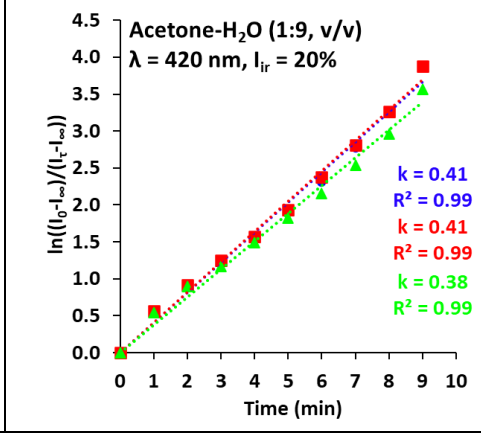

1g in DMSO-PBS (pH 7.4) (1:9, v/v), λ_{ir} = 420 nm, I_{ir} = 20%

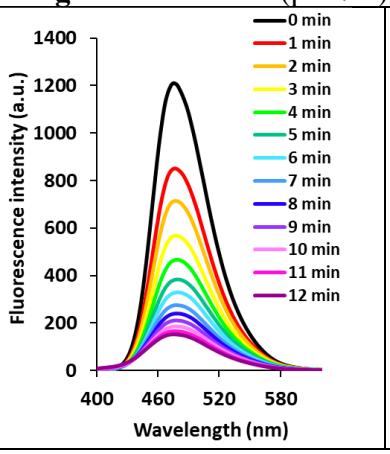

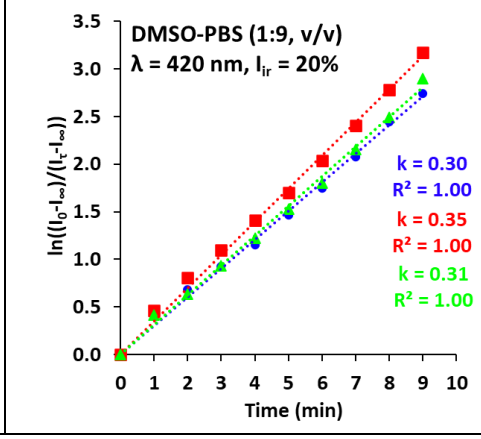

1g in DMSO-PBS (pH 7.4) (1:1, v/v), λ_{ir} = 420 nm, I_{ir} = 20%

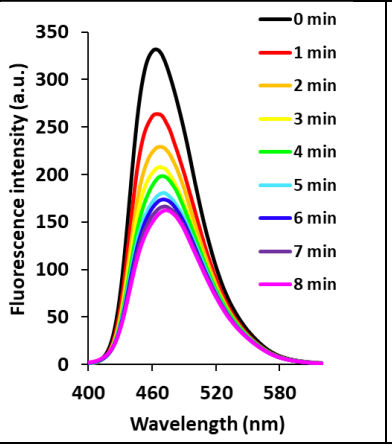

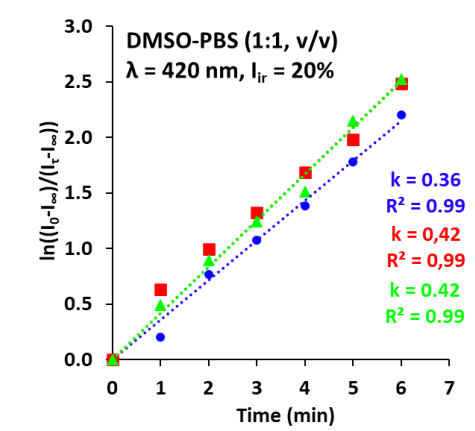

1g in MeCN-H_2O (1:9, v/v), λ_{ir} = 420 nm, I_{ir} = 20%

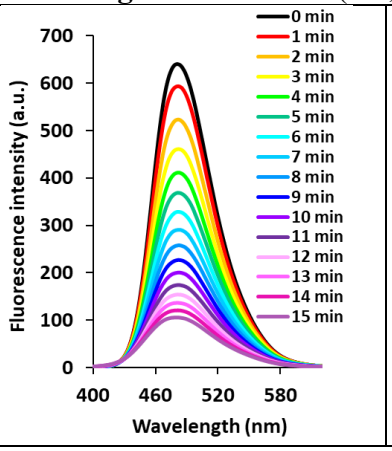

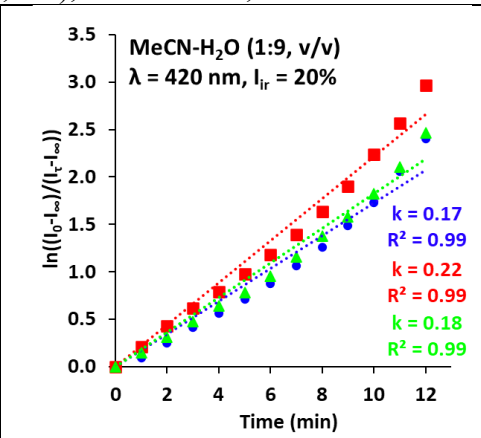

1g in DMSO-PBS (pH 7.4) (1:9, v/v), λ_{ir} = 365 nm, I_{ir} = 10%

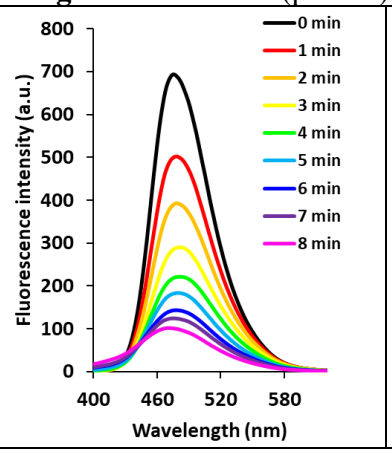

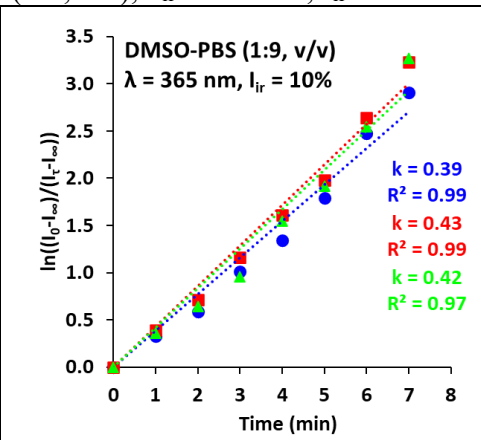

1g in DMSO-PBS (pH 7.4) (1:9, v/v), λ_{ir} = 365 nm, I_{ir} = 20%

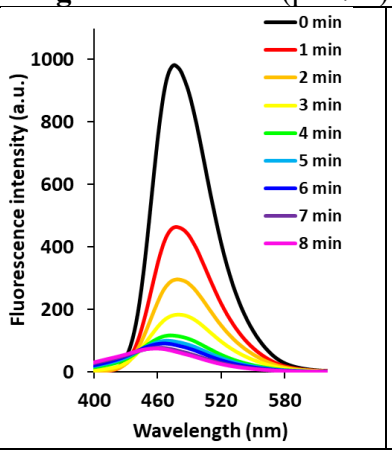

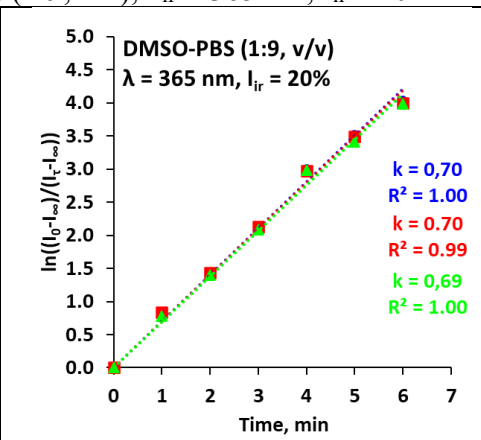

1g in MeCN, λ_{ir} = 420 nm, I_{ir} = 20%

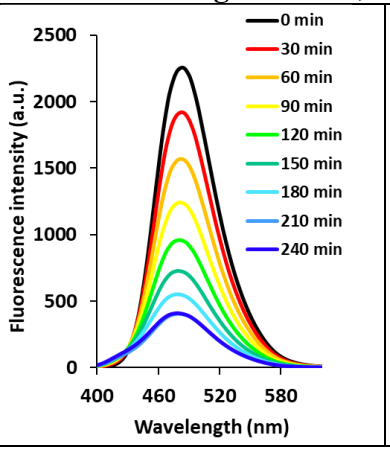

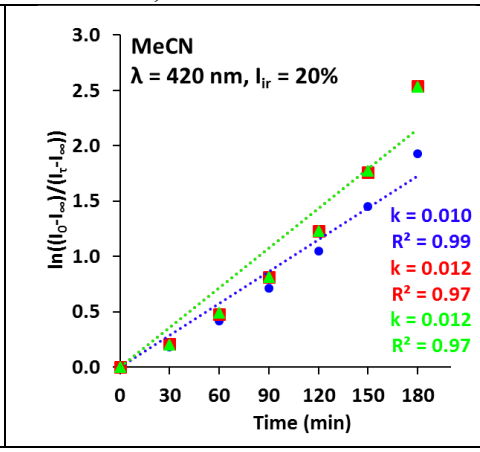

1h in DMSO-PBS (pH 7.4) (1:9, v/v), λ_{ir} = 420 nm, I_{ir} = 20%

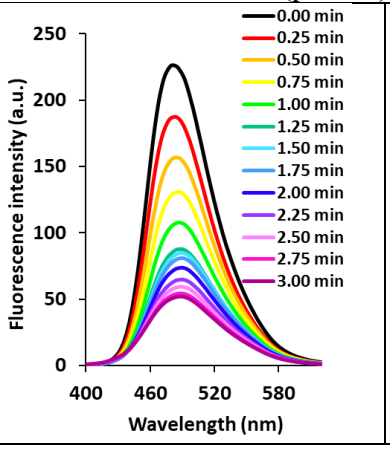

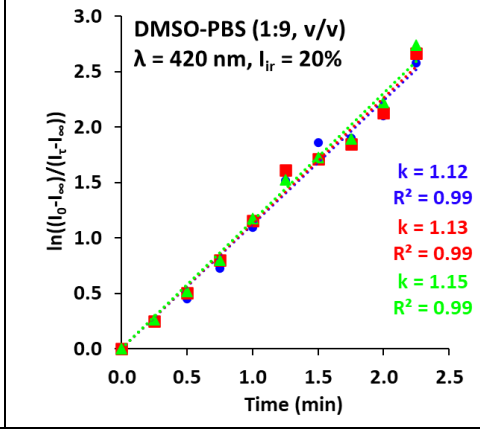

1i in MeCN-H_2O (1:9, v/v), λ_{ir} = 420 nm, I_{ir} = 20%

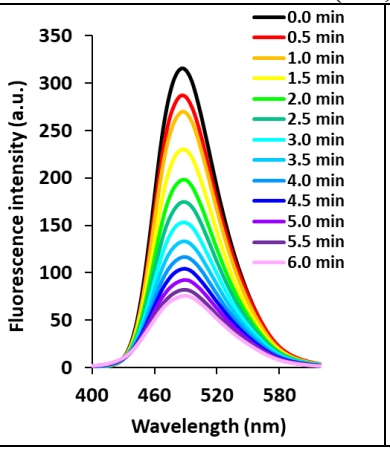

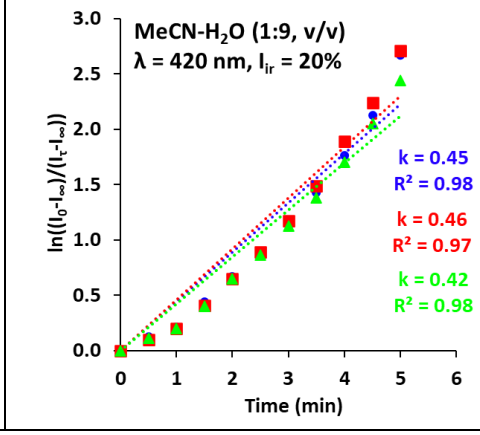

1i in DMSO-PBS (pH 7.4) (1:9, v/v), λ_{ir} = 420 nm, I_{ir} = 20%

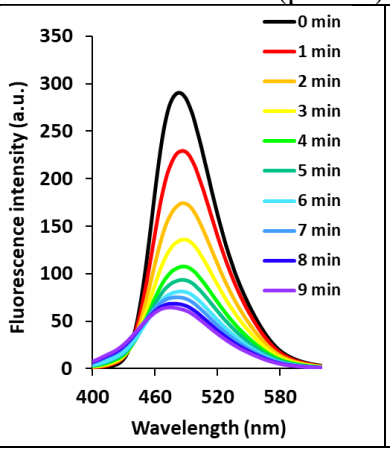

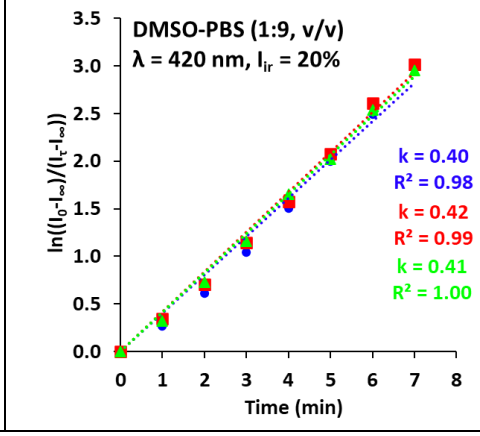

1j in DMSO-PBS (pH 7.4) (1:9, v/v), λ_{ir} = 420 nm, I_{ir} = 20%

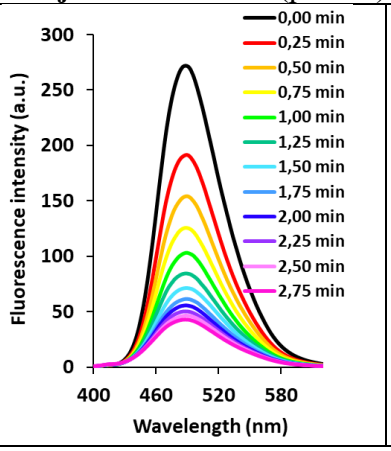

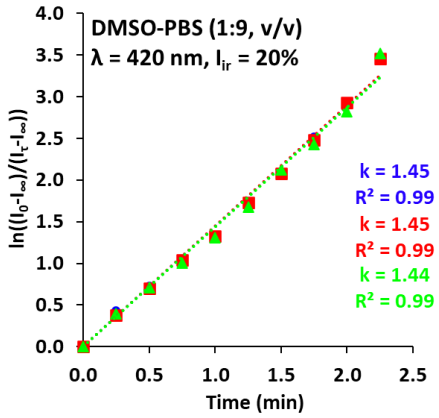

1k in DMSO-PBS (pH 7.4) (1:9, v/v), λ_{ir} = 420 nm, I_{ir} = 20%

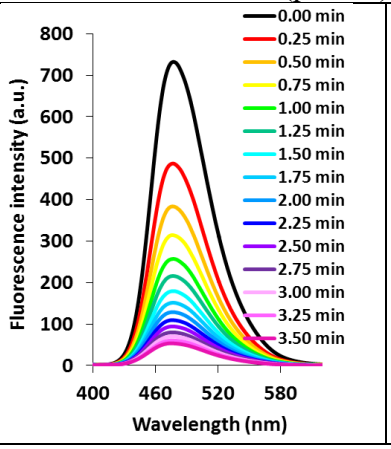

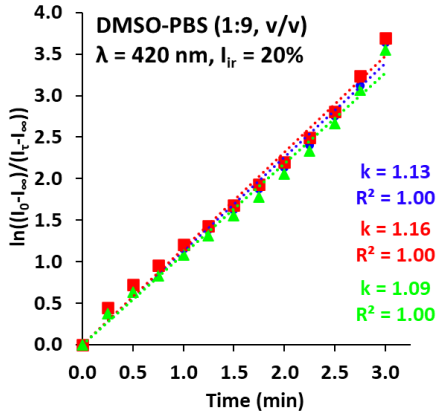

1m in DMSO-PBS (pH 7.4) (1:9, v/v), λ_{ir} = 420 nm, I_{ir} = 20%

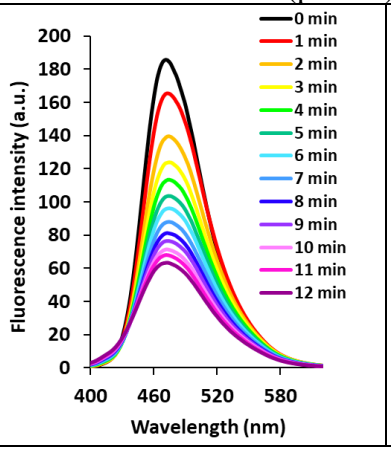

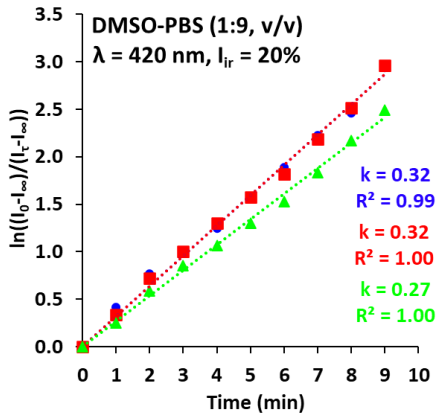

1n in DMSO-PBS (pH 7.4) (1:9, v/v), λ_{ir} = 420 nm, I_{ir} = 20%

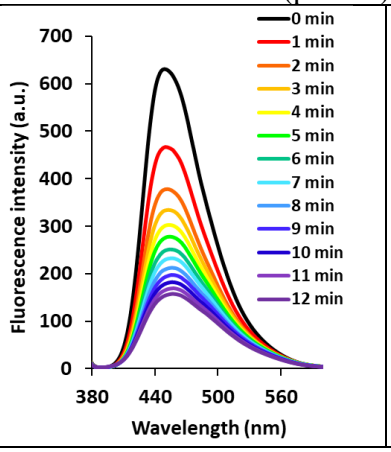

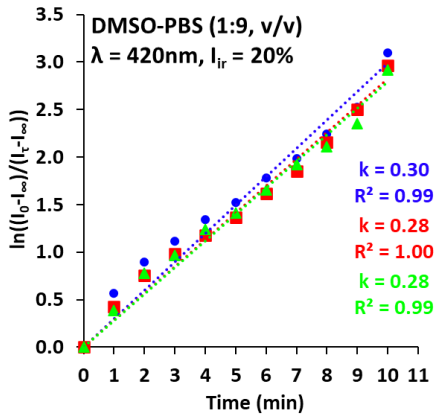

1n in DMSO-PBS (pH 7.4) (1:9, v/v), λ_{ir} = 365 nm, I_{ir} = 20%

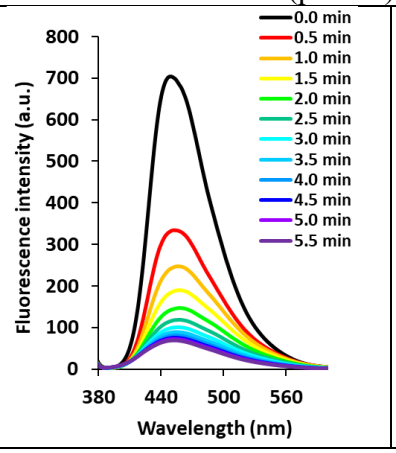

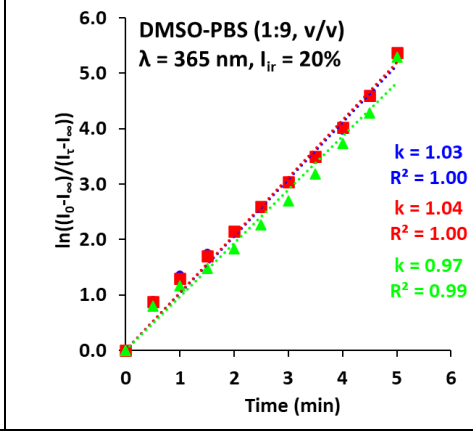

1o in DMSO-PBS (pH 7.4) (1:9, v/v), λ_{ir} = 365 nm, I_{ir} = 20%

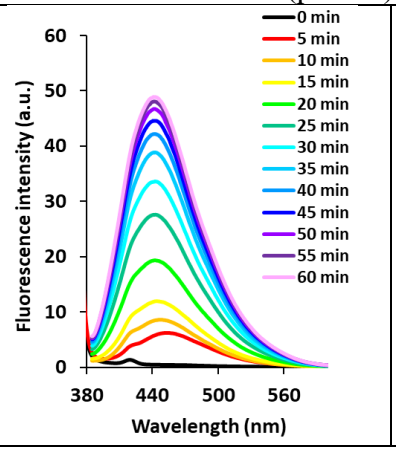

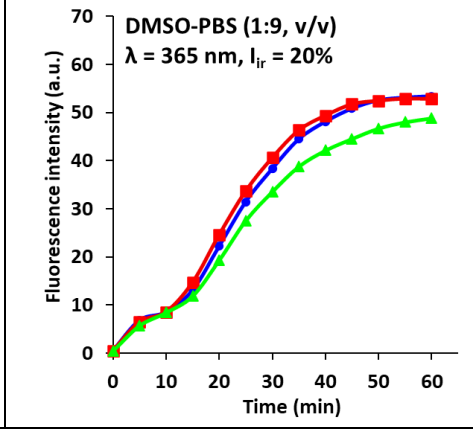

1p in DMSO-PBS (pH 7.4) (1:9, v/v), λ_{ir} = 420 nm, I_{ir} = 20%

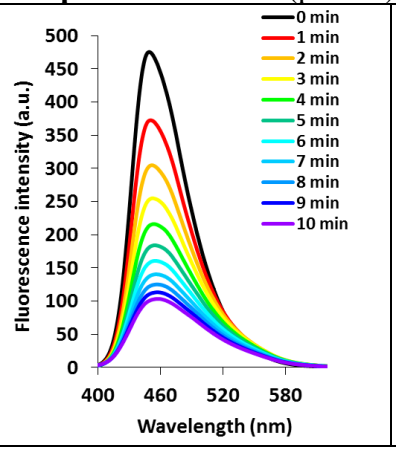

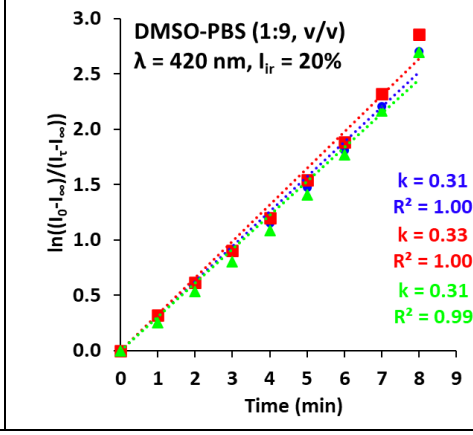

1q in DMSO-PBS (pH 7.4) (1:9, v/v), λ_{ir} = 420 nm, I_{ir} = 20%

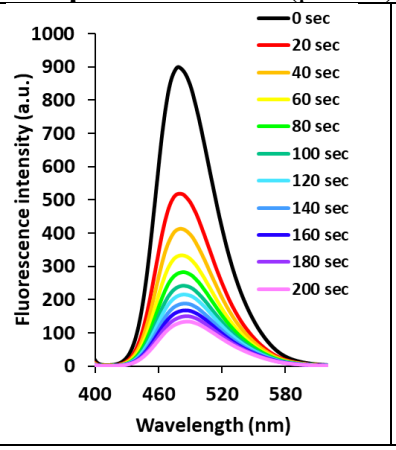

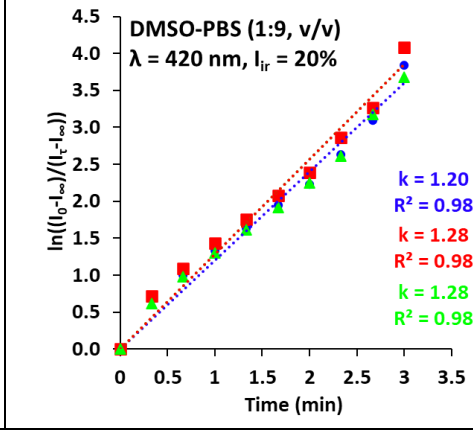

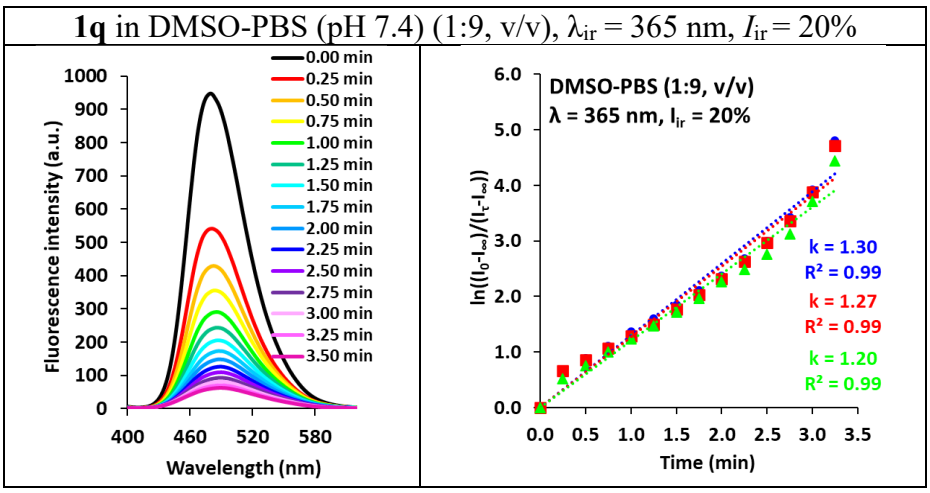

Fig. S56. Evolution of emission spectra for ATT-PCs **1a–q** (c = 1×10^{-5} M) in different media (DMSO-PBS 1:1 or 1:9 v/v, pH 7.4; MeCN-H_2O 1:9 v/v; MeCN) upon irradiation (λ_{ir} = 365 or 420 nm; I_{ir} = 10% or 20%). Corresponding first-order kinetic plots according to $\ln[(I_0 - I_\infty)/(I_t - I_\infty)]$ vs. time (t) for selected ATT-PCs.

Table S22. Kinetic data for the phodissociation of ATT-PCs **1a-q**.

Entry	Compd	Structure	Conditions	k, min^{-1}	$\bar{k}$, min^{-1}	$\tau_{1/2}$, min	R^2	Q_u (%)
1	**1a**	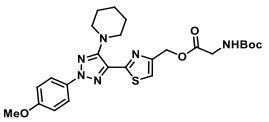	λ = 420 nm, I_{ir} = 20%, DMSO-PBS 1:9	0.12	0.12 ± 0.01	5.81	1.00	-
2				0.11			1.00	
3				0.12			0.99	
4	**1b**	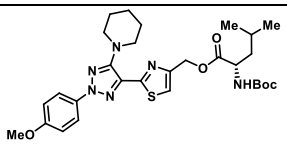	λ = 420 nm, I_{ir} = 20%, DMSO-PBS 1:9	0.92	0.87 ± 0.04	0.80	0.99	-
5				0.84			0.99	
6				0.84			1.00	
7	**1d**	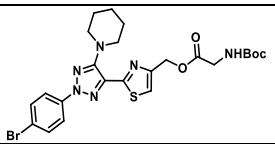	λ = 420 nm, I_{ir} = 20%, DMSO-PBS 1:9	0.20	0.199 ± 0.003	3.48	0.97	-
8				0.22			0.98	
9				0.20			0.97	
10	**1e**	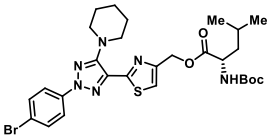	λ = 420 nm, I_{ir} = 20%, DMSO/PBS (1/9, v/v)	0.20	0.20 ± 0.01	3.46	0.99	-
11				0.21			0.99	
12				0.20			0.99	
13	**1f**	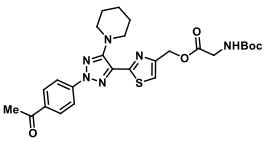	λ = 420 nm, I_{ir} = 20%, DMSO-PBS 1:9	0.47	0.48 ± 0.02	1.43	0.99	0.67 ± 0.03
14				0.51			0.99	
15				0.47			1.00	
16			λ = 420 nm, I_{ir} = 20%, MeCN-H_2O 1:9	0.42	0.41 ± 0.02	1.69	1.00	-
17				0.39			1.00	
18				0.42			0.99	
19			λ = 420 nm, I_{ir} = 20%, Acetone-H_2O 1:9	0.41	0.40 ± 0.02	1.74	1.00	-
20				0.41			1.00	
21				0.38			1.00	
22	**1g**		λ = 420 nm,	0.30		2.16	1.00	

23			I_{ir} = 20%, DMSO-PBS 1:9	0.35	0.32 ± 0.02		1.00	0.48 ± 0.04
24				0.31			1.00	
25			λ = 420 nm, I_{ir} = 20%, DMSO-PBS 1:1	0.36	0.40 ± 0.03	1.74	1.00	-
26				0.42			0.99	
27				0.42			1.00	
28			λ = 420 nm, I_{ir} = 20%, MeCN-H_2O 1:9	0.17	0.19 ± 0.03	3.60	0.99	-
29				0.22			0.99	
30				0.18			0.99	
31			λ = 365 nm, I_{ir} = 10%, DMSO-PBS 1:9	0.39	0.41 ± 0.02	1.69	0.99	0.49 ± 0.03
32				0.43			0.99	
33				0.42			0.97	
34			λ = 365 nm, I_{ir} = 20%, DMSO-PBS 1:9	0.70	0.70 ± 0.01	1.00	1.00	0.414 ± 0.004
35				0.70			1.00	
36				0.69			1.00	
37			λ = 420 nm, I_{ir} = 20%, MeCN	0.010	0.011 ± 0.001	62.07	0.99	-
38				0.012			0.97	
39				0.012			0.97	
40	**1h**		λ = 420 nm, I_{ir} = 20%, DMSO-PBS 1:9	1.12	1.12 ± 0.02	0.62	1.00	1.13 ± 0.02
41				1.13			1.00	
42				1.15			1.00	
43	**1i**		λ = 420 nm, I_{ir} = 20%, DMSO-PBS 1:9	0.40	0.41 ± 0.01	1.68	0.99	0.59 ± 0.01
44				0.42			1.00	
45				0.41			1.00	
46			λ = 420 nm, I_{ir} = 20%, MeCN-H_2O 1:9	0.45	0.44 ± 0.02	1.56	0.98	-
47				0.46			0.97	
48				0.42			0.98	
49	**1j**		λ = 420 nm, I_{ir} = 20%, DMSO-PBS 1:9	1.45	1.44 ± 0.01	0.48	1.00	3.74 ± 0.02
50				1.45			1.00	
51				1.44			1.00	
52	**1k**		λ = 420 nm, I_{ir} = 20%, DMSO-PBS 1:9	1.13	1.13 ± 0.03	0.62	1.00	1.55 ± 0.05
53				1.16			1.00	
54				1.09			1.00	
55	**1m**		λ = 420 nm, I_{ir} = 20%, DMSO-PBS 1:9	0.32	0.30 ± 0.03	2.29	1.00	-
56				0.32			1.00	
57				0.27			1.00	
58	**1n**		λ = 420 nm, I_{ir} = 20%, DMSO-PBS 1:9	0.30	0.29 ± 0.01	2.42	0.99	-
59				0.28			1.00	
60				0.28			0.99	
61			λ = 365 nm, I_{ir} = 20%, DMSO-PBS 1:9	1.03	1.01 ± 0.04	0.69	1.00	-
62				1.04			1.00	
63				0.97			0.99	

64 65 66	**1o**	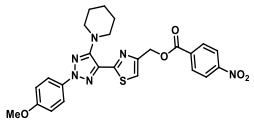	λ = 365 nm, I_{ir} = 20%, DMSO-PBS 1:9	- - -	-	22.08	- - -	-
67 68 69	**1p**	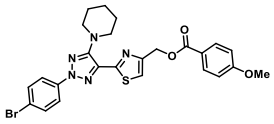	λ = 420 nm, I_{ir} = 20%, DMSO-PBS 1:9	0.31 0.33 0.31	0.32 ± 0.01	2.19	1.00 1.00 0.99	-
70 71 72	**1q**	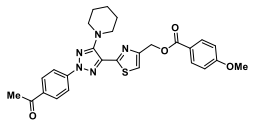	λ = 420 nm, I_{ir} = 20%, DMSO-PBS 1:9	1.20 1.28 1.28	1.25 ± 0.05	0.55	0.99 0.99 0.99	-
73 74 75			λ = 365 nm, I_{ir} = 20%, DMSO-PBS 1:9	1.30 1.27 1.20	1.26 ± 0.05	0.55	0.99 0.99 0.99	-

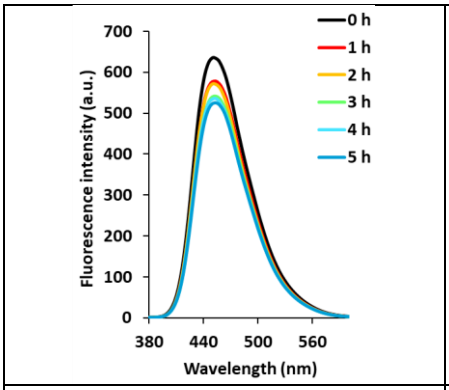	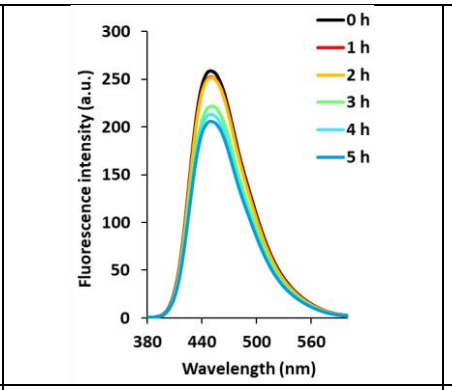	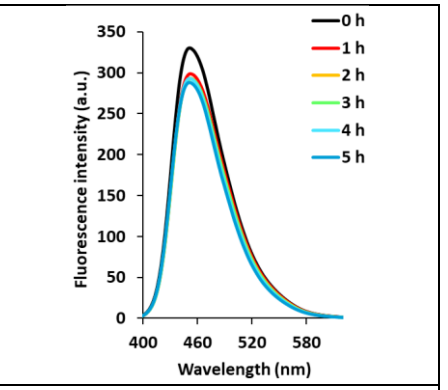
1a	**1b**	**1d**
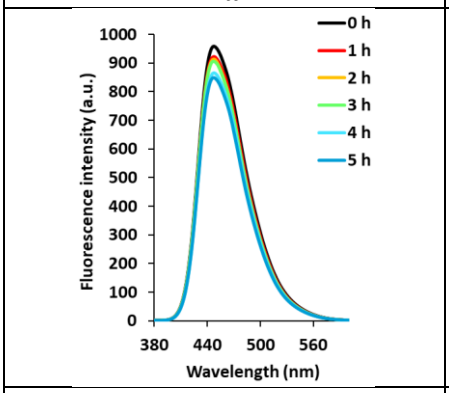	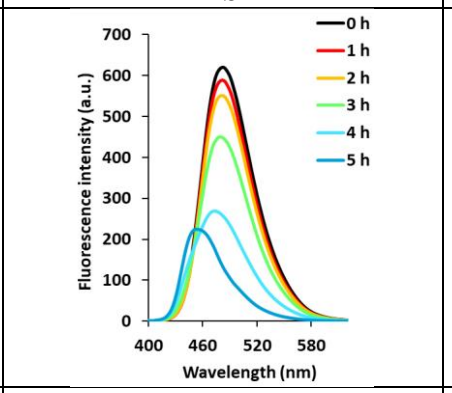	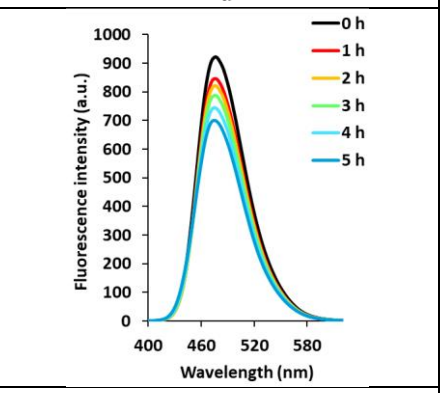
1e	**1f**	**1g**
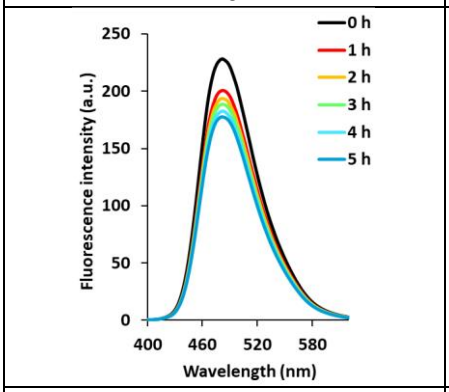	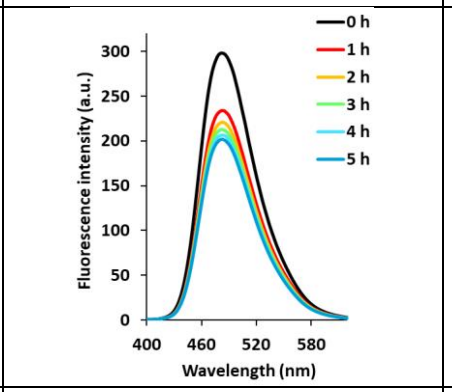	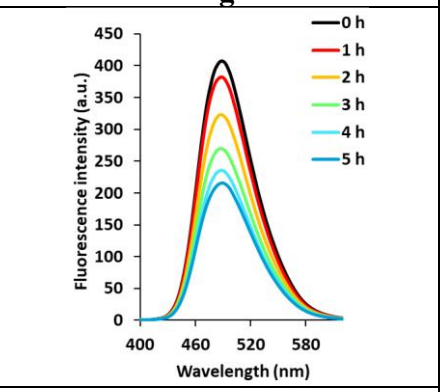
1h	**1i**	**1j**

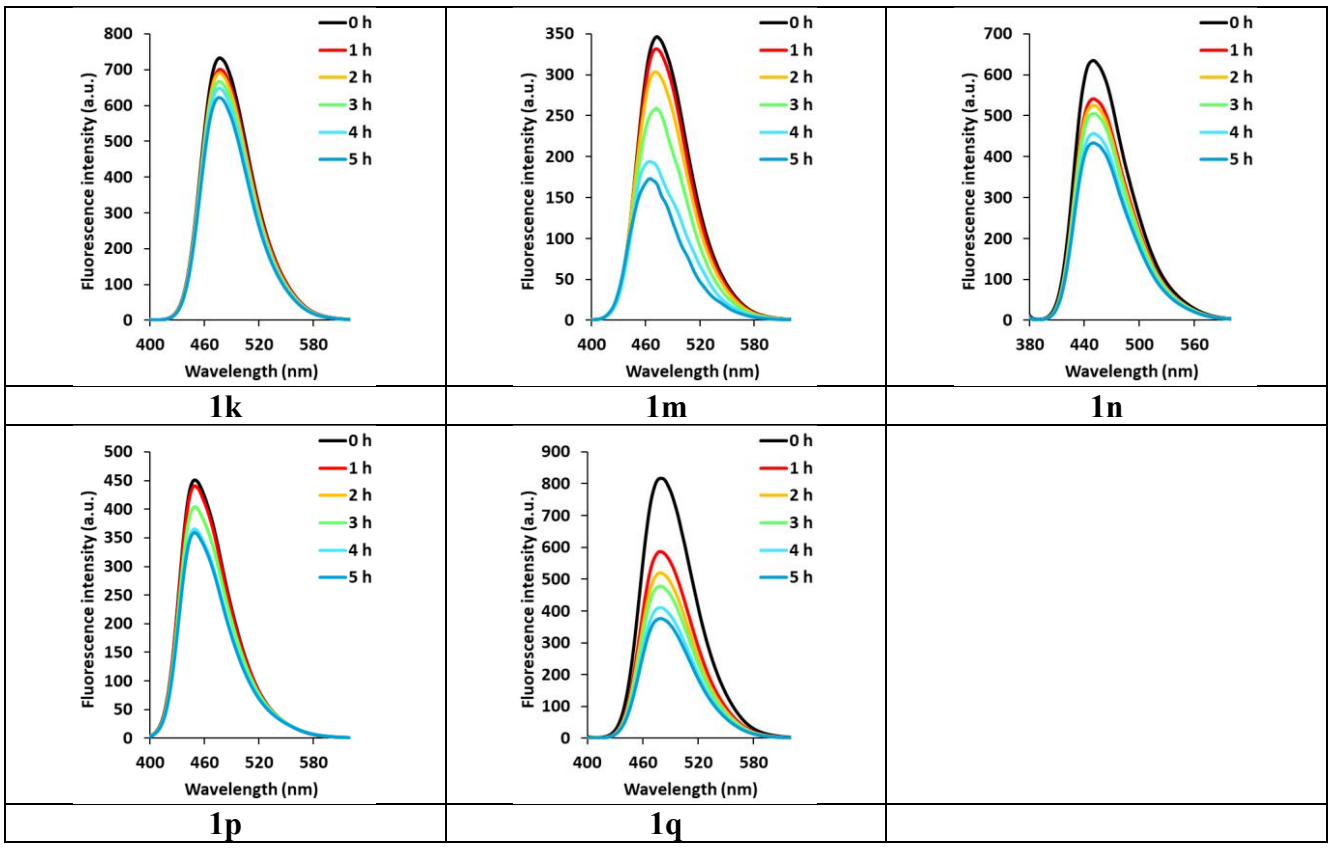

Fig. S57. Evaluation of emission spectra recorded during hydrolytic dissociation of ATT-PCs **1a**, **b**, **d-k**, **m-q** (c = 1×10^{-5} M) in a mixture of solvents DMSO-PBS (1:9, v/v, pH 7.4) in the dark over 5 hours, with measurements taken at 1-hour intervals.

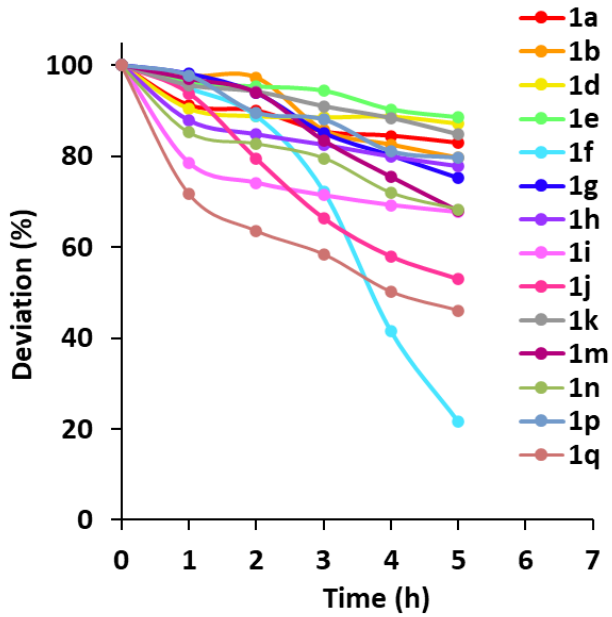

Fig. S58 Evaluation of the stability of ATT-PCs to hydrolytic dissociation of ATT-PCs **1a**, **b**, **d-k**, **m-q** (c = 1×10^{-5} M) in a mixture of solvents DMSO-PBS (1:9, v/v, pH 7.4) in the dark over 5 hours, with measurements taken at 1-hour intervals.

Table S23. The change in fluorescence intensity (%) of ATT-PCs **1a, b, d–k, m–q** (1×10^{-5} M) in DMSO–PBS (1:9, v/v, pH 7.4) was monitored in the dark over 5 hours, with measurements taken at 1-hour intervals.

Entry	Comp	Time, h					
		0	1	2	3	4	5
1	**1b**	100	91.2	90.0	85.4	84.5	82.9
2	**1d**	100	97.6	97.3	85.7	82.5	79.6
3	**1e**	100	90.5	88.8	88.6	88.7	87.2
4	**1f**	100	96.2	95.3	94.4	90.3	88.6
5	**1g**	100	94.9	88.8	72.3	41.6	21.7
6	**1h**	100	98.1	93.9	85.1	80.1	75.2
7	**1i**	100	87.9	84.9	82.6	80.0	77.9
8	**1j**	100	78.5	74.1	71.4	69.2	67.7
9	**1k**	100	93.8	79.4	66.3	57.9	52.9
10	**1m**	100	95.6	94.2	91.1	88.5	84.9
11	**1n**	100	97.0	94.0	83.5	75.6	68.1
12	**1p**	100	85.2	82.7	79.6	71.9	68.3
13	**1q**	100	97.7	89.6	88.0	81.0	79.6

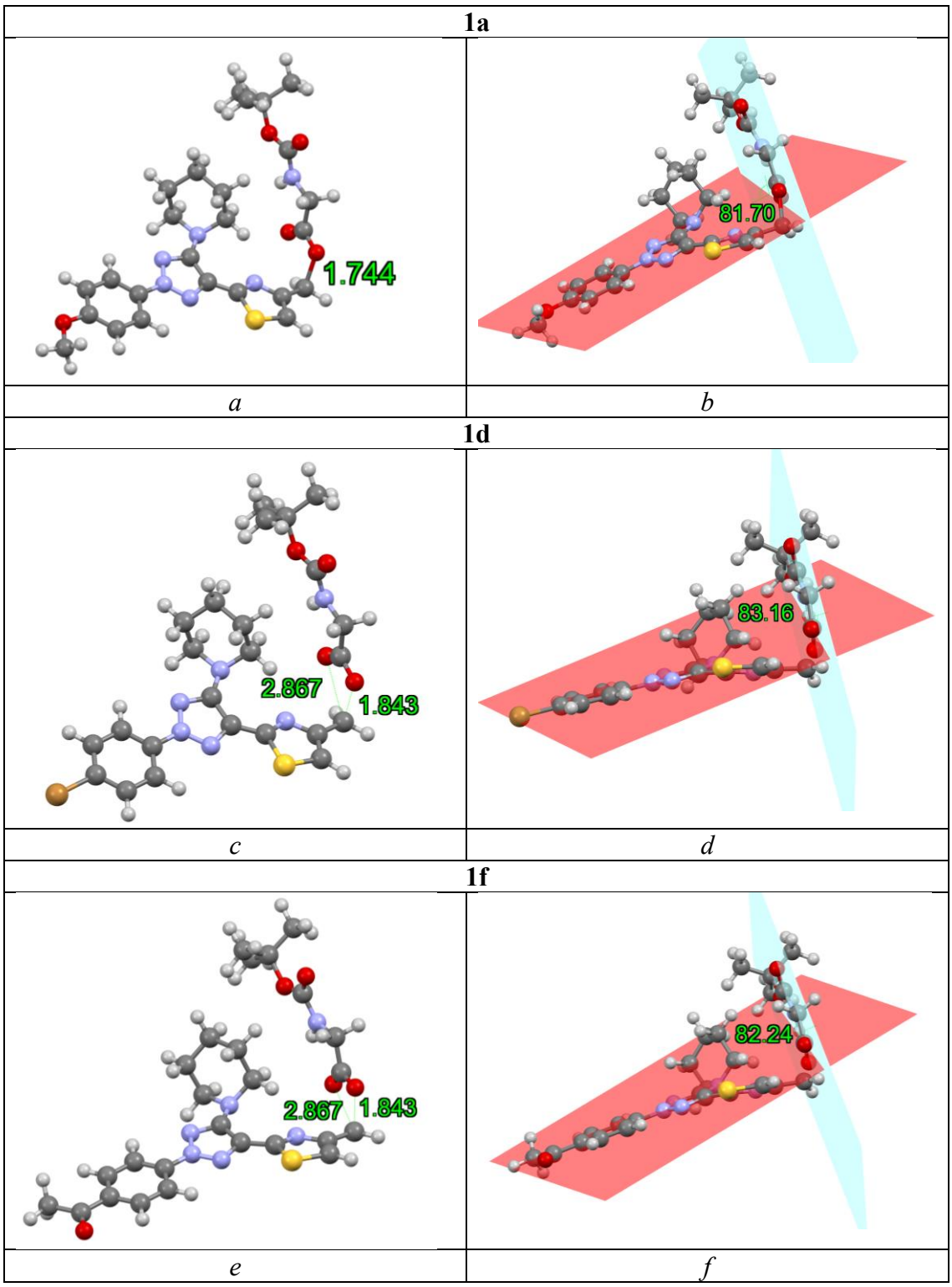

Fig. S59. The structure of ionic pairs during the cleavage of the C-O bond ATT-PCs **1a, d** and **f**. (*a*, *c*, *e*) - Front veiw ; (*b*, *d*, *f*) - Side view.

Table S24. The cation charge on C-atom of ATT-PCs **1a, d**, **f** in GS (S_0) and ES (S_1)

Compd	**1a**		**1d**		**1f**	
State	S_0	S_1	S_0	S_1	S_0	S_1
q/|e|	0.565	0.402	0.560	0.469	0.560	0.437

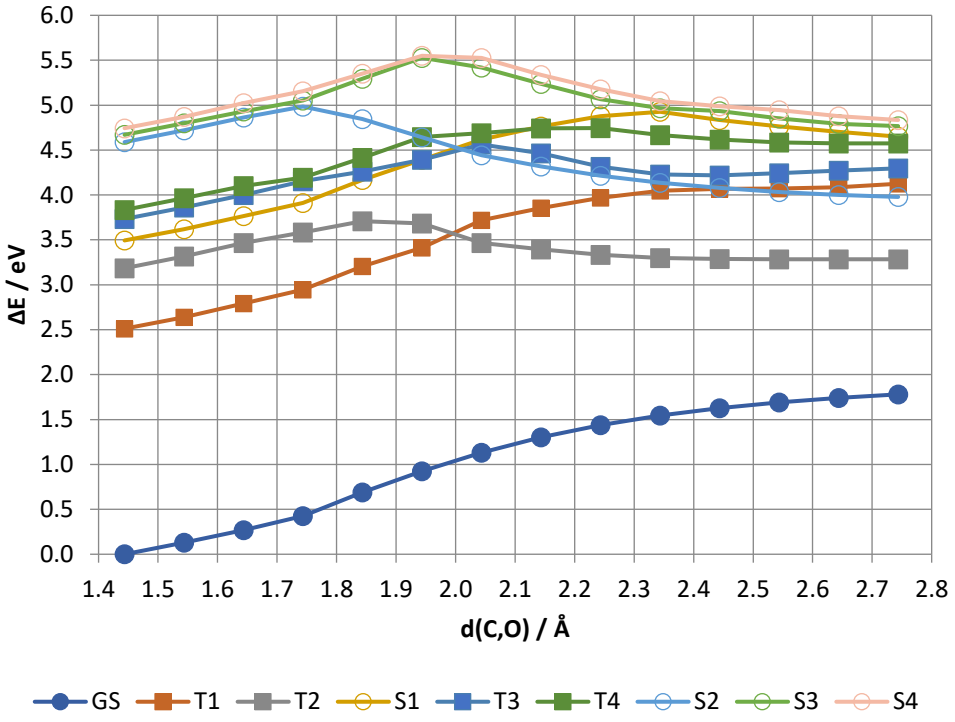

1a

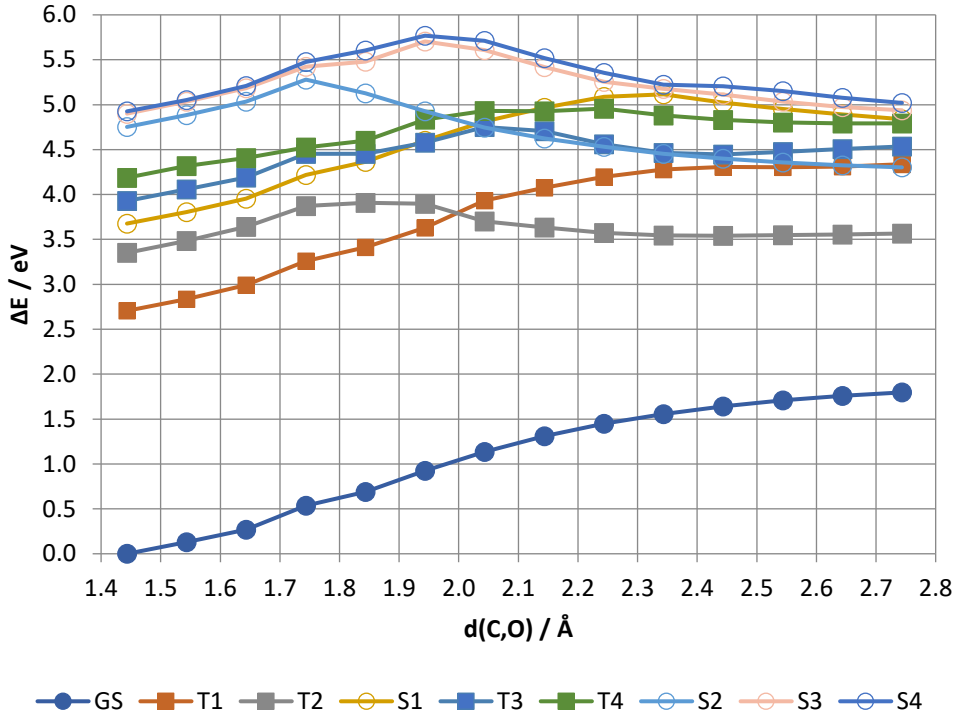

1d

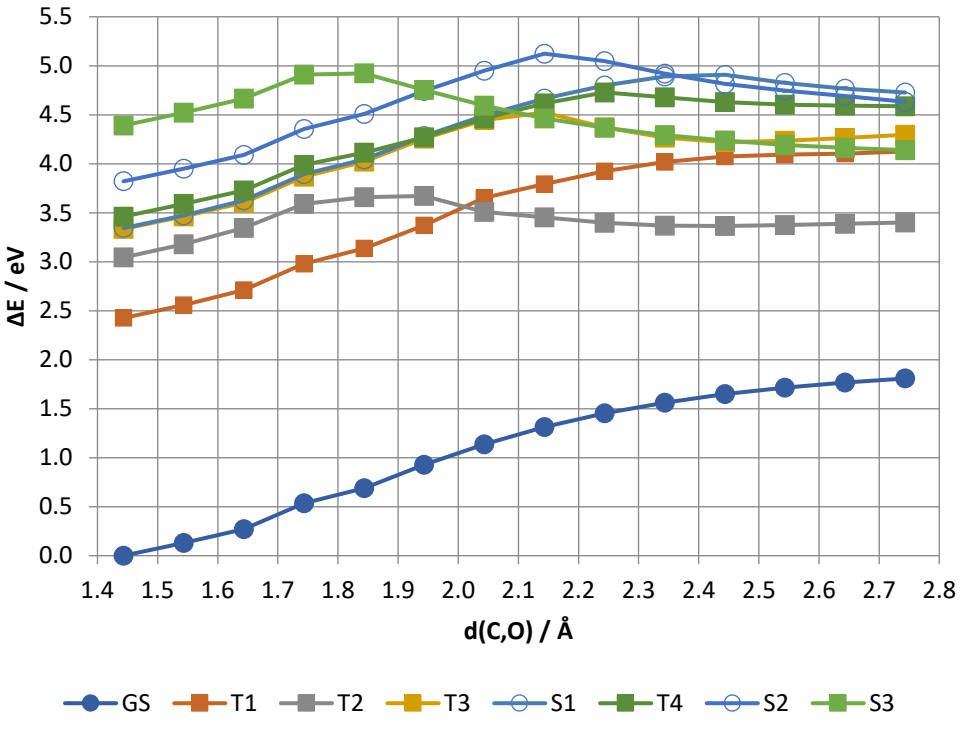

1f

Fig. S60. Changes in the energy levels S and *T* states of an increase in the distance between the carbon (C) and oxygen (O) atoms during bond cleavage.

Experiment with Potassium Sorbate. Solutions of ATT-PCs **1b**, **1e**, and **1g** (c = 1 × 10^{-5} M) in DMSO–PBS (1:9, v/v, pH 7.4) were prepared in cuvettes. Potassium sorbate was added to achieve final concentrations of 1.0 and 2.0 equivalents relative to the photocage. The emission spectrum of each sample was recorded at regular time intervals following irradiation (λ_{ir} = 420 nm, I_{ir} = 20%).

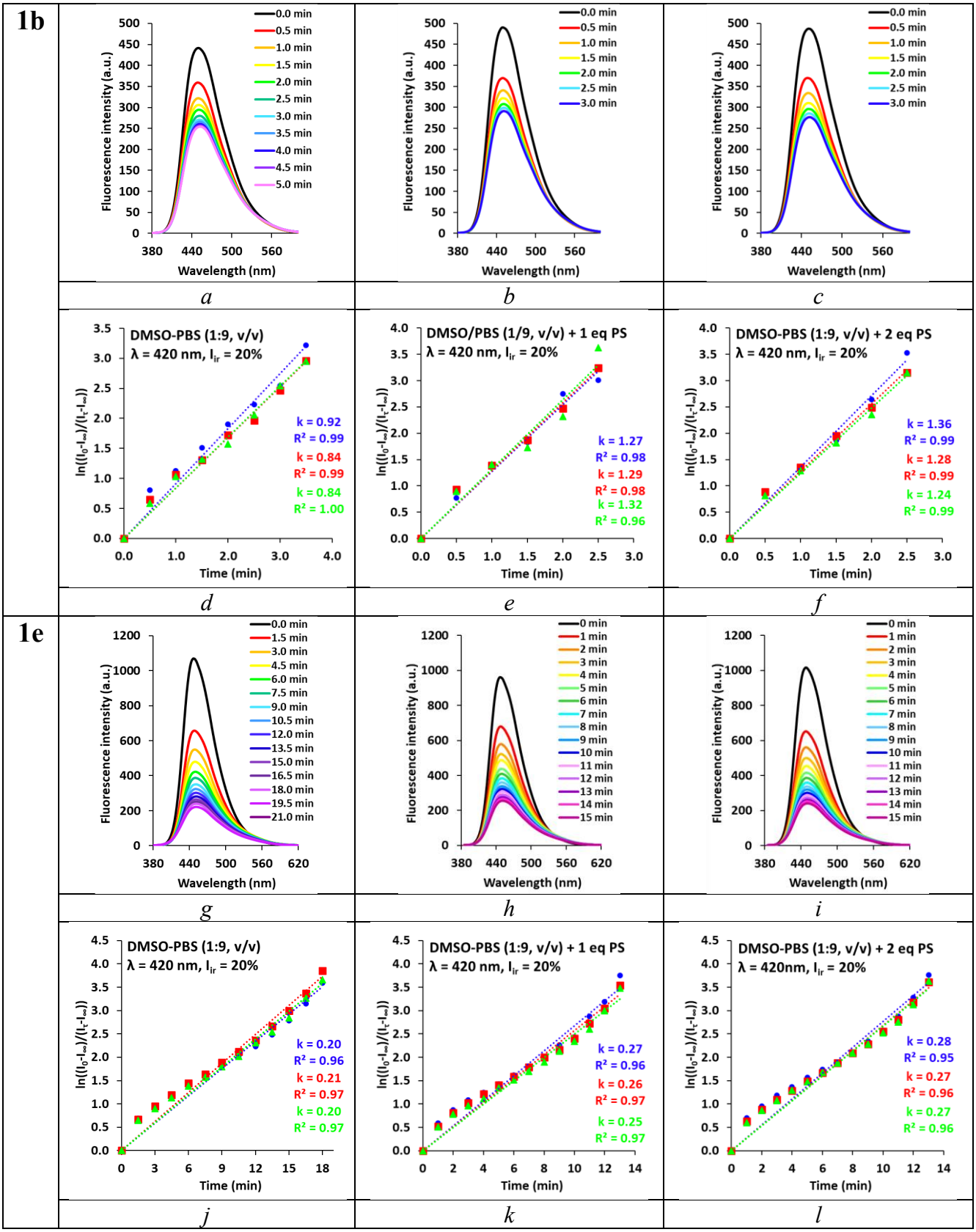

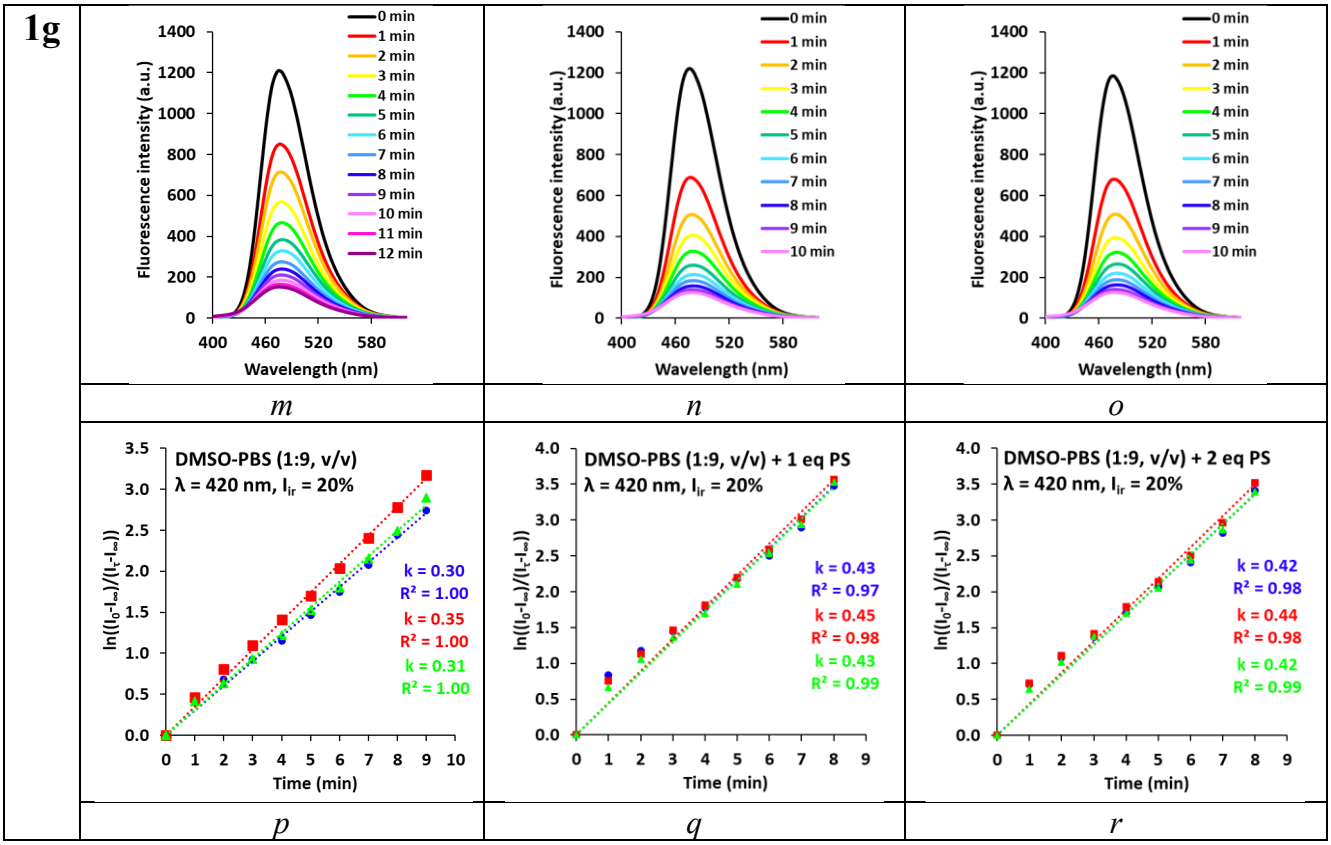

Fig. S61. (*a*, *b*, *c*, *g*, *h*, *i*, *m*, *n*, *o*) Evolution of the emission of solutions of ATT-PCs **1b**, **1e**, **1g** (c = 1×10^{-5} M) in a binary mixture of solvents DMSO-PBS (1:9, v/v, pH 7.4) upon irradiation (λ_{ir} = 420 nm, I_{ir} =20%): (*a*, *g*, *m*) without potassium sorbate (PS) (*b*, *h*, *n*) with 1.0 equiv. PS, (*c*, *i*, *o*) with 2.0 equiv. PS. (*d*, *e*, *f*, *j*, *k*, *l*, *p*, *q*, *r*) Plot of $\ln[(I_0 - I_\infty)/(I_t - I_\infty)]$ versus *t* for ATT-PCs **1b**, **1e**, **1g**: (*d*, *j*, *p*) without PS, (*e*, *k*, *q*) with 1.0 equiv. PS, (*f*, *l*, *r*) with 2.0 equiv. PS.

Table S25. Kinetic parameters for the photodissociation of ATT-PCs **1b**, **1e**, and **1g** (c = 1 × 10^{-5} M) in DMSO–PBS (1:9, v/v, pH 7.4) in the absence and presence of potassium sorbate (PS; 1.0 and 2.0 equiv.) under irradiation (λ = 420 nm, 20% power). Data obtained from fluorescence measurements.

Entry	Compd	Structure	PS, equiv.	k, min^{-1}	$\overline{k}$, min^{-1}	$\tau_{1/2}$, min	R^2
1				0.92			0.99
2			-	0.84	0.87 ± 0.04	0.80	0.99
3				0.84			1.00
4				1.27			1.00
5	**1b**	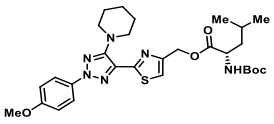	1	1.29	1.29 ± 0.02	0.54	1.00
6				1.32			0.99
7				1.36			1.00
8			2	1.28	1.29± 0.06	0.54	1.00
9				1.24			1.00
10				0.20			0.99
11			-	0.21	0.20 ± 0.01	3.46	0.99
12				0.20			0.99
13				0.27			0.99
14	**1e**	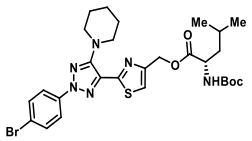	1	0.26	0.26± 0.01	2.68	0.99
15				0.25			0.99
16				0.28			0.99
17			2	0.27	0.27 ± 0.01	2.56	0.99
18				0.27			0.99
19				0.30			1.00
20			-	0.35	0.32 ± 0.02	2.16	1.00
21				0.31			1.00
22				0.43			0.99
23	**1g**	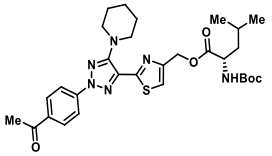	1	0.45	0.44 ± 0.01	1.58	1.00
24				0.43			1.00
25				0.42			0.99
26			2	0.44	0.43 ± 0.01	1.63	1.00
27				0.42			1.00

8. Biological experiments

Materials and methods. Vero cell cultures (green monkey kidney epithelium) and human fibroblast cultures were obtained from the Russian Collection of Cell Cultures (Institute of Cytology, Russian Academy of Sciences).

Cells were cultured in T-25 ventilated flasks (JetBiofil, China) using DMEM nutrient medium (HiMedia, India) supplemented with 3% fetal calf serum (Biolot, Russia) and a gentamicin-streptomycin solution (Biolot, Russia). Cultures were maintained in a humidified incubator at 37°C with 5% CO_2. Cells were passaged every three days or upon reaching 90% confluence using a trypsin-Versene solution (Bioinlabs, Russia).

Resazurin-assay. After 24 hours of incubation, 20 µL of a 0.42 mM resazurin solution (Thermo Scientific, USA) was added to each well. DMSO (a cytotoxic agent used to induce cell death) was added to the corner wells to serve as a positive control for cytotoxicity/blank. Fluorescence intensity was recorded using Chemidoc MP (Biorad, USA) in three ranges: Green Epi with a Green 605/50 filter for recording resazurin, Red Epi with a 695/55 filter for recording resazurin, and Blue Epi with a 530/28 filter for recording the plate itself. Acquired images were processed using CellProfiler to segment the cells of the plate and measure the fluorescence intensity in each of them, and then subsequent calculations were performed using a Python script (https://github.com/arteys/Resazurin_ChemiDoc).

Statistical processing. The results were analyzed using a python script available in the repository at the link: https://github.com/arteys/MTT_assay_multi. Raw data **are** also provided in this repository. Statistical processing was carried out using the Statannotations 3 library, using a two-tailed Mann-Whitney-Wilcoxon test, taking into account the Bonferroni correction for multiple comparisons. The designation ns corresponds to the absence of statistical significance, * significance at 1.00e-02 < p <= 5.00e-02, ** reliability at 1.00e-03 < p <= 1.00e-02, *** reliability at 1.00e-04 < p <= 1.00e-03, **** reliability at p <= 1.00e-04.

Confocal and optical microscopy. Microscopic examination was performed using the equipment of the Shared Research Center of Scientific Equipment SRC IIP UrB RAS. After staining and washing, living cells were examined using a confocal laser scanning microscope LSM-710 (Carl Zeiss) has a multichannel QUASAR detector (34 channels). Images were acquired using an immersion lens 40x/1.3 Oil. To obtain an informative fluorescent image in special software ZEN a special lambda mode (λ-mode) was used, which allows determining the emission range with the maximum contrast for this preparation.

To minimize the light effect on the sample, the initial focus adjustment was carried out under illumination with a laser with a wavelength of 633 mm, as the lowest energy available. The emission spectra of substances were also extracted from images obtained in the lambda mode. However, it is

necessary to clarify that the confocal microscope is not a spectrofluorometer, and the fluorescence spectra obtained with it can be unreliable. The images were processed using FIJI, a Python script was written to process the lambda images obtained with the confocal microscope, allowing the processing of the .lsm file format. The script is available on the Github (https://github.com/arteys/PyLSM).

The initial focus adjustment on a confocal microscope was carried out using the light of a laser with a wavelength of 633 nm, as the least energetic available. To study the phenomenon of a decrease in the brightness of the dye under the action of light radiation (photobleaching), the cells were stained with a dye according to the procedure described above. The light exposure was carried out with the same laser intensity, which is necessary to obtain an image with adequate contrast. Without changing the laser intensity, a series of images was recorded sequentially for 30 seconds. Then, the integrated fluorescence intensity was determined from the images and graphs were plotted.

Cell staining. To clarify the localization of the tested substance, cells were additionally stained with fluorescent dyes staining known cell organelles.

Additional cell staining and colocalization experiments. To clarify the localization of the tested substance, cells were additionally stained with fluorescent dyes staining known cell organelles. The colocalisation of dye with the tested substance was assessed using ImagJ (FIJI), specifically the JACoP BIOP plugin. Noise was removed from the images using the standard Despeckle function, as well as the background using the Subtract Background function at default settings. Next, the JACoP BIOP plugin was used to obtain a fluorogram (colocalisation scatterplot) as well as numerical data (namely Manders overlap coefficient).

Preliminary cells grown in specialized confocal dishes were stained with the investigated substance, for this purpose a solution of the substance at a concentration of 10 μM in nutrient medium was added to the cells, after which they were incubated for half an hour. Then the medium was removed, the cells were washed three times with phosphate buffer, after which the cells were stained with commercial dye.

All work with photosensitive substances was performed in a Bioinnelix laminar flow cabinet (BioinnLabs, Russia) using red LED illumination (625 nm) to minimize the effect of light on the substance.

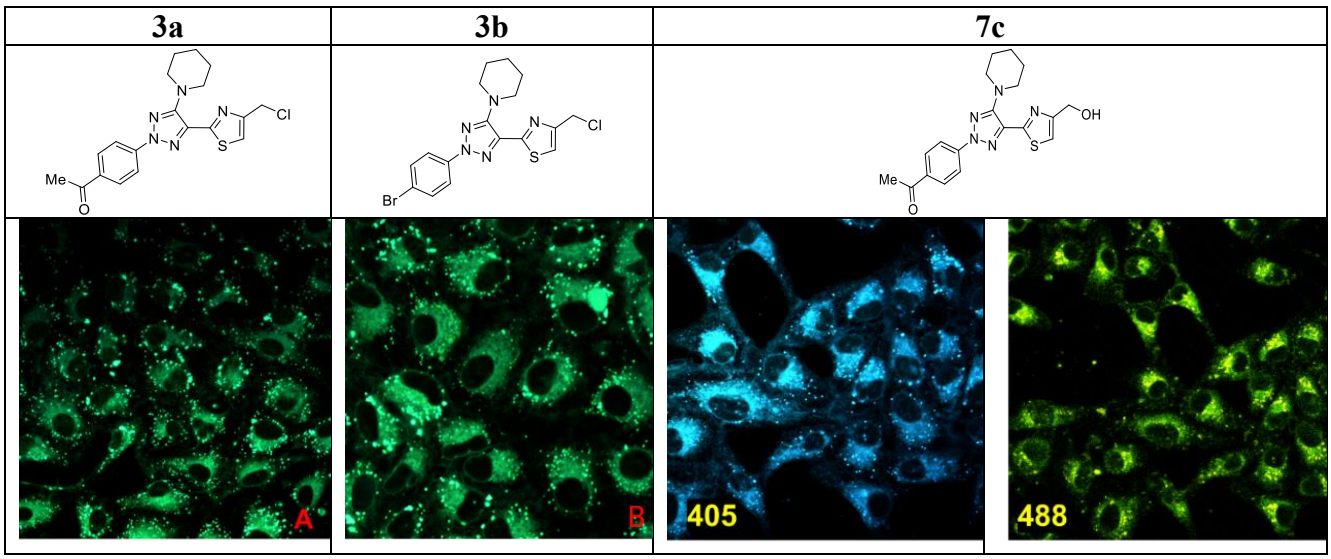

Fig. S62. Fluorescence microscope images of Vero cells treated with (A, B) ATT-CH_2Cl **3a-b** (0.1 μM, 0.5 h) under irradiation with laser λ= 405 nm at 37°C and (C, D) ATT-CH_2OH **7c** (0.1 μM, 0.5 h) under irradiation (C) λ= 405 nm and (D) λ= 488 nm at 37°C.

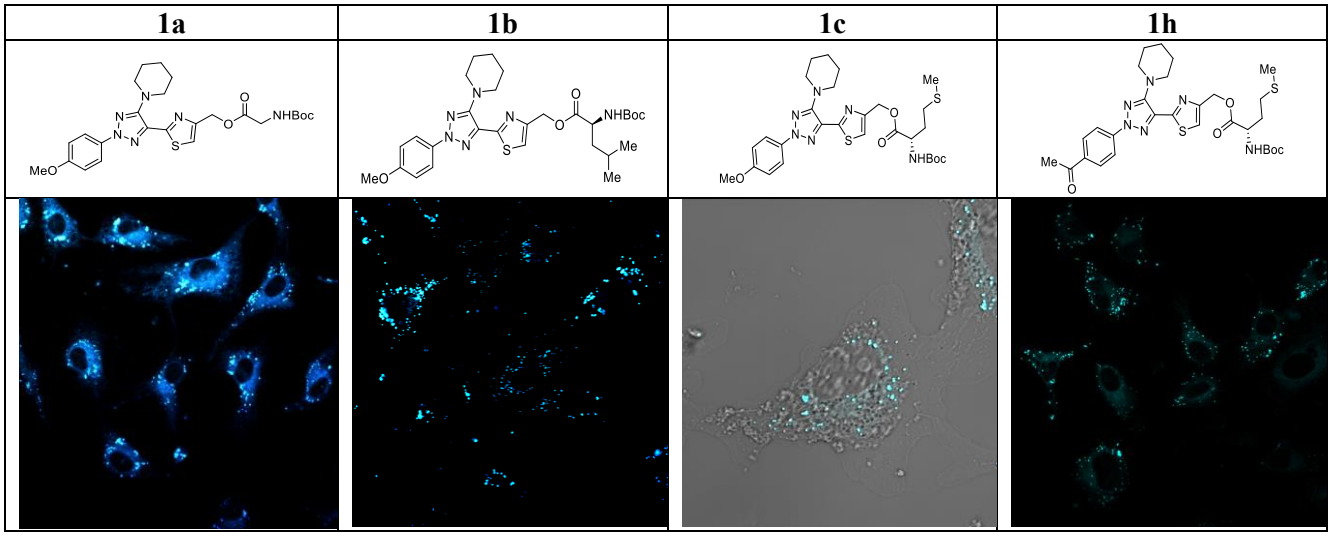

Fig. S63. Fluorescence microscope images of Vero cells treated with ATTs-PC **1a-c, h** (0.1 μM, 0.5 h) under irradiation with laser λ= 405 nm at 37°C.

References:

1 K. D. Gavlik, S. G. Lesogorova, E. S. Sukhorukova, J. O. Subbotina, P. A. Slepukhin, E. Benassi and N. P. Belskaya, *Eur. J. Org. Chem.*, 2016, 2700–2710.

2 M. L. Kondratieva, A. V. Pepeleva, N. P. Belskaya, A. V. Koksharov, P. V. Groundwater, K. Robeyns, L. V. Meervelt, W. Dehaen and Z.-J. Fan, *Tetrahedron*, 2007, **63**, 3042–3048.

3 N. P. Belskaya, V. A. Bakulev, T. G. Deryabina, J. O. Subbotina, M. I. Kodess, W. Dehaen, S. Toppet, K. Robeyns and L. V. Meervelt, *Tetrahedron*, 2009, **65**, 7662–7672.

4 T. G. Deryabina, N. P. Belskaya, M. I. Kodess, W. Dehaen, S. Toppet and V. A. Bakulev, *Tetrahedron Lett.*, 2006, **47**, 1853–1855.

5 A. A. Gagarin, A. S. Minin, V. A. Shevyrin, E. Benassi and N. P. Belskaya, *J. Mater. Chem. B*, 2024, **12**, 11402–11413.

6 A. A. Gagarin, A. S. Minin, V. A. Shevyrin, I. P. Kostova, E. Benassi and N. P. Belskaya, *Chem. Eur. J.*, 2023, **29**, e202302079.

7 A. D. Becke, *J. Chem. Phys.*, 1993, **98**, 5648–5652.

8 Y. Zhao and D. G. Truhlar, *Theor. Chem. Acc.*, 2008, **120**, 215–241.

9 S. Grimme, S. Ehrlich and L. Goerigk, *J. Comput. Chem.*, 2011, **32**, 1456–1465.

10 J. Tomasi, B. Mennucci and E. Cancès, *J. Mol. Struct.: THEOCHEM*, 1999, **464**, 211–226.

11 A. K. Rappé, C. J. Casewit, K. S. Colwell, W. A. Goddard and W. M. Skiff, *J. Am. Chem. Soc.*, 1992, **114**, 10024–10035.

12 A. V. Marenich, C. J. Cramer and D. G. Truhlar, *J. Phys. Chem. B*, 2009, **113**, 6378–6396.

13 J.-D. Chai and M. Head-Gordon, *J. Chem. Phys.*, 2008, **128**, 084106.

14 T. Yanai, D. P. Tew and N. C. Handy, *Chem. Phys. Lett.*, 2004, **393**, 51–57.

15 J. C. Taylor, *Phys. Rev.*, 1954, **95**, 1313–1317.

16 C. M. Breneman and K. B. Wiberg, *J. Comput. Chem.*, 1990, **11**, 361–373.

17 a) R. F. W. Bader and H. Essen, *J. Chem. Phys.*, 1983, **80**, 1943–1960; b) R. F. W. Bader, *Atoms in Molecules: A Quantum Theory*, Oxford University Press, 1990; c) R. F. W. Bader, *Chem. Rev.*, 1991, **91**, 893–928.

18 a) H. J. Bohórquez, C. F. Matta and R. J. Boyd, *Int. J. Quantum Chem.*, 2010, **110**, 2418–2425; b) E. R. Johnson, S. Keinan, P. Mori-Sánchez, J. Contreras-Garcia, A. J. Cohen and W. Yang, *J. Am. Chem. Soc.*, 2010, **132**, 6498–6506; c) P. Cacciani, P. Čermák, J. Cosléou, J. El Romh, J. Hovorka and M. Khelkhal, *Mol. Phys.*, 2014, **112**, 2476–2485; d) J. Andres, S. Berski, J. Contreras-Garcia and P. Gonzalez-Navarrete, *J. Phys. Chem. A*, 2014, **118**, 1663–1672.

19 G. B. Bacskay, *Chem. Phys.*, 1981, **61**, 385–404.

20 a) F. W. Biegler-König, R. F. W. Bader and T. H. Tang, *J. Comput. Chem.*, 1982, **3**, 317-328; b) AIMPAC, http://www.chemistry.mcmaster.ca/aimpac/imagemap/imagemap.htm, (accessed August 2025); c) N. Keith, Ph.D. Thesis, McMaster University, Canada, 1993.

21 M. J. Frisch, *et al.*, GAUSSIAN 16 (Revision C.01), Gaussian, Inc., Wallingford, CT, 2016.